UiT
THE ARCTIC
UNIVERSITY
OF NORWAY

Faculty of Science and Technology

Department of Chemistry

MD simulations reveal how synthetic antimicrobial peptides interact with membrane models

—

Ravna Sarre

KJE-3900 Master's Thesis in Chemistry, December 2014

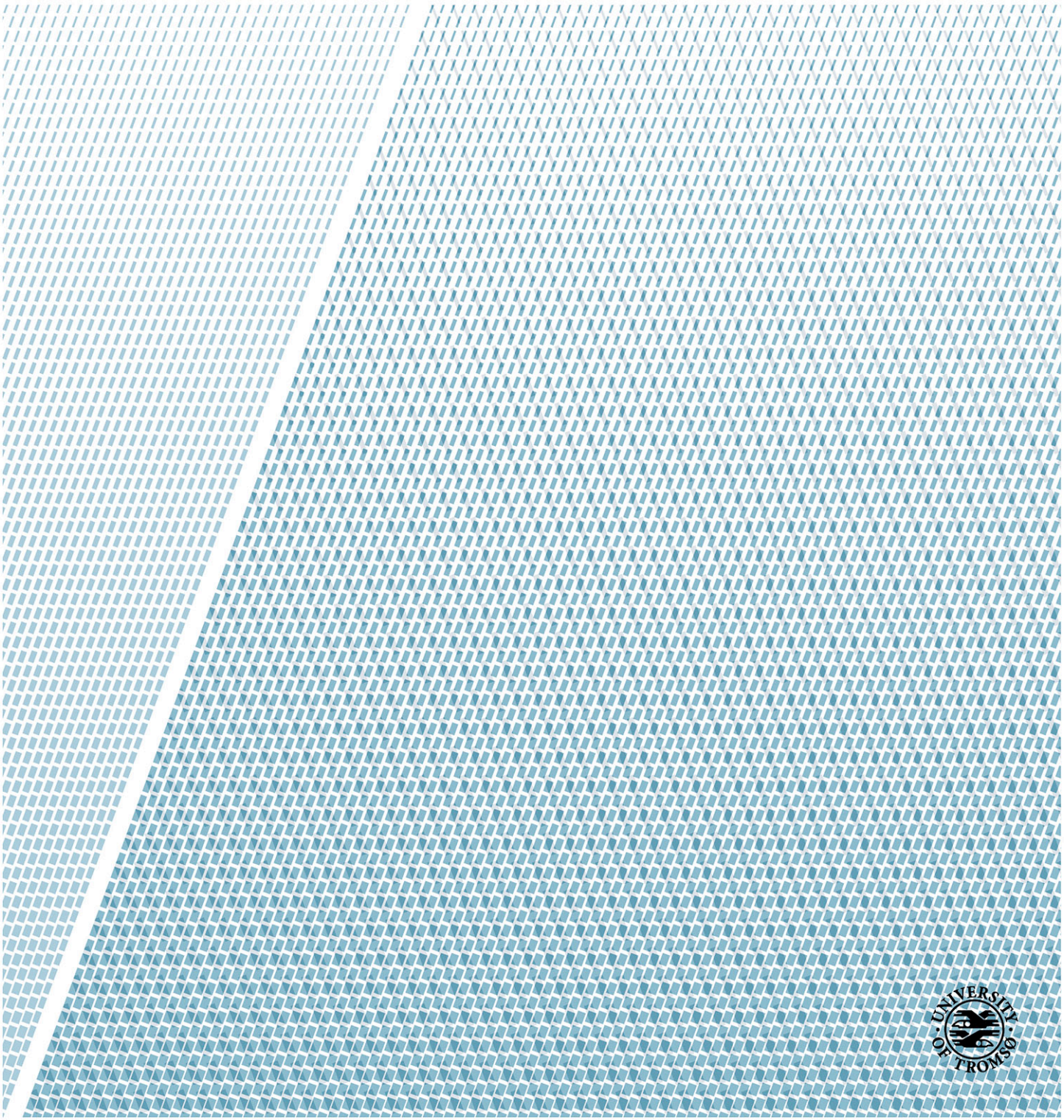

Abstract

Since the discovery of antibiotics the extensive use in health care and agriculture has led to the development of resistant bacterial strains. Antimicrobial peptides (AMPs) exists in nature where they are believed to play an important role in the innate immune system in vertebrates. Due to their antibacterial properties and apparent ability to elicit very low bacterial resistance, researchers have been hopeful that they can alleviate the challenges of progressing multiresistance, but this has not become a reality yet.

In this project, molecular dynamics simulations are used to explore the interactions of AMPs with model lipid bilayers. An important step in this process is to obtain a lipid bilayer with structure and properties that resembles those of the biological relevant fluid phase (Lα) bilayer. By applying molecular dynamics it is possible to study the interaction at an atomic level. Atomic level studies of fluid phase (Lα) lipid bilayers are not possible with the present experimental methods.

To examine the atomic level interactions of the synthetic antimicrobial peptides RWR-NHBn and RTbtR-NHBn with a bacterial like membrane, various DMPC and DMPG lipid bilayers are simulated with different combinations of the ions Na^+, K^+ and Cl^-. Most combination of ions yield membrane properties in good agreement with experimental values. A binary mixture of DMPC/DMPG with K^+ as counter-ions is used for the simulation with peptides. Interesting effects on the membrane is seen in a system with 4 TRTbtR-NHBn peptides where one peptide cause a large groove in the membrane surface by suppressing many DMPG lipids in the region. This may be a pre-stage to pore formation.

Acknowledgements

I would like to thank my supervisor Professor Bjørn Olav Brandsdal for guidance and encouragements during this project.

I would also like to thank Geir Isaksen, Johan Isaksson, Davide Michetti, Davide Bon and Elena Malkin for good discussions and advice.

I would also like to express my apreciation for the support and encouragments from my friends Laura Liikanen, Martin Ernstsen and my fiancé Martin

Contents

List of Figures

Chapter 1

Introduction

1.1 Antimicrobial Resistance

Since the discovery of bacteria in the late 19th century, the search for appropriate preventative and therapeutic drugs has been an ongoing task. Antibiotics was first discovered in 1929, when the British scientist Alexander Fleming isolated the antibacterial compound *penicillin* from the fungus *Penicillium chrysogenom*. Penicillin was introduced into clinical use in 1945, near the end of World War II, and proved effective in treating infections in wounded soldiers. At this time pharmaceutical companies also begun to look for and develop other antibiotics. Due to its effectiveness in treating infectious diseases, and also due to unexpected non-antibiotic effects such as being antiviral, antitumor and anticancer agents [8], the discovery of antibiotics is considered one of the most significant health-related events of modern time.

Infectious diseases have been a major cause of disorder throughout the history of mankind. In earlier centuries, epidemics caused by viruses such as smallpox and poliomyelitis, have resulted in the death of large parts of the affected populations. Today these diseases are a rarity in wealthy industrialized nations, due to effective vaccines and vaccination programs [9]. Although smallpox was declared globally eradicated by the *World Health Organization* (WHO) on 8 May 1980 [10], there are still many other infectious diseases [11] which constitute a serious health threat in some developing countries.

Unfortunately, the extensive use of antibiotics in health-care and agriculture has led to the appearance of resistant strains. Bacterial species can develop

resistance through several mechanisms, including antibiotic inactivation, target modification, efflux pumps and spontaneous mutation. The development of antibiotic resistance can take as little as one year, after the introduction of a new antimicrobial agent [12]. To put this evolutionary pace into perspective, humans have acquired 2% difference in genome sequence in about 8 million years, the same amount that poliovirus manage in five days [9]. This rapid evolution is a result of several factors which together encourage genetic adaption by destroying pathogens that fail to change:

- Rapid genetic replication of the pathogen.
- The ability to horizontally transfer genes even between different species.
- Selective pressure by the host's adaptive immune system.
- Human application of antibiotics.

In 1941, penicillin G had an effect on virtually all strains of *Staphylococcus aureus*. Three years later, by the end of 1944 the *S. aureus* was capable of braking the structure of penicillin by means of β-lactamase [13]. By 1992 in excess of 95% of *S. aureus* were resistant to penicillin, ampicillin, and the antipseudomonal penicillins. As a result of increasing resistance, the pharmaceutical industry synthesized methicillin, a semisynthetic penicillin. The emergence of methicillin-resistant *Staphulococcus aurerus* (MRSA) has lead to increased use of vancomycin, being the only agent effective against these bacteria. The increased use of vancomycin, has in turn lead to vancomycin-resistance in other species such as *Enterococcus faecium* (VRE). MRSA and VRE are both examples of pathogens that have developed multi-resistance. Today, the new discovery of natural antimicrobial agents is rare. Although the novel semisynthetic compounds have extended the useful life of several classes of antibiotics, the approach of chemical modifications of antibiotics is not a permanent solution [8]. To slow the evolution of antibiotic resistant bacteria, measures must be taken to reduce unnecessary use of antibiotics in health-care and agriculture, and also to avoid dumping of antibiotics into the environment.

1.2 Antimicrobial Peptides

Antimicrobial peptides (AMPs) are essential components of the host defense against infections in virtually every life form, ranging from fungi and plants to

insects and animals. In animals, AMPs are mostly found in tissues and organs such as the skin, the respiratory tract, the intestines, as well as in neutrophilic leukocytes [14]. These are all areas frequently exposed to pathogens. Thus, AMPs are believed to be part of the innate immune system as the first line of defense against a variety of invading microbes. AMPs were first discovered in 1939 when Dubos [15] extracted an antimicrobial agent from a soil *Bacillus* strain. It showed to be bactericidal and capable of lyzing the living cells of several Gram-positive microbial species (e.g. *S. pneumoniae*). Since then a variety of AMPs has been discovered in various organisms [16, 17, 14, 18]. One of these is defensin, which is the first reported AMP with an animal-origin [19]. It is a typical bactericidal peptide, which in humans are known as α-defensins [20]. It has been established that collectively, AMPs and structurally related peptides also possess functions distinct from this broad-spectrum antimicrobial activity. These include antiviral, antiparasite and antitumor qualities as well as realization of roles in inflammation, immunity, wound healing and fertility. Thus, the term antimicrobial is only kept in use because it was the first-described and the most prevalent attribute of AMPs [21, 22, 20].

As of 2013 more than 5000 AMPs have been discovered or synthesized and various databases [23, 24] have been developed to keep track of them. Naturally occurring AMPs range from 12 to over 100 amino acids [25]. They are classified according to the source organisms, biological activity, peptide features (charge, length, hydrophobic residue content, chemical modifications and three-dimensional structure), binding targets (membranes and non-membranes), and mechanism of action of the peptides. The broad spectrum of activities these peptides have, and also the occurrence of several different variants in one species, has led to the suggestion that the evolution of antimicrobial peptides is driven by the variety of microbes that at all time threatens a particular organism [21].

Since their discovery, researchers have been hopeful that AMPs can be part of a solution for the problem of antibiotic resistant bacteria [20]. Antimicrobial peptides apparent ability to elicit very low bacterial resistance makes them promising candidates to replace current antibiotic therapies. However, should AMP-resistant strains appear, it would be a great threat to public health considering AMPs being a part of the innate immune system of virtually all organisms [21].

1.2.1 Antibacterial Peptides

As of 2014, antibacterial AMPs are the most studied AMPs. Most of them are cationic under physiological conditions with an amphipathic structure. This is due to spatial segregation of hydrophobic and cationic amino acid residues [21]. One factor that is believed to be essential for the selectivity of AMPs towards bacterial cells over eucaryotic cells is the interaction with negatively charged components of the cytoplasmic membrane of bacteria. The interaction mechanisms leading to cell lysis is mainly divided in two groups. The first group of AMPs translocate across the membrane and inhibits important pathways inside the cell such as DNA replication and protein synthesis [1]. The second group interacts directly with the membrane, increasing permeability to ions and solutes by formation of transient channels or dissolution of the membrane. There are several suggested models for the exact mechanism leading to cell death by the AMPs in the second group. Some of these are illustrated in Figure 1.1. The barrel-stave model suggests that the peptides aggregate on the membrane surface and then insert into the membrane bilayer, aligning hydrophobic peptides with the lipid core region. In the carpet model, the peptides orients parallel to the membrane surface forming an extensive carpet which leads to membrane disruption in a detergent-like manner. In the toroidal model the attached peptides aggregate and induce the lipids in each monolayer to bend continuously through the pore. The peptides are aligned in between the lipids with their hydrophobic regions interacting with the lipid bilayer core and their hydrophilic regions interacting with the lipid head groups as well as the water [1]. A common feature to these models is the need of a certain threshold concentration of peptides for the insertion or disruption to occur. The concentration can be given as a peptide:lipid ratio or the minimum inhibitory concentration (MIC), which is the lowest concentration of an antimicrobial that will inhibit the visible growth of a microorganism after overnight incubation.

1.2.2 Short Antimicrobial Peptides

Cationic antimicrobial peptides (CAPs) occurring in nature are defined as short peptides (10-50 amino acids). They are either gene-encoded or derived from precursor peptides through one or more proteolytic activation steps. There is an increased interest in the pharmacological application of antimicrobial peptides to treat infections, but unfavorable properties like poor therapeutic index, toxicity and lability to proteases, creating potentially un-

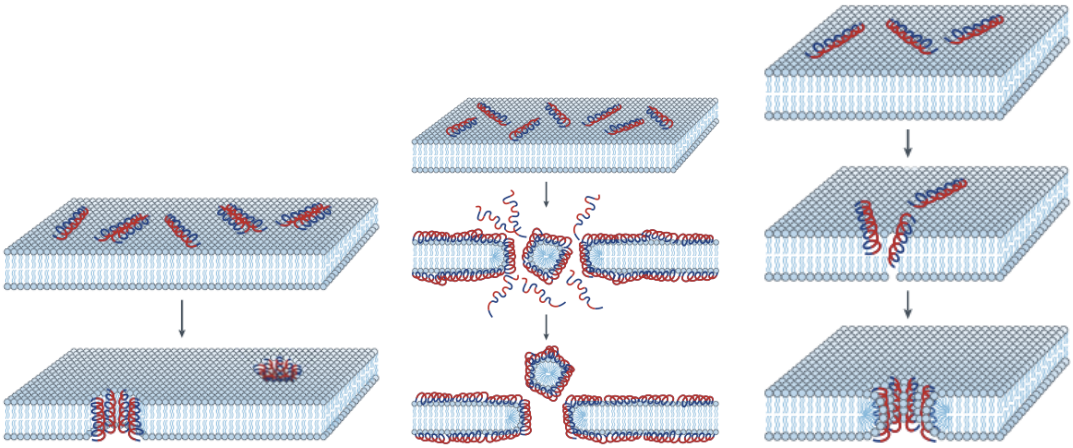

Figure 1.1: *Starting from left, the barrel-stave, carpet and toroidal models show peptide interactions with a membrane model. Figures are adapted from Brogden [1].*

favorable pharmacokinetics are issues that must be addressed [26, 27]. The largest issue, however, is the high cost of manufacturing peptides. To overcome these problems, researchers have tried to develop minimalistic mimics of CAPs using as few as two or three amino acids, while retaining the basic features of membrane-active natural CAPs such as cationic charge and amphipathic structures [28]. Synthetic and modified AMP studies have showed that small modifications can change the characteristic of the peptides significantly. However, predicting the result of these changes is a challenging task, and a deeper knowledge regarding the physiochemical properties of AMPs is necessary to fully understand the effect of structural modifications. The increasing number of computational studies in the field can help focus experimental work which can eventually verify the modes of action of these AMPs [22, 29].

The two tripeptide models used in this study (Figure 1.2) are active antimicrobial tripeptides with stability towards chymotryptic degradation. The stability towards chymotryptic degradation was examined in a previous study [26, 30, 31] where introduction of hydrophobic C-terminal amide modifications and bulky synthetic side chains on the central amino acid showed to be an effective way of increasing the half-life time. The tripeptides in these studies were based on the general scaffold Arg-X-Arg-NHBn (R-X-R-NHBn) shown in Figure 1.3, where "X" represents a non-natural bulky amino acid side chain.

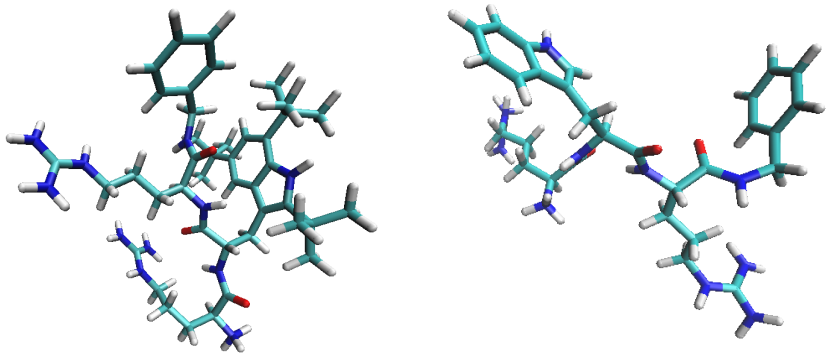

(a) (b)

Figure 1.2: *The tripeptides RTbtR-NHBn (a) and RWR-NHBn (b) used in this study.*

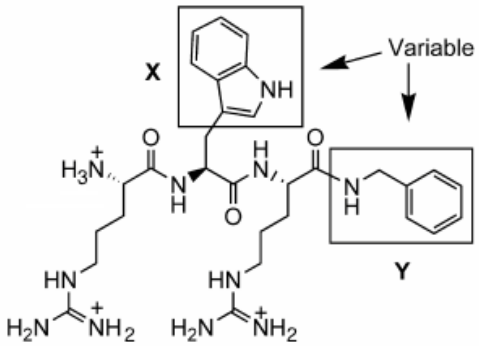

Figure 1.3: *General scaffold RWR-NHBn, with the two different groups X and Y which were subject to modifications.*

In the RTbtR-NHBn the central tryptophan is modified by adding three *tert*-butyl side chains (Tbt), whereas the RWR-NHBn only has the C-terminal modification with the benzylamide. Thus, both peptides has two hydrophobic elements and three cationic charges.

1.3 Cell Membranes

Biological membranes are complex dynamical structures which are essential components of cells and their organelles. They mainly consist of amphiphilic

lipids which self-assemble due to the hydrophobic effect and thus form two leaflets, into which proteins are embedded (Figure 1.4).

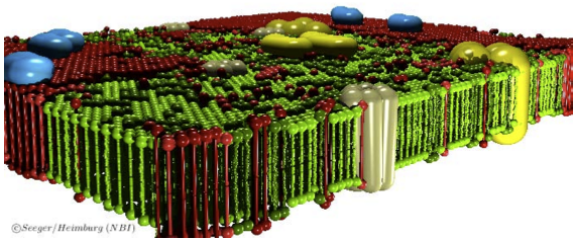

Figure 1.4: *A schematic representation illustrating the compounds of a biological membrane. It is composed of lipids with different physical properties partly organized in domains, and various inserted proteins. Figure adapted from Heimburg [2].*

In eukaryotic cells the membrane separates the various cellular compartments from their respective external environments, a structure which enables segregation of specific chemical reactions, leading to increased biochemical efficiency. The semipermeable nature of cellular membranes allow the passage of small molecules like nutrients and waters. The lipids of biological membranes can exist in multiple possible phase states, which affects properties like thickness of the membrane, area per lipid and translational diffusion of lipids. Studies of synthetic membranes have shown that the adopted phase depends on lipid structure such as acyl chain length and saturation. The lipids in these studies have also shown different dependencies of temperature variation resulting in different phase characteristics [32]. Considering the fact that biological membranes contains a great variety of different lipids, the idea that different regions might adopt various fluid and solid phases is not inconceivable. In fact, coexisting phases has been shown to occur in studies of the phase behavior of artificial membranes [33]. The fluid phase (L_α) is still the most biological relevant, and it has to be precisely regulated for the function of enzymes and efficient rearrangement of of lipids between momolayers and lateral in one monolayer [9]. Thus, the lipid composition greatly affects the overall structure of the biological membranes, which in turn might influence the distribution and function of proteins embedded in the membrane, as well as interactions with proteins and peptides in the extra- and intracellular environment [34, 2].

1.3.1 Eukaryotic Cell Membranes

About 50% of the mass in most mammalian cell membranes are lipid molecules, while the remaining is mainly proteins. In addition to lipids and proteins, the lipid bilayers contain sterols like cholesterol (phytosterols in plants). Eukaryotic cells in general invest substantial resources in generating different lipids and contains more than 1000 different species. This is possible due to variation in headgroups and aliphatic chains. The major structural lipid in eukariotic membranes are glycerophospholibids, such as phosphatidylcholine (PC), phosphatidylethanolamine (PE), and phosphatidylserine (PS) (Figure 1.5) [3, 34]. However, the distribution of phospholipids and sterols differs throughout the main organelles of mammals and yeast, and the actual synthesis of lipids is geographically restricted. The plasma membrane has a majority of the glycerophospholibid phosphatidylcholine, and the PE lipids in these membranes are located in the inner leaflet. In addition it is enriched in sphingolipids (e.g. glycolipids and sphingomyelin) and sterols (e.g. cholesterol), which are packed more densely than glycerolipids [34]. The ratio of cholesterol:phospholipid can be as high as 1:1. The cholesterol makes the lipid bilayer less deformable in the region of insertion, and thereby decreases the permeability to small water-soluble molecules. The distribution of lipid species is not homologous between the monolayers of the plasma membrane.

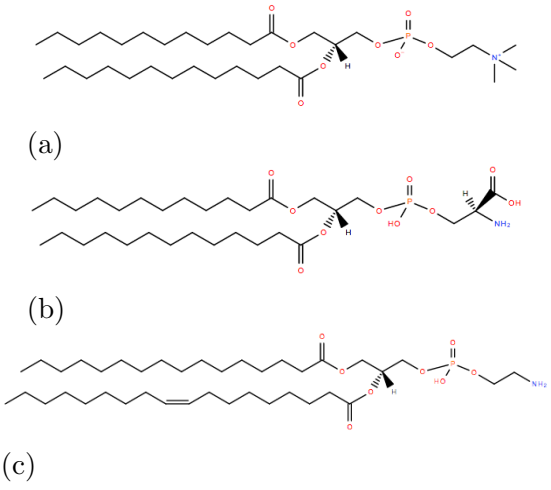

Figure 1.5: *Examples of glycerophospholibids; 1-dodecanoyl-2-tridecanoyl-sn-glycero-3-phosphocholine (a), 1-dodecanoyl-2-tridecanoyl-sn-glycero-3-phosphoserine(b), 1-hexadecanoyl-2-(9Z-octadecenoyl)-sn-glycero-3-phosphoethanolamine(c). Figures are adapted from the LIPID MAPS database [3].*

Glycolipids are sugar-containing lipids found exclusively in the noncytosolic monolayer of the lipid bilayer, where they generally constitutes about 5% of the lipids. The function of these lipids are thought to be many, ranging from protecting the membrane, signaling, and partition i lipid rafts giving favorable environment for certain proteins [9].

1.3.2 Prokaryotic Cell Membrane

In contrast to the plasma membrane of most eukaryotic cells, the prokarytic plasma membranes are often composed of mainly one type of phospholipid [9]. For bacterial membranes this phospholipid is to a large extend phosphatidylethanolamine (PE) (Figure 1.5c). The remaining lipids are usually negatively charged at physiological conditions, where phosphatidylglycerol (PG), or PG derivatives such as diphosphatidylglycerol (DPG) or cardiolipin (CL) are predominant [35, 36, 37]. Furthermore, the lipid composition also depends on whether the bacterium belongs to the class of *Gram-negative* or *Gram-positive* bacteria (Figure 1.6).

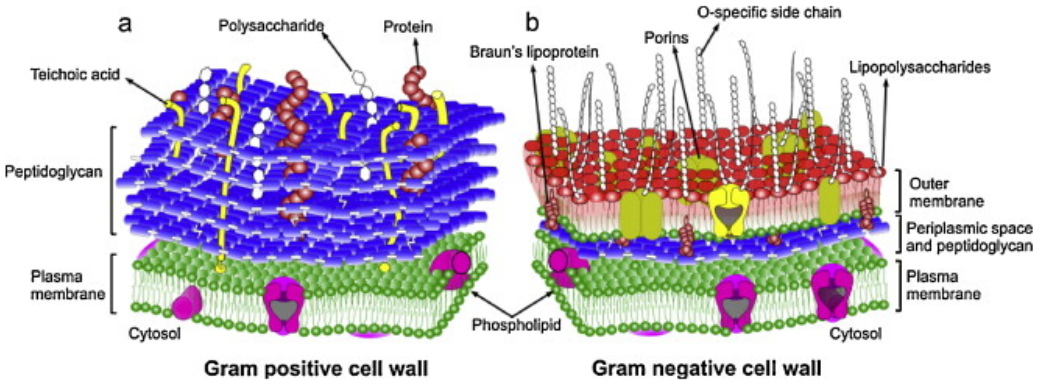

Figure 1.6: *Schematic representation of the cell membranes of Gram-positive (a) and Gram-negative (b) bacteria. Figure adapted from Tripathi et al. [4].*

The plasma membrane of mammalian cells are built for stability through lipid composition and high content of sterols. The bacterial membrane lacks sterols and has adopted other means of strengthening their structure. Bacteria with single membranes are called *Gram-positive*, they have a thick peptidoglycan layer with attached proteins and different glycopolymers like polysaccharides and teichoic acids [38]. The layer encases their cytoplasmic cell membrane and takes up the crystal violet stain used in the Gram staining method,

hence the name. In *Gram-negative* bacteria, the cytoplasmic membrane is surrounded by a thin peptidoglycan layer overlayed by an asymmetrical bilayer of phospholipids and lipopolysaccharides containing membrane proteins such as porins [4]. In general, higher amounts of PE lipids are found in the membranes of Gram-negative bacteria, while the cytoplasmic membrane of Gram-positive bacteria are rich in PG lipids. The lipids composition of various Gram-negative and Gram-positive bacteria are given in Table 1.1.

Table 1.1: *The lipid composition of various Gram-negative and Gram-positive bacteria.*

Bacterial species	Lipid composition (%)		
	PE[a]	PG[b]	CL[c]
Gram-positive			
B. polymyxa	60^{α}	3^{α}	8^{α}
B. cereus	43^{α}	40^{α}	17^{α}
B. subtilis	12^{β}	70^{β}	4^{β}
E. faecalis	- $^{\alpha}$	27^{α}	19^{α}
S. epidermis	- $^{\alpha}$	90^{α}	1^{α}
S. aureus	- $^{\alpha}$	57^{α}	19^{α}
MRSA	- $^{\alpha}$	57^{α}	19^{α}
Gram-negative			
E. coli	$85^{\alpha}79^{\gamma}$	$15^{\alpha}17^{\gamma}$	$5^{\alpha}4^{\gamma}$
K. pneumoniae	82^{α}	5^{α}	6^{α}
P. aeruginosa	60^{α}	21^{α}	11^{α}

[α] Adapted from Epand et al. [35]; [β] Adapted from Clejan et al.[39]; [γ] Adapted from Morein et al.[40], the values are for inner and outer membrane together, only inner membrane has lipid composition of 75, 19, 6 respectively.
[a] Phosphatidylethanolamine; [b] Phosphatidylglycerol; [c] Cardiolipin

Bacteria has the ability to adapt to their environment by adjusting their fatty acid composition to maintain the fluidity of their membranes [9]. Thus, the lipid composition might be slightly different at different growth conditions.

1.3.3 Membrane Electrostatics

Electrostatic interactions have an important role in many biological processes. Biological membranes carry numerous ionized and polar groups,

which either are part of the lipid, glycolipid, inserted protein, or other charged molecules absorbed onto the membrane surface. The electrostatic effects of all these groups influence the conformation and function of molecules involved in signaling and transport, as well as the actual structure and stability of the membrane. The net charge of biological membranes are slightly negative in most cases, due to that the membrane proteins and the native lipids have isoelectric points below neutral pH [41, 42]. The charged groups are not uniformly distributed throughout the membrane surface, which in turn leads to different orientation of water dipoles in the membrane water interface region. The charged headgroups also influence the concentration of ions in the region. Thus, the electrical potential (Ψ, surface potential) which exists due to structural charges will differ at any point across a cell membrane. In addition to the surface potential the total electric potential of a membrane is made up of the transmembrane potential ($\Delta\Psi$, due to gradients in ion concentrations across the membrane) and the dipole potential (Ψ_D). The latter arises from the alignment of dipolar lipid headgroups and water dipoles in the interface region between the hydrophobic membrane interior and the aqueous phase [43]. Charges on membrane surface or transmembrane ion concentration gradients creates electric fields. These electric fields in the membrane-solution interface act on, and depends upon, the distribution of ions in the region. The fields also regulate the absorption and binding of charged species to the membrane surface [42].

In Gouy-Chapman electrostatic theory the ion concentration within a finite distance of the membrane (Debye length) differs from the bulk, and this finite zone is called the ionic diffuse double-layer. The ionic charge within the double-layer is deduced to be identical in size but opposite in sign to the membrane. The Gouy-Chapman approximation is a model often used to describe phenomena at the interface of charged membranes submerged into ionic solutions [41, 32]. Due to the complexity of membrane surfaces, no existing model can give a complete description of them. Thus, one have to choose which variables and quantities that are of interest before choosing a model to compare with. In the Gouy-Chapman approximation all charges are confined to an infinitely narrow plane and the ion distribution is governed by Coulombic forces [42]. These approximations might not be appropriate for all cases, in particular when considering phenomena which arise due to polarizing effects. In the field of molecular modeling, the development of sufficient polarizable force fields is an ongoing task [44]. The first membrane simulation in salt solution using a polarizable force fields was performed by Vácha et al. [45], where they found that the adsorption properties of anions follows the Hofmeister series [46].

1.4 Molecular Modeling

Molecular modeling is the common term used to describe any theoretical method or computational technique that provides understanding and ability to predict the the behavior of a molecular system. There are different approaches to how a system can be modeled. In the *quantum mechanical model* the nucleus is considered a positive charge with a cloud of negative electrons around it. It is a model applying quantum physics and mathematical equations to describe how the molecule is held together by attractive and repulsive forces among the charges. In the *force field model* the system is considered as atoms and bonds moving in a classical mechanical sense, as "balls" attached by "springs" creating a harmonic potential. The electrons are not considered in this model, which makes the calculations less time-consuming. The force field model can therefore be used on larger system such as biological membranes, where the quantum mechanical model is computationally intractable. Molecular modeling has become an important tool, which gives a unique perspective of atomic level (or electron) interactions and processes in complex biological systems. It provides an opportunity to compare many different configurations in a system and thus reduce costs in the experimental setup.

1.4.1 Force Field

Force field methods relies on simple functional forms and sets of parameters empirically adjusted to reproduce the experimental or quantum chemical properties of molecules. The energy of a system is calculated as a function of the nuclear positions - positions that have occurred due to the intra- and inter-molecular forces acting within the system. The force field parameters describing the system are bond stretching, angle bending, bond rotation, electrostatic and van der Waals forces. Energetic penalties in this force field are associated with the deviation of bonds and angles from their ideal values [47]. A basic functional form of the total potential energy U_{total}, is given by:

$$U_{total} = U_{bond} + U_{angle} + U_{dihedral} + U_{non-bonded} \tag{1.1}$$

The sum of the three first terms in equation 1.1 make up the bonded interactions:

$$U(r^N)_{bonded} = \sum_{bonds} \frac{k_i}{2}(l_i - l_{i,0})^2 + \sum_{angles} \frac{k_i}{2}(\theta_i - \theta_{i,0})^2 + \sum_{torsions} \frac{V_n}{2}(1 + \cos(n\omega - \gamma)) \tag{1.2}$$

Where $U(r^N)$ is the potential energy of N atoms, as a function of position r. The first terms in equation 1.2 represents all the bonds between a pair of covalently bonded atoms in the molecule. This is modeled by Hooke's law which is an harmonic potential. Thus, there will be an increase in energy as the bond length l_i deviates from the reference values $l_{i,0}$. A true bond-stretching potential in a "real" molecule would not be harmonic due to vibrational motion. This means that the average length of the bond in a vibrating molecule will deviate from the equilibrium value for the hypothetical motionless state [47]. Hooke's law, however, gives a good approximation for the small oscillations in covalent bonds. k_i is the force constant.

The second term, also modeled by a harmonic potential, reflects the deviation of the valence angle θ_i from a specific reference values $\theta_{i,0}$. The contribution of each angle is characterized by a specific force constant k_i. Less energy is required to distort an angle away from equilibrium than to stretch or compress a bond, thus the force constant is proportionately smaller.

The third term in equation 1.2 represents the torsional potential, which models the energy change caused by rotation of bonds. In this term, ω is the dihedral angle, V_n is the force constant referring to the "barrier height", n refers to the multiplicity- number of minimum points as the function is rotated 360°, and γ is the phase factor which determines where the torsion angle passes through its minimum value. Most of the variation in structure and relative energies are a result of the interplay between the torsional and non-bonded contributions. As the bond rotates the conformation passes through minimum-energy in staggered structure and maximum-energy in eclipsed structure.

Some force fields, like MM2, uses more than one term to describe each torsion. This is to take into account the effects of hyperconjugation in alkanes, conjugation in alkenes and steric interactions between 1-4 atoms. To achieve the desired planar geometry in e.g. aromatic rings, an *out-of-plan* bending term is applied. This term can be added to the force field in several ways but the definition of "improper" torsion is widely used. This is because it can easily be included with the "proper" torsional terms in the force field, its functional form being $\nu(\omega) = k(1 - \cos 2\omega)$ [47]. Cross terms of the various

contributions in the force field should be included to achieve good performance. Most cross terms are functions of two internal coordinates and the ones that are found to be necessary in order to reproduce structural properties accurately are; bond-bond, bond-angle, angle-angle, bond-torsion and angle-torsion.

The last two terms in equation 1.1 make up the non-bonded interactions:

$$U(r^N)_{non-bonded} = \sum_{i=1}^{N} \sum_{j=i+1}^{N} \left(4\varepsilon_{ij} \left[\left(\frac{\sigma_{ij}}{r_{ij}} \right)^{12} - \left(\frac{\sigma_{ij}}{r_{ij}} \right)^{6} \right] + \frac{q_i q_j}{4\pi\varepsilon_0 r_{ij}} \right) \quad (1.3)$$

There are two non-bonded terms contributing to the total potential energy. Coulomb potential, which often is used to models the electrostatic interactions and Lennared-Jones potential which models van der Waals interactions (vdW). These term are given in equation 1.3. The electrostatic properties of a molecule is determined by the distribution of fractional point charges q for all atoms i and j throughout the molecule. The charge distribution occurring is a result of the difference in electronegativity of the elements. When using Coulomb's law, the electrostatic interactions between two molecules are calculated as a sum of interactions between pairs of point charges $q_i q_j$. ϵ_0 is the permittivity of free space and r_{ij} is the inter-atomic distance.

The van der Waals interactions are a combination of attractive and repulsive forces. The attractive contribution is due to dispersive forces, which occur as a result of instantaneous dipoles arising during fluctuations in the electron clouds. The repulsive contribution can be understood in term of the Pauli principle, which prohibits any two electrons in a system having the same set of quantum numbers [47]. The interaction is a result of electrons having the same spin occuring in overlapping orbitals. The effect of this interactions is to reduce the electrostatic repulsion between pairs of electrons by forbidding them to occupy the same region of space, resulting in repulsion between nuclei due to the reduced electron density in the internuclear region. Thus the attractive forces are said to be long-range whereas the repulsive forces act at short distances. The Lennard-Jones 12-6 potential in equation 1.3 describes these interactions. The attractive forces varies as r^{-6} and the repulsive forces varies as r^{-12}. r_{ij} is the separation of atom i and j. σ_{ij} is the collision diameter and ε_{ij} is the minimum potential energy of interaction for the two interacting species at the ideal radius of separation.

1.4.2 Concepts of Statistical mechanics

Statistical mechanics can be thought of as a branch of physics which tries to explain the laws of thermodynamics from the mechanical properties of collections of molecules. Through a probabilistic description it provides the link between the microscopic properties of matter and its bulk properties. Consider a system of N particles. Each particle will at any given time have a momentum $\mathbf{p}^N$ and occupy a position $\mathbf{r}^N$ of a uniquely defined state $\mathbf{p}^N\mathbf{r}^N$ in a 6N-dimensional phase space. A phase space trajectory visiting all the states on an energy surface having a probability of existence, give the true properties of a system at thermodynamic equilibrium. Thus, summing the Boltzmann factor $e^{(-E/k_BT)}$, of each state, gives the partition function:

$$q = \sum_{i=1}^{N} e^{(-E_i/k_BT)} \tag{1.4}$$

where E is the state energy and k_BT is the product of Boltzmann's constant and thermodynamic temperature. When the partition function is used to normalize the average energy of a system, the probability density of the system follows the Boltzmann distribution:

$$\rho(\mathbf{p}^N, \mathbf{r}^N) = \frac{e^{(-E(\mathbf{p}^N,\mathbf{r}^N)/k_BT)}}{q} \tag{1.5}$$

where any two microstates with the same energy would have the same probability of existence. An *ergodic* phase space trajectory of all microstates is not achievable, due to the sampling time which would reach infinity. However, a *time average* of a property equals the *ensemble average* of that property at equilibrium. Simulation techniques such as molecular dynamics (MD) produces a time average of a system with a manageable number of atoms and molecules. By applying statistical mechanics the time average can be replaced by an ensemble average. The ensemble average, or expectation value, of a given macroscopic property can then be given as:

$$\langle A \rangle = \iint d\mathbf{p}^N d\mathbf{r}^N A(\mathbf{p}^N, \mathbf{r}^N)\rho(\mathbf{p}^N, \mathbf{r}^N) \tag{1.6}$$

which is the multidimensional integral over all the 6N microstates of the N particles weighted by their probabilities. $\mathrm{A}(\mathbf{p}^N(t), \mathbf{r}^N(t))$ is the instantaneous

value of property A. The ensemble average of property A is determined by integrating over all possible configurations of the system. Since the members of the ensemble follows the Boltzmann distribution, an estimate of the thermodynamic properties is possible [47].

1.4.3 Molecular Dynamics

Molecular dynamics (MD) is a sampling method, generating states in phase space that are connected in time. The states of the system are sampled as atoms are moved to new positions accordingly to the forces acting upon them. Knowledge of the systems potential energy function and Newton's laws of motion allows the calculation of these forces and movements. Newton's laws of motion are empirically justified and makes up the foundation of classical dynamics[47]. They state the following:

1. A particle stays in its condition of rest or continues to move in a straight line at constant velocity unless an external force $\sum \mathbf{F}$ acts upon it.

$$\sum \mathbf{F} = 0 \Rightarrow \frac{d\mathbf{v}}{dt} = 0 \tag{1.7}$$

   where $\mathbf{v}$ is the velocity of the of the particle.

2. The net force acting on a particle is equal to the rate of change of its linear momentum.

$$\sum \mathbf{F} = \frac{d\mathbf{p}}{dt} = m\frac{d\mathbf{v}}{dt} \tag{1.8}$$

   where $\mathbf{p}$ is the momentum of the of the particle.

3. To every force, there is an equal and opposite directed counterforce.

$$\mathbf{F}_{AB} = -\mathbf{F}_{BA} \tag{1.9}$$

Because of the deterministic nature of Newton's laws, this information is sufficient to generate a trajectory of the simulated system over time, when starting from a well prepared configuration. The total energy of the system is conserved by the application of Newton's laws, thus MD simulations naturally

form the NVE ensemble. Algorithms that connect the system to a thermostat or barostat allow the sampling of the NVT or NPT ensemble [47].

The first MD simulations (e.g. Alder and Wainwright 1957 [48]) were performed using very simple potentials, such as the hard-sphere potential. In the hard-sphere model there is no force between particles until they collide. The collisions are perfectly elastic and the particle velocities after the collision are calculated according to the principle of conservation of linear momentum. Today algorithms use a continuous potential, where the force between two atoms or molecules changes continuously with their separation (e.g. Lennard-Jones potential). This is a more realistic way of calculating the potential, but since the motion of all particles are coupled together, the equations can not be solved analytically[47]. As an alternative, the finite difference method can be used to integrate the equations of motion. The essential idea of this method is to break down the integrations into very small time steps δt. The total force acting on a particle at time t is calculated as the vector sum of its interactions with other particles. From the forces the acceleration can be determined by applying Newton's second law (equation 1.8). The positions and velocities at time $t + \delta t$ can then be calculated combining the acceleration with positions and velocities at time t. The force is assumed to be constant during a time step. The algorithms using the finite difference method also assume that the positions and dynamic properties can be approximated as Taylor series expansions:

$$\mathbf{r}(t+\delta t) = \mathbf{r}(t) + \delta t\mathbf{v}(t) + \frac{1}{2}\delta t^2\mathbf{a}(t) + \frac{1}{6}\delta t^3\mathbf{b}(t) + \frac{1}{24}\delta t^4\mathbf{c}(t) + \cdots \quad (1.10)$$

$$\mathbf{v}(t+\delta t) = \mathbf{v}(t) + \delta t\mathbf{a}(t) + \frac{1}{2}\delta t^2\mathbf{b}(t) + \frac{1}{6}\delta t^3\mathbf{c}(t) + \cdots \quad (1.11)$$

$$\mathbf{a}(t+\delta t) = \mathbf{a}(t) + \delta t\mathbf{b}(t) + \frac{1}{2}\delta t^2\mathbf{c}(t) + \cdots \quad (1.12)$$

$$\mathbf{b}(t+\delta t) = \mathbf{b}(t) + \delta t\mathbf{c}(t) + \cdots \quad (1.13)$$

The choice of time step is important to avoid an overlap of high energies as atoms get too close, or an inefficient sampling of phase space if the time step is too large. A rule of thumb is to have a time step approximately one-tenth of the shortest period of motion. In a biological system this is the stretching of a C-H bond, vibrating with a repeat period of $\sim$10 fs. Thus a time step of 1 fs would be appropriate. It is often necessary to constrain many degrees of freedom to achieve a more efficient sampling. Algorithms such as the SHAKE method applies such constrains without affecting the general motion of the

molecule[49, 47]

1.4.4 Modeling of Lipid Bilayers

Model membranes used in experiments to mimic natural systems are often pure component membranes or have only a few components. This makes it easier to precisely control the environment of the membrane constituents and their properties. The study of pure component membranes can still help understand basic biological membrane functions, its interaction with the environment and mechanisms of protein insertion. However, the detailed structure of a bilayer that is in the biological relevant fluid (L_α) phase, is not possible to obtain experimentally. The fluctuation of fluid phase bilayer results in many equally correct structures, and the right way to represent them all are through a statistical distribution function of the constituents [50]. Molecular modeling can help to guide the interpretation of experimental results since the level of detail is much greater than what can be obtained experimentally. The reliability of simulations, on the other hand, must be evaluated against existing experimental data. There are several techniques which to a certain degree complement each other, that can give information of properties such as area per lipid, bilayer thickness and acyl chain order parameters. The latter is obtained from deuterium NMR quadrupole splitting [51]. The electron density profiles (z-coordinates) obtained from x-ray diffraction data of the L_α phase bilayers, can only give a measure of the location of the phosphate groups, which in turn gives an indication of the bilayer thickness. In addition to uncertainty regarding detailed interactions in a lipid bilayer there is some scatter in literature values of known parameters, due to different ways of calculating them from data sets [50].

The lack of detailed experimental data is reflected in molecular modeling of lipid bilayers, in terms of force field parameterization. High level *ab initio* calculations which are required for force field parametrization, presently (as of 2009) only allows evaluation of 10-12 heavy atoms at the time to gain accurate results. In addition, there are limitations in low-level QM calculations with respect to London's dispersion interactions for small clusters of molecules. Thus, QM methods and resulting data can not be used alone in parametrization [44]. Thermodynamic properties deduced from experiments are fitted to the QM minimum energies of small components at different stages of the parametrization to better mimic the ensemble of molecules. The lack of experimental data for lipid properties and also mixtures of lipids

thus creates challenges in the field [52].

Chapter 2

Methods

2.1 Preparation of Lipid Bilayers

Seven fully hydrated lipid bilayers were constructed using the CHARMM-GUI[53]. All systems are given in Table 2.1, with the right number and distribution of ions and water molecules. Three systems contained 336 zwitterionic DMPC lipids of which one system had no ions and two systems had an ionic strength of 154 mM using either NaCl or KCl. Two systems contained 336 anionic DMPG lipids with either K^+ or Na^+ as counter-ions. Finally, two mixed systems with 140 DMPC lipids and 196 DMPG lipids each with either K^+ or Na^+ as counter-ions. Each of the DMPG and mixed bilayers were also prepared with an ionic strength of 154 mM corresponding to physiological conditions. The preparations were done using the graphical program Visual Molecular Dynamics (VMD) [54] by assigning water and ions to the lipid bilayers obtained from CHARMM-GUI. In addition to the above mentioned systems, the three different lipid bilayers were prepared in aqueous solution containing a random distribution of the ions Na^+, K^+ and Cl^-.

2.2 Simulation Details

The CHARMM36 All-Hydrogen Lipid Parameters[52] were used for the lipids in this study. The water was modeled using the TIP3P model (W.L. Jorgensen et al.). The ions were employed the parameters developed by Noskov and Roux [55], which includes non-bond pairwise exceptions for the Na^+ and

Table 2.1: *The systems generated with charmm-gui and further ten systems which were rebuild containing different compositions of ions. All systems with ions in addition to counter-ions has an ionic strength of 154 mM.*

Lipid System	Na^+	K^+	Cl^-	number of water[c] molecules
DMPC				13144
DMPC	39		39	13120
DMPC		39	39	13135
DMPC	27	27	54	18471
DMPG[a]	336			13754
DMPG[a]		336		13761
DMPG	393		57	19738
DMPG		393	57	19397
DMPG	194	196	55	18759
MIX[ab]	196			13538
MIX[ab]		196		13297
MIX[b]	252		56	19029
MIX[b]		252	56	19029
MIX[b]	126	126	56	19029

[a] *Counter-ions only;* [b] *Mixed DMPC/DMPG lipid bilayer (70/98 per leaflet);* [c] *The recommended water model to use with CHARMM parameters is TIP3P [44], which was applied to all systems.*

Cl^- ion pair from Lou and Roux [56]. Exceptions can be applied to any pair of atoms and are donated the keyword NBFIX in CHARMM force fields. The incorporated NBFIX terms for Na^+ ions interaction with carbonyl ester and phosphate ester oxygens developed by R. M. Venable et al. [57] were also applied. The NAMD software package was used for the MD simulations [58], which were performed under periodic boundary conditions in the NpT ensemble.

The equilibration process of the lipid bilayers were divided into six stages followed by a last production run. The first three stages consisted of 25000 simulation steps (time step; 1fs) each, followed by three stages of 100000 simulation steps (time step; 2fs) each. Evaluation of the bonded interactions, the short-range non-bonded interactions and long-range electrostatics was done every step. The cutoff distance for the short-range interactions (i.e. van der Waals and electrostatics) was 12.0 Å using a switching function

starting at 10 Å. The bilayer was oriented in the x-y plane with geometrical center set to zero for the z-coordinate. During the first six stages velocities' were reassigned every 500 steps and the applied force keeping the atoms in the upper head groups at a constant distance (17 Å) from the z-center was gradually removed. The dihedral restraints were also gradual removed. The 500000 step (time steps; 2fs) production run was unconstrained. The total equilibration time was 1175 ps.

The following settings applies for the 110 ns calibration of the lipid bilayers as well as the MD simulations of the lipid bilayer systems also containing peptides. A target pressure of 1 atm was imposed using the Langevin piston method[59], with a oscillation period of 100 fs and damping timescale of 50 fs. Langevin dynamics was used to control the temperature at the physiological temperature 310 K, with a damping coefficient of 1 ps^{-1}. The Particle Mesh Ewald (PME) method was used for computation of the long-range electrostatic forces [60] with a grid density of approximately 1 Å and a six-order interpolation of the charges to the grid. The geometry of the TIP3 water molecules was constrained using the SHAKE algorithm [49]. The bonded forces were evaluated every 1 fs, short-range nonbonded forces every 2 fs, and long-range electrostatics every 4 fs. A smooth cutoff was used between 8 and 10 Å.

2.3 Peptide Topology and Parameters

The topology and parameters for the two tripeptides were generated using the automatic CGenFF program ParamChem [61]. The atomic charges in the generated topology files were manually examined and compared to charges of similar residues in the CHARMM36 All-Hydrogen Topology File for Proteins [5]. For the RTbtRNH-MtPh peptide the charges differed from those applying for equivalent residues in the protein topology file. This might be due to the program not recognizing the *tert*-butyl side groups in the central 2,5,7-tri(*tert*-butyl)tryptophan residue. All the charges that differed were reassigned accordingly to those given in the topology file for proteins. The *tert*-butyl side groups are attached to the atoms CD1, CZ2 and CZ3 in Figure 2.1. These atoms were given the charges of their respective equivalent merged with the charge of the equivalents attached hydrogen. Further the central carbon of the *tert*-butyl side groups was given a zero charge as for the *neopentane* in the general CGenFF topology file [61].

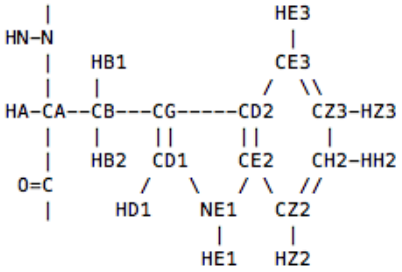

Figure 2.1: *The amino acid tryptophan with the atom types as given in the CHARMM36 All-Hydrogen Topology File for Proteins [5].*

The atomic charges in the generated topology file for the RWRNH-MtPh peptide were in agreement with the CHARMM36 Protein topology file.

2.4 Preparation of Peptide Lipid Bilayer Systems

The DMPC/DMPG mixed bilayer system with K^+ as counter ions was chosen to build the systems containing peptides. The last frame of the calibrated lipid bilayer trajectory was used, where the bilayer and all ions within 4 Å of the bilayer surface were retained. In total 6 systems were build, three containing the peptide RWR-NHBn and three with the RTbtR-NHBn peptide. Each of the three systems had a combination of 1, 4 or 8 of their respective peptide, which corresponds to a peptide:lipid ratio of 1:168, 4:168 and 8:168 at the bilayer surface facing the peptides. The peptides were placed at a distance of approximately 4 Å from the nearest atom of the lipid bilayer. The systems containing 336 lipids, a variety number of peptides and ions within 4 Å of the membrane surface were then solvated. Each simulation box had approximately 30000 water molecules. Finally all systems were neutralized by randomly replacing water molecules with counter-ions corresponding to the ion type already in the system. All the steps involving building of the systems including generating PDB and PSF files for the MD simulations were performed using the VMD program [54]. The PSF files for the peptides were not accurately generated due to to many characters in the topology files atom type column. Hence, the PSF file was manually corrected regarding the atom types of the peptides, and also regarding some missing charges in the peptides. Three MD simulations were performed for each system, initially

minimized for 10000 steps and then started with different random velocity distributions.

2.5 Analysis of the Lipid Bilayers

The time evolution of the average area per lipid, $\langle Å^2 \rangle$, was analyzed using the membrane analysis tool MEMBPLUGIN [62], which can be run within the VMD environment. The total area per lipid as well as the area per lipid of each lipid species was calculated, using the atoms C2 C21 C31 (figure 3.4) to project onto the plane delimited by the simulation box. MEMBPLUGIN uses Voronoi method [63] to calculate the areas.

Ordering of nonpolar hydrocarbon chains in lipid bilayers is typically characterized by the deuterium order parameters S_{CD}. The order parameters are easily obtained from deuterium NMR quadripole splittings [64]. The order parameters S_{CD} were calculated from the average angle θ along the last 100 ns of the simulations using a script implemented by Justin Gullingsrud []. If θ is the angle between a CD bond (carbon-deuterium bond) and the bilayer normal, the order parameters are given by:

$$S_{CD} = \frac{3}{2}\langle cos^2\theta \rangle - \frac{1}{2} \tag{2.1}$$

the angular brackets donate a time and assembly average.

The membrane thickness was calculated as the average distance between phosphate atoms using the membrane analysis tool MEMBPLUGIN [62]. The inter-facial width was calculated for each leaflet of the membrane, as the standard deviation of the distribution of phosphate atoms along the z-axis. Before doing the calculations of phosphate distribution the trajocteris were properly wrapped using the PBCTools blugin of VMD [54]. All frames were moved, yielding z = 0 at the membrane center.

2.6 Analysis of Peptide Insertion

As for the calculation of the distribution of phosphate atoms, the bilayer systems containing peptides were wrapped and all frames were moved to

obtain z = 0 at the membrane center. The z-coordinates of atoms NE1 and CH2 on the tryptophan residue (Figure 2.1) were extracted for each peptide at every frame. These atoms have the same name in the RWR-NHBn- and the RTbtR-NHBn peptides. In addition the z-coordinate of the first carbon atom in the benzyl-ring (Figure 1.3) of the C-terminal capping were extracted. The name of this atom is C76 and CG4 for RTbtR-NHBn and RWR-NHBn respectively. The positions of the atoms were then plotted as a function of simulation time in reference to the average position of phosphate atoms (Appendix D and E).

Chapter 3

Results and Discussion

3.1 Selection of Lipid Bilayers

The antimicrobial tripeptides RTbtR-NHBn and RWR-NHBn have a selectivity towards negatively charged bacterial membranes [26]. Thus, for the purpose of studying the interactions of these tripeptides with a bacteria-like membrane, a binary mixture of dimyristoylphosphatidylcholine (DMPC) and dimyristoylphosphatidylglycero (DMPG) was chosen. DMPG is an anionic lipid at physiological conditions, whereas DMPC is a zwitter-ionic lipid. They are both glycerophospholipids with two acyl chains comprising 14 carbons each (Figure 3.1).

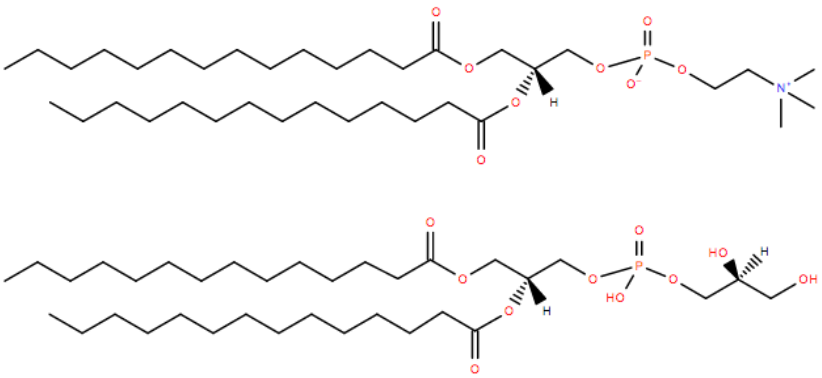

Figure 3.1: *The lipids used in this study, top, dimyristoylphosphatidylcholine (DMPC) and, bottom, dimyristoylphosphatidylglycerol (DMPG).*

In Gram-positive bacteria, such as *S.aureus* and MRSA, 57% of the cytoplasmic cell membrane consists of DMPG lipids. In other species, such as *S.epidermis*, this number can be as high as 90% [35]. Hence, the mixed lipid bilayers where built with 70 DMPC lipids and 98 DMPG lipids per leaflet, which corresponds to 58.3% DMPG lipid. There is little literature on structural properties, such as order parameters, for DMPG lipids in pure bilayers. The choice of DMPC as the zwitter-ionic component was due to the relatively large amount of experimental data available for such homogeneous lipid bilayers [65, 50]. In addition, since both lipids have fully saturated hydrocarbon chains of equal length, one might expect similar behavior of the chains upon mixing. This assumption is supported by studies of the behavior of binary mixtures of DMPC and DMPG lipids [66, 67]. To better evaluate whether the behavior of the mixed bilayers corresponds to the experimental data, homogeneous bilayers of each of the DMPC- and DMPG lipids were simulated, in addition to the binary mixture of the two. It is important to study the interactions of lipid molecules to be in a better position to explore more complex systems such as interactions between lipids and peptides and their assemblies.

Several experimental studies have examined the interactions of various monovalent cations, divalent cations and anions, with lipid bilayers. A common conclusion is that the type of ion and also the ion-concentration has an effect on physical properties of the bilayer, such as the temperature at which phase transition between the more compact gel phase (L_β) and the biological relevant [50] liquid crystalline (L_α) phase occur [68, 69, 67]. In a study of metal cations and their effect on phase behavior, Bindre *et al.* [68] found that the effect of the the ions on the phase transition is linearly correlated with the electrostatic solvation free energy of the ions in water, which in turn is inversely related to ionic radius. This study also found that monovalent ions such as Na^+ and K^+ do not differ to a great extend, but they both weakly affect the hydration of the polar interface making carbonyl groups of the POPC lipid slightly more accessible to water molecules. The POPC lipid has a phosphatidylcholine (PC) head group as the DMPC lipid in this thesis. In a study by Garcia *et al.* [69], Na^+ ions were found to have a slightly greater affinity towards the lipid surface of a phosphatidylcholine (PC) membrane than K^+ ions. They also studied the effect of charged head groups (phosphatidylglycerol, PG), and found a weaker binding of K^+ ions with the bilayer compared to Na^+ ions. However, one might expect a stronger effect of cations on anionic lipids, due to stronger attractive Coulombic forces [68].

Numerous molecular dynamic studies have been conducted addressing the issue of various ionic effects on membrane properties [70, 71, 72, 73], using either the GROMOS- [74] or the CHARMM force field packages [75]. Effects observed in these studies, such as shrinking of area per lipid as a function of time, and also a considerable underestimate of area per lipid, have later been assigned to the force field parameters. The problem was partly due to a too high affinity of Na^+ ions towards the carbonyl oxygens in the lipids. This issue and other issues regarding properties of lipid bilayers, have been addressed, and updated CHARMM force field parameters exists as of June 2010 [52] and September 2013 [57]. Nevertheless, considering the observed effects in experimental studies and there can be room for improvement in force field parameters, the lipid bilayer systems in this study were prepared with a variation of the Na^+, K^+ and Cl^- ions. In addition, Na^+ and K^+ are two of the most abundant cations in a biological cell environment.

The parameters used to evaluate the properties of the bilayers, and which bilayer to use in the study of peptide interactions, are average area per lipid, $\langle Å^2 \rangle$, and order parameters, S_{CD}. In addition, the time evolution of the coordination number, N_C, of cations with carbonyl-, phosphate-, glycol-, and water oxygens, was examined. The time evolution of N_C, together with average area per lipid gives a good indication on whether and when the system is fully equilibrated. Figure 3.2 shows N_C for K^+ and Na^+ ions in each of the bilayer systems (homogeneous DMPC bilayer, homogeneous DMPC bilayer, and a mixed bilayer) with either NaCl or KCl, respectively. The remaining N_C data are given in appendix B, where it is organized by lipid bilayer system with various ion compositions. All systems, regardless of ion composition, shows convergence of the coordination number of the cations throughout the 110 ns simulation. This indicates that the migration of cations from solution to lipid oxygens stabilized during the equilibration phase prior to the simulation. Thus, the results in previous studies [72, 73], implying the need for longer simulation time before the system is fully equilibrated regarding migration of Na^+ ions may not be valid.

The average area per lipid, $\langle Å^2 \rangle$, a widely used quantity to characterize lipid bilayer systems. It gives a direct indication of lipid packing, which in turn gives an indication of whether one can expect the examined bilayer to be in the liquid crystalline phase (L_α)[50]. The area per lipid also affects a variety of physiological properties such as lateral diffusion, membrane elastic properties, and permeation [72]. The time evolution of the area per lipid supports the trend observed for the coordination number (N_C) of the cations in the equilibration of the systems.

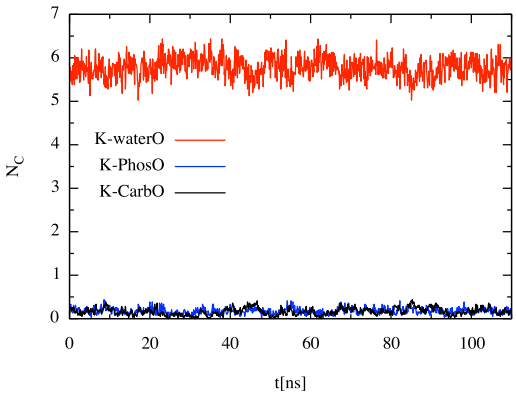

(a) N_C *of* K^+ *ions (DMPC lipids).*

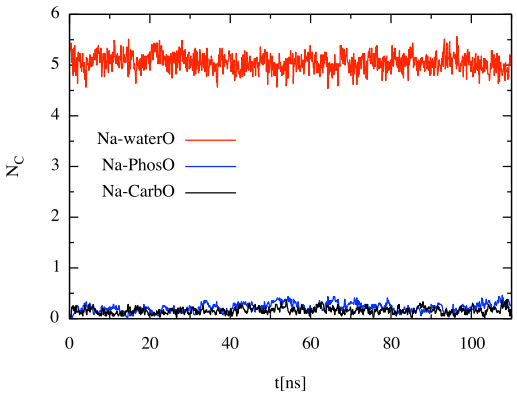

(b) N_C *of* Na^+ *ions (DMPC lipids).*

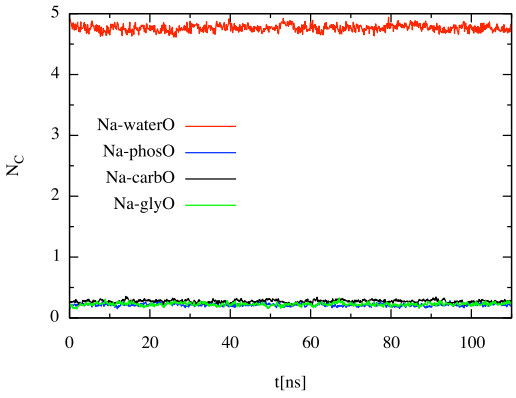

(c) N_C *of* Na^+ *ions (DMPG lipids).*

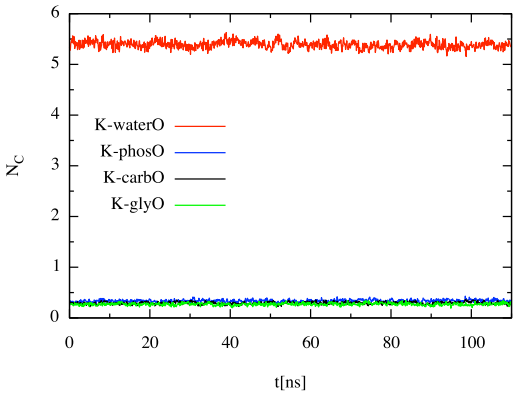

(d) N_C *of* K^+ *ions (DMPG lipids).*

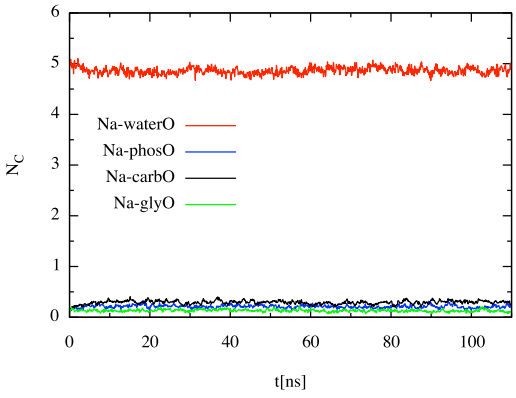

(e) N_C *of* Na^+ *ions (mixed bilayer)*

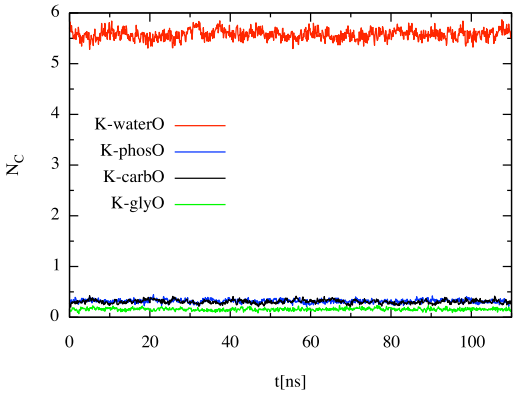

(f) N_C *of* K^+ *ions (mixed bilayer)*

Figure 3.2: *Time evolution of coordination number* N_C *for* K^+ *or* Na^+ *ions with water-, carbonyl- or phosphat oxygens in the DMPC, DMPG and mixed lipid systems with either KCl or NaCl. In addition, the* N_C *of both ions with glycol oxygens in systems with DMPG lipids.*

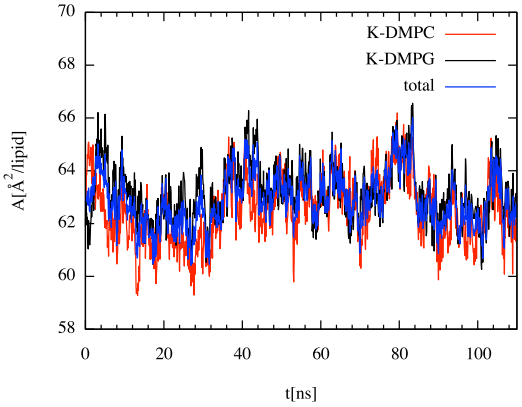

(a) *With K^+ as counter-ions.*

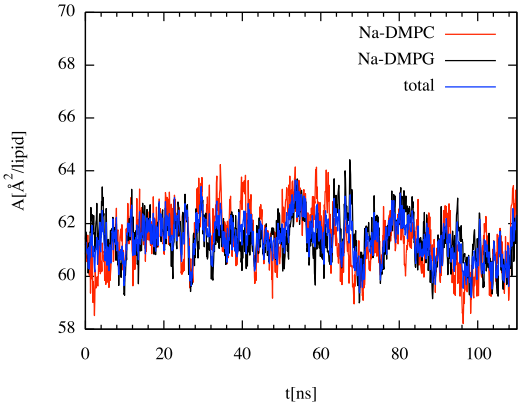

(b) *With Na^+ as counter-ions.*

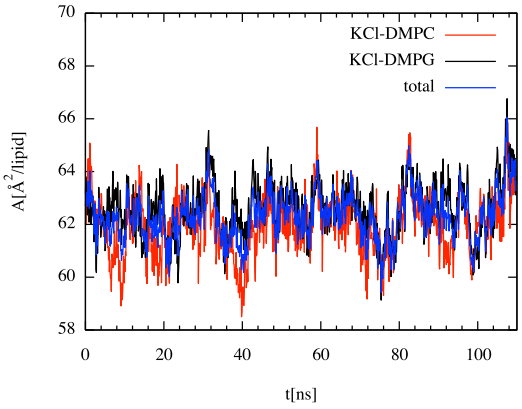

(c) *With 154 mM KCl.*

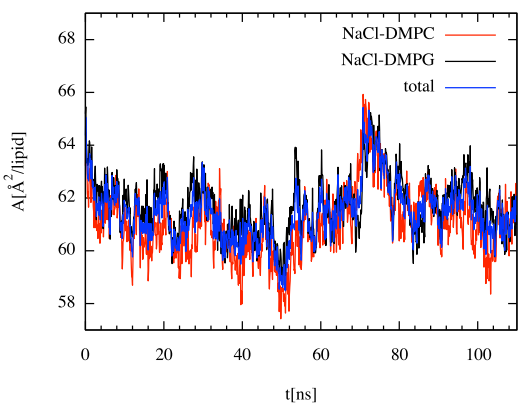

(d) *With 154 mM NaCl*

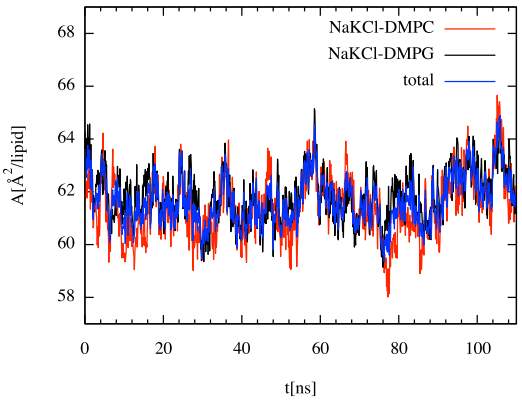

(e) *With ions; K^+ Na^+ Cl^-*

Figure 3.3: *Time evolution of the area per lipid of various DMPC/DMPG lipid bilayer.*

A correlation between these two parameters is expected, considering results in prior studies which showed a notable decrease in the area per lipid over time due to increasingly tight binding of Na^+ ions to the lipid bilayer [73]. Figure 3.3 shows the 110 ns simulation of lipid bilayers containing a mixture of DMPC and DMPG lipids. The time dependent area per lipid for systems of homogeneous DMPC and DMPG lipids are given in appendix A. The average area per lipid for all systems are also given in Table 3.1. These values were obtained from averaging over the fluctuating areas which occurred during a single simulation run of 110 ns.

Table 3.1: *Time average of area per lipid in systems generated with charmm-gui, where some systems are rebuild containing different compositions of ions. All systems with ions in addition to counter-ions has an ionic strength of 154 mM.*

Label	Lipid	Na^+	K^+	Cl^-	Area per lipid Å^2		
	System				DMPC	DMPG	TOTAL
A.1	DMPC				61.413		
A.2	DMPC	39		39	60.682		
A.3	DMPC		39	39	61.023		
A.4	DMPC	27	27	54	61.315		
B.1	DMPG[a]	336				64.056	
B.2	DMPG[a]		336			65.228	
B.3	DMPG	393		57		63.573	
B.4	DMPG		393	57		64.806	
B.5	DMPG	194	196	55		64.156	
C.1	MIX[ab]	196			61.394	61.393	61.393
C.2	MIX[ab]		196		62.537	63.159	62.900
C.3	MIX[b]	252		56	61.061	61.726	61.449
C.4	MIX[b]		252	56	61.947	62.603	62.329
C.5	MIX[b]	126	126	56	61.430	61.837	61.668

[a] *Counter-ions only,* [b] *Mixed DMPC/DMPG lipid bilayer (70/98 per lefleat)*

The average area per lipid obtained for the four DMPC lipid bilayer were similar in size, ranging from 60.682 Å^2 in the system with NaCl to 61.413 Å^2 in the system with no ions. Literature values of area per lipid for phosphatidylcholine (PC) lipids show some variance, depending on which experimental techniques have been used. An overview of the varying results obtained are given in a review done by Nagle *et al.* [50]. The review addresses the problem of experimental uncertainty in the structure of fully hydrated fluid (Lα) phase lipid bilayers, which leads to a less accurate base of data to compare

with, for instance, computer simulations. The review concluded that the great uncertainty in values can be reduced by carefully considering adjustments to older literature values, which might have been deduced without fully considering the fluidity of (Lα) phase lipid bilayers. Nagle *et al.* [50] concluded that the area per lipid for DMPC lipids is 59.6 Å^2 at 30°C. This is in agreement with the value 60.0 Å^2 obtained by Petrache *et al.* [65] at the same temperature. Petrache *et al.* also found that the area per lipid for DMPC at 50°C is 65.4 Å^2. Extrapolation of the two later values yield an area per lipid of 61.6 at 37°C. Thus, all values obtained for area per lipid of systems with DMPC lipids are in good agreement with experiments.

In contrast to DMPC lipid bilayers, experimental estimates of the area per lipid of homogeneous DMPG bilayers is not abundant in the literature. However, Pan *et al.* [32] have determined the molecular structure of various phosphatidylglycerol (PG) lipids in the biological relevant fluid phase. The group has developed a new method, scattering density profile or SDP model, which combines experimental data obtained from neutron and X-ray scattering with MD simulations. The latter is used to calculate the probabilities of lipid volumes. For DMPG lipid bilayers they found an area per lipid of 66.2 Å^2 at 37°C. The DMPG lipid bilayers simulated with K^+ as counter-ions, and the system containing KCl are in good agreement with this value, having an area per lipid of 65.2 Å^2 and 64.8 Å^2, respectively. The DMPG bilayer systems, which had different amounts of Na^+ ions present, resulted in a value of area per lipid slightly below the result obtained by Pan *et al.*. The simulation of the lipid bilayer system with DMPC lipids and NaCl resulted in an area per lipid slightly smaller than the other DMPC lipid bilayer systems. The overall trend for both DMPC- and the DMPG lipid bilayers, indicates that Na^+ and K^+ ions have different influence of area per lipid and the DMPG bilayer seemed to be more affected. However, considering that the systems contain different amounts of Na^+ ions, there is no clear correlation between a decrease in area per lipid and an increase in concentration of Na^+ ions. One has to take into account that these are results from a single simulation run per system.

To evaluate which of the mixed lipid bilayers to use in further simulations with peptides, the area per lipids of DMPC and DMPG in mixture were compared to the homogeneous bilayers. The total average area per lipid for the mixed bilayers shows a similar trend as the homogeneous bilayers with a slightly smaller value for the bilayer systems containing Na^+ ions. By examining the separate average area per lipid of the DMPC and DMPG lipid in the mixed bilayer (Table 3.1), it is clear that the average area per lipid

of DMPG is affected to a greater extent as a result of the mixing. In this case it seems to be a correlation between the decrease of DMPG $\langle Å^2 \rangle$ and increase in number of Na^+ ions. In all systems containing Na^+ ions the $\langle Å^2 \rangle$ of DMPG resembled that of the homogeneous DMPC bilayers.

Lewis *et al.* [76] have examined the thermotropic phase behavior of hydrated binary mixtures of DMPC and DMPG, using calorimetric and spectroscopic methods. As other studies have suggested [77, 78], they found that the two lipids are highly miscible in all proportions, and that the overall behavior is consistent with the fact that the temperature and enthalpy changes associated with gel/liquid crystalline phase transitions of the two lipids are similar, and that the DMPC and DMPG exhibits near ideal mixing behavior. However, Lewis *et al.* also obtained data indicating that the midpoint temperatures for pretransitions and gel/liquid crystalline phase transitions were higher for mixtures containing 5-50 mol% DMPG compared to either of the homogeneous bilayers. This behavior is inconsistent with the two lipids forming ideal mixtures [76].

Experimental values of the area per lipid of DMPG in pure bilayers are about 4 $Å^2$ larger than that of their neutral counterpart DMPC, despite of the phosphatidylglycerol (PG) head groups volumes being smaller. Pan *et al.* [32] argue that this is in agreement with the double layer Gouy-Chapman theory, which predicts a larger lipid area being energetically more favorable for the anionic DMPG lipids. A larger area yields a smaller surface charge density. The Gouy-Chapman theory predict that the unit free energy of a charged interface submerged in an ionic solution is proportional to its surface charge density [42]. As observed in the simulation of the mixed lipid bilayers, one might expect some decrease in the area per lipid of DMPG lipids due to less repulsion between the charged head groups when DMPC is present. The mixture of the zwitter-ionic PC head groups and anionic PG head groups might stabilize the lipid bilayer, resulting in the higher midpoint temperature for the pre- and main phase transitions observed by Lewis *et al.* [76]. However, DMPG is still the major component in the presented simulations, thus one might not expect a too large compression.

The order parameters, S_{CD}, of the saturated *sn*-1 and *sn*-2 chains were calculated separately for both DMPC and DMPG lipids. The attachment of the two chains to the glycerol backbone is illustrated in Figure 3.4.

Experimental values of order parameters reflect the average orientation of internuclear C-D vectors with respect to the direction of the external magnetic field [64]. Lipids in fluid bilayers are highly dynamic. Thus, one expects con-

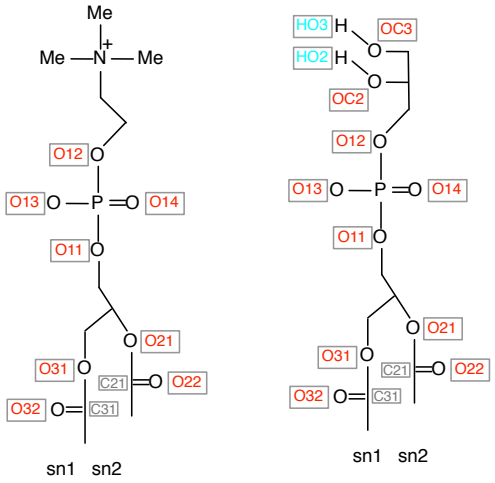

Figure 3.4: *Schematic structure of the DMPC and DMPG lipids.*

tributions from many movements occurring at different time scales. Segment motions such as rotation around chemical bonds and trans-gauche isomerisations occur during picoseconds. Molecular motions such as rotation around the lipid axis and wobbling occur at time scales of nanoseconds, whereas lateral diffusion occurs during microseconds. In addition, there is collective fluctuation of the bilayer itself [64, 65]. When comparing order parameters calculated from MD simulations, it is important to remember that the relatively short simulation time (from ten to a few hundred nanoseconds) will not capture some of the slower processes which take place. The order parameters obtained from the 110 ns simulation of DMPC lipids in systems with different ion composition compared to experimental values are presented in Figure A.1.

The order parameters, S_{CD}, are plotted as a function of acyl segment position, which gives a profile that indicates the average degree of order along the lipid acyl chain [65]. The order parameters of the segments close to the glycerol and head group region (from C2 to C8) resembles a plateau which is followed by a reduction in S_{CD} when approaching the center of the bilayer. The *sn*-2 S_{CD} for the simulated DMPC bilayers plateau region are in good agreement with the experimental values from Douliez *et al.* [7].

Figure 3.6a and 3.6b represents the order parameters, S_{CD}, of DMPG lipids in homogeneous bilayers, together with S_{CD} of the two lipids in the binary mixture (DMPC/DMPG), as well as the S_{CD} of DMPC lipids in a system without ions. The systems containing DMPG lipids have Na^+ ions as counter-

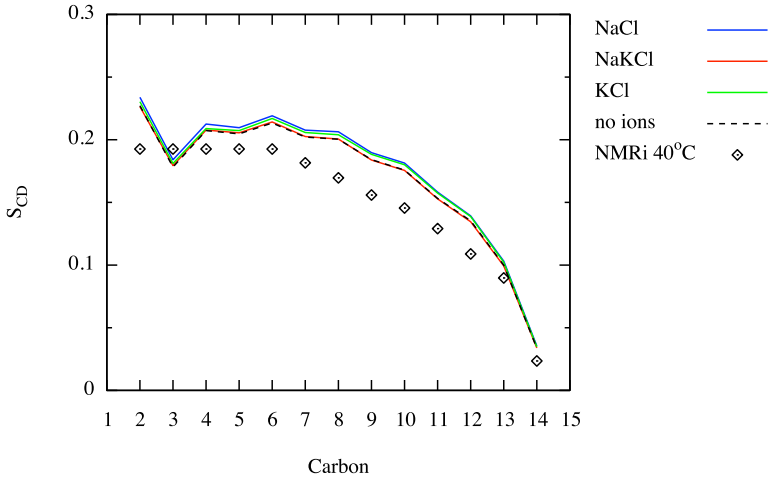

(a) *sn-1*

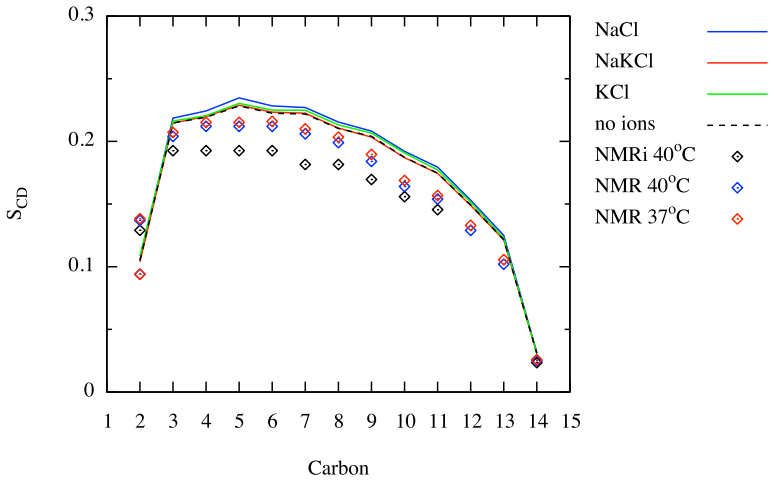

(b) *sn-2*

Figure 3.5: *sn-1- (a) and sn-2- (b) acyl chain order parameters (S_{CD}) for all the DMPC systems containing 154 mM NaCl, 154 mM KCl, 154 mM NaCl and KCl, or no-ions respectively. The black points in both plots are NMR data collected at 40° C, adapted from Nevzorov et al. [6]. The blue (40° C) and red points are NMR data adapted from Douliez et al. [7]. The NMR data corresponding to the red points (37° C) are found by extrapolation from data collected at 40° C and 35° C.*

ions. Figure 3.6c and 3.6d shows the same comparison, with K^+ ions as counter-ions. As expected, the result closely follows the change in the average area per lipid. The DMPC lipid bilayer is more compressed compared to the pure DMPG bilayer, which results in a higher ordering of the acyl chains. An interesting result is that the DMPC and DMPG lipids adapts the same order parameters upon mixing. As for the area per lipid (Table 3.1), when using Na^+ as counterion, both lipids in the mixture adapt the characteristics of the pure DMPC bilayer. When the counter-ion is K^+, the area per lipid and order parameters of DMPG and DMPC coincide, which, is also the case for the mixed bilayer system containing KCl to a lesser extent (shown in Figure C.3f, appendix C). Considering the findings of Lewis *et al.*, questioning the assumption that DMPC and DMPG exhibit near ideal mixing behavior, and the results of Garidel *et al.* yielding slightly lower main phase transition enthalpies for various DMPC/DMPG mixtures compared to pure component bilayers, the mixed bilayer system containing K^+ ions was chosen for the peptide simulations. The area per lipid and order parameters of the two lipids in the latter system differs from the pure component bilayers. However, due to inconclusive experimental results for the properties of binary mixtures of DMPC and DMPG, it may be a good idea to simulate a system containing Na^+ ions as well to compare the differences.

3.2 First Peptide Interaction and Insertion to The Lipid Bilayer

The DMPC/DMPG lipid bilayer with K^+ as counter-ion was built with six different combinations of peptides. Three parallel simulations of each of the systems, containing different numbers of either of the two peptides RWR-NHBn or RTbtR-NHBn, were simulated. The time of each simulation is given in Table 3.2, in addition to the peptide:lipid ratio at the leaflet facing the peptides and association occurring between peptides. The peptides, initially randomly placed in solution close to the surface of the membrane, rapidly bound to the lipid interface. However, the two peptides RWR-NHBn and RTbtR-NHBn (Figure 1.2) adapts different conformations in the solution, resulting in somewhat different modes of initial interactions and development throughout the simulation.

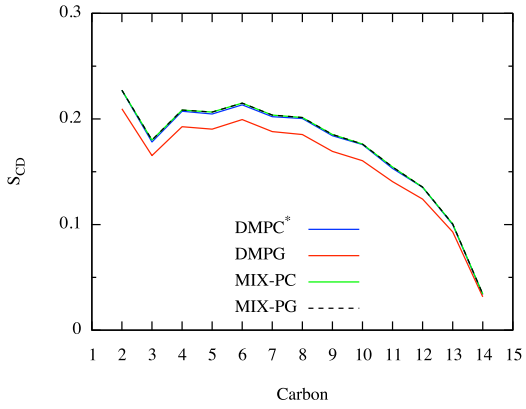

(a) S_{CD} *of sn-1-chain with* Na^+ *as counter-ions.*

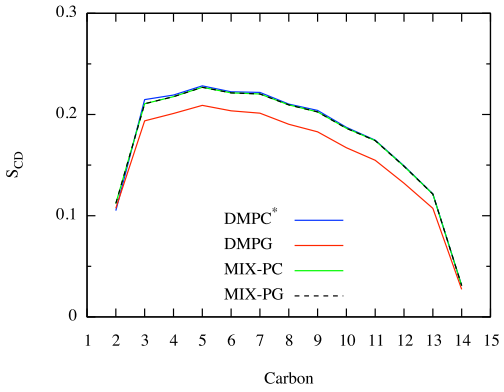

(b) S_{CD} *of sn-2-chain with* Na^+ *as counter-ions.*

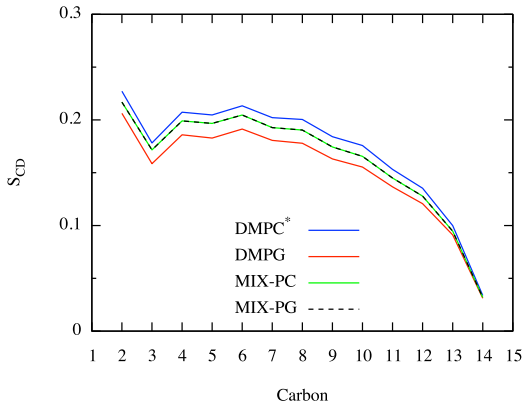

(c) S_{CD} *of sn-1-chain with* K^+ *as counter-ions.*

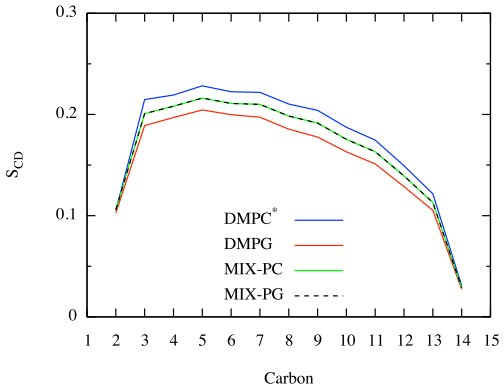

(d) S_{CD} *of sn-2-chain with* K^+ *as counter-ions.*

Figure 3.6: *The order parameters* (S_{CD}) *of DMPC * lipids in system without ions and DMPG lipids in homogeneous bilayer compared with the* S_{CD} *of a binary mixture of the two lipids with* Na^+ *or* K^+ *as counter-ions.*

Table 3.2: An overview of MD simulations performed with peptides present and with potassium as counter-ion.

Label	Peptide	Peptide/Lipid	Time (ns)	Association
A.1	RWR-NHBn	1/168	100	
A.2	RWR-NHBn	1/168	100	
A.3	RWR-NHBn	1/168	100	
A.4	RWR-NHBn	4/168	200	
A.5	RWR-NHBn	4/168	200	
A.6	RWR-NHBn	4/168	200	
A.7	RWR-NHBn	8/168	250	Dimer
A.8	RWR-NHBn	8/168	250	
A.9	RWR-NHBn	8/168	250	Trimer
A.1	RTbtR-NHBn	1/168	100	
A.2	RTbtR-NHBn	1/168	100	
A.3	RTbtR-NHBn	1/168	100	
B.4	RTbtR-NHBn	4/168	200	
B.5	RTbtR-NHBn	4/168	200	Dimer
B.6	RTbtR-NHBn	4/168	200	
B.7	RTbtR-NHBn	8/168	250	
B.8	RTbtR-NHBn	8/168	250	Dimer, Trimer
B.9	RTbtR-NHBn	8/168	250	3 x Dimer $\rightarrow$ Tetramer

The RWR-NHBn peptide generally adapts a nonamphipathic conformation, with each of the Arginine (Arg) residues stacked with either the Tryptophan (Trp) residue or the C-terminal benzylamide. Depending on the spatial orientation of the peptide, initially either of the positive Arg or N-terminal forms electrostatic interactions with the negatively charged phosphate head groups of the membrane. Issakson *et al.* [28] performed a NMR and MD simulation study, examining the correlation between different stereoisomers of a synthetic antimicrobial peptide (SAMP) and the MIC values obtained. The synthetic antimicrobial peptide (SAMP) used in their study (LTX 109) differ from the RTbtR-NHBn peptide only by the C-terminal being phenylethyl instead of benzylamide. They found that the stereoisomers resulting in a nonamphipathic conformation led to a higher MIC value, meaning lower antimicrobial activity. Issakson *et al.* further suggested that the stacking of guanidyl with the π-electron system of the aromatic Trp residue effectively

increases the water solubility of the peptide molecule.

Figure 3.8 shows the z-coordinates of the atoms NE1, CH2 (Trp residue, see Figure 2.1) and the CG4 atom (first atom on the C-terminal benzyl ring) as a function of time, for one RWR-NHBn peptide in a system simulated with 8 RWR-NHBn. The black line shows the mean trend of all phosphate atom's z-coordinates in the lipid bilayer leaflet facing the peptides. The indole nitrogen of the Trp residue (NE1) has a blue trend-line, the CH2 atom z-coordinates are illustrated with a red trend-line and the CG4 atom on the benzylamide capping has a yellow trend-line. Figure 3.9 demonstrates the position of the RWR-NHBn peptide at different time points during the simulation (dashed lines in Figure 3.8). By examining the trend-lines in Figure 3.8 it is possible to get an impression of the spacial orientation of the peptide as well as whether the conformation is amphipathic or not. A nonamphipatic conformation yields a larger separation of the respective trend-lines (Figure 3.9a). However, a smaller spacing of the trend-lines while the RWR-NHBn peptide still is on the lipid bilayer surface, might be due to a planar orientation were both Arg residues of the nonamphipathic peptide interacts with different lipid phosphate groups. The insertion trend of the RWR-NHBn peptide in all systems containing four or eight peptides (six systems in total) is given in Appendix D. The trends are shown for each individual peptide for the full simulation time. Similarly the insertion trends for the RTbtR-NHBn peptides are given in Appendix E.

The RWR-NHBn peptides tends to stay in the lipid water interface region with either the benzylamide C-terminal or the Trp residue somewhat deeper embedded in the membrane. The conformational change resulting in both hydrophobic components of the peptide being deeply embedded within the membrane only occurs once, twice and once for the three systems simulated with 4 peptides respectively. The insertion does not occur until the last 100 ns of the 200 ns simulation (Appendix D). As for the systems containing 8 RWR-NHBn peptides, the insertion of both hydrophobic components into the hydrophobic core of the lipid bilayer occurred with 3, 4 or 5 peptides in each of the simulations respectively. In six of these cases the insertion happened during the first 100 ns of a 250 ns simulation. Considering the fraction of peptides (1:4, 2:4, 1:4 versus 3:8, 4:8, 5:8) which insert it seems like the probability of insertion and insertion at an earlier time increases with a larger number of peptides in the system. By examining the behavior of the RWR-NHBn peptides in the trajectories it appears that some of the Trp residues which are inserted into the hydrophobic interior of the membrane, seeks to interact with the interfacial region of the lipid bilayer over

again. This behavior can also be seen in the trend-lines of the Trp atom's z-coordinates for several of the RWR-NHBn peptides given in Appendix D. The Trp residues preference of being in the interfacial region of the lipid bilayers has previously been documented [79, 80]. The π-electron system of the Trp results in a negatively charged cloud which can participate in cation-π binding with positively charged lipid head groups, in a similar way as with guanidyl. The π-electron system also results in the aromatic Trp having quadrupole moment. Thus, it cannot strictly be considered as a hydrophobic residue [80, 81].

In system A.7 (Table 3.2), a cluster of 2 peptides form, and in system A.9, a cluster of 3 peptides form. The Dimer and Trimer in each system remain for 200 ns, but the the peptides separate again towards the end of the 250 ns simulation. By examining the trajectories with clusters of RWR-NHBn peptides it seems like these clusters make a greater impact on the membrane than singularly inserted peptides. The phosphate head groups of the lipids interact with the Arg residues and N-terminal in the cluster of peptides, but also form hydrogen bonds with the backbone nitrogens and Trp indole. The interactions seem to "lock" the involved lipid head groups in position, while the cluster of peptides forces them towards the membrane center as the peptides embed deeper. The impact on the membrane resulting from a cluster of two RWR-NHBn peptides is illustrated in Figure 3.7.

The RTbtR-NHBn peptide tends to adapt a amphipathic conformation, which can easily be observed as relatively close trend-lines for the z-coordinates of the atoms in the Tbt residue (NE1 and CH2) and benzylamide (C76) (Appendix E). Figure 3.10 and 3.12 illustrate the movements of two different RTbtR-NHBn peptides, A and E, relative to the membrane surface. Both peptides A and E are from system 1, containing 8 RTbtR-NHBn peptide (Figure E.4a and E.5a). Multiple snapshots are taken during the simulation to better illustrate how to interpret the trend-lines of the various atom positions during the simulation (Figure 3.11 and 3.13). In the case of peptide A (Figure 3.10), the two hydrophobic components Tbt and benzylamide, are grouped together with the two Arg residues oriented towards the phosphate groups of the membrane. Peptide A does not embed deeper into the hydrophobic membrane core until the last 50 ns of a 250 ns simulation. The benzylamide capping of peptide E "flips" into the membrane interior after approximately 70 ns, closely followed by the Tbt residue. This sudden "flipping" of both hydrophobic components into the membrane interior is characteristic for most of the RTbtR-NHBn peptides in this study (Appendix E). In the three systems containing 4 RTbtR-NHBn peptides insertion of both benzylamide and

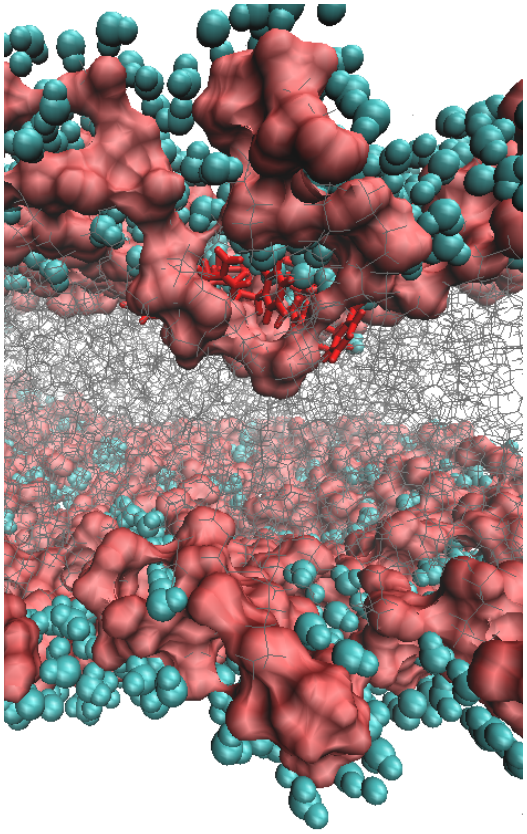

Figure 3.7: *The figure illustrates the impact on the membrane resulting from a cluster of two RWR-NHBn peptides. The surf graphics is applied to the polar head group of lipids including the carbonyl esters.*

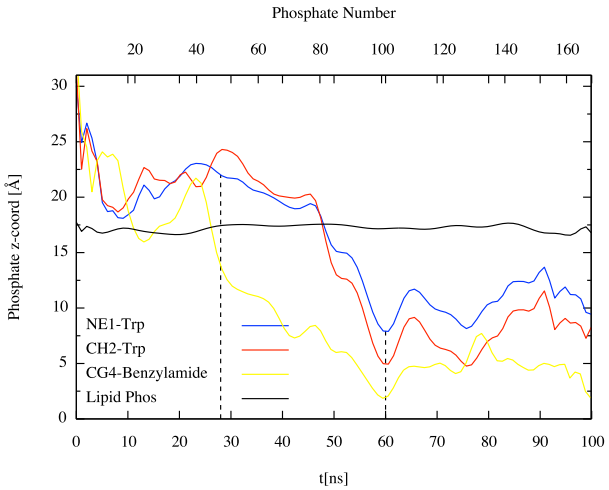

Figure 3.8: *The trend-lines for the z-coordinate of atoms NE1, CH2 (TRP Figure 2.1) and CG4 which is the first atom on the C-terminal benzyl ring (A-RWR-NHBn), as a function of time (ns). The black line shows the trend of all phosphate atoms z-coordinates in the lipid bilayer leaflet facing the peptides, blotted individually. The dashed lines refers to the snapshots of the trajectory taken at 28 and 60 ns respectively shown in Figure 3.9.*

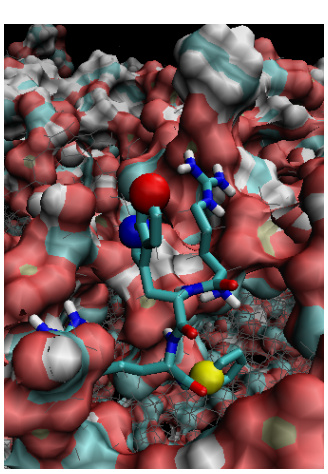

(a) *RWR-NHBn peptide at 28 ns.*

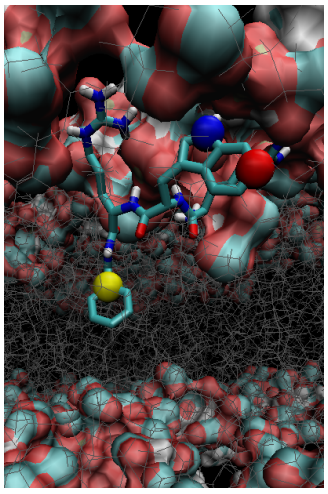

(b) *RWR-NHBn peptide at 60 ns.*

Figure 3.9: *Snapshots taken of peptide A, which movement is illustrate by trend-line in Figure 3.8. Taken from a simulation with 8 RWR-NHBn peptides. The color of the atoms in the figure match the trend-lines in Figure 3.8.*

Tbt occurred with 2, 0 and 2 peptides respectively. In the three systems containing 8 RTbtR-NHBn peptides, insertion of both hydrophobic components occurred with 4, 5 and 3 peptides, respectively. In addition the Tbt residue of peptide G in system 1 (Figure E.5c) embeds into the hydrophobic core of the membrane. Unlike the Trp residue of the RWR-NHBn peptides, the Tbt residue remains deeply embedded after insertion. This is expected, considering the far more hydrophobic character of the bulkier Tbt residue. In all systems with 4 RTbtR-NHBn peptide (first three systems in Appendix E), peptide D did not insert as it might appear from the graphs. This peptide had a similar effect on the membrane as the clusters of 2 RWR-NHBn peptides, "locking" down several DMPG lipids buy interaction with phosphate head groups (Figure 3.18).

In the case of the system with 8 RTbtR-NHBn peptides (B.8 and B.9 in Table 3.2), multiple cluster formations are observed. The hydrophobic components of different peptides rapidly interacts with each other. These hydrophobic interactions seem to "lock" the involved peptides together at the lipid bilayer surface. In system 2 (Appendix E), the RTbtR-NHBn peptides not involved in any cluster, rapidly insert into the membrane. Thus, overall the same number of peptides are inserted in systems of RTbtR-NHBn and RWR-NHBn peptides, at least at the time scale of these simulations. The antimicrobial activity of both synthetic antimicrobial peptides (SAMPs) in this study has been examined in previous studies [30, 26]. The RWR-NHBn has an observed MIC value of 83 μM with *S. aureus* and 50 μM with MRSA [26], whereas RTbR-NHBn has a MIC value of 3.2 μM for both of these bacterial species [30]. If the mechanism of membrane rupture and killing of these bacterial species is a result of pore formation due to peptide insertion, one can expect more inserted RTbR-NHBn peptides if the simulation time is increased.

3.3 The effect of RWR-NHBn and RTbtR-NHBn on The Lipid Bilayer

The average area per lipid $\langle \text{Å}^2 \rangle$ of all three parallels for each system is given in Table 3.3. The areas obtained during the last half of the simulation time is given in parenthesis, to detect any changes throughout the simulation. Irrespectively of how many peptides and whether the peptide is RWR-NHBn or RTbtR-NHBn the area per lipid of both DMPG and DMPC is slightly larger than the values of the equilibrated lipid bilayer. The total area per

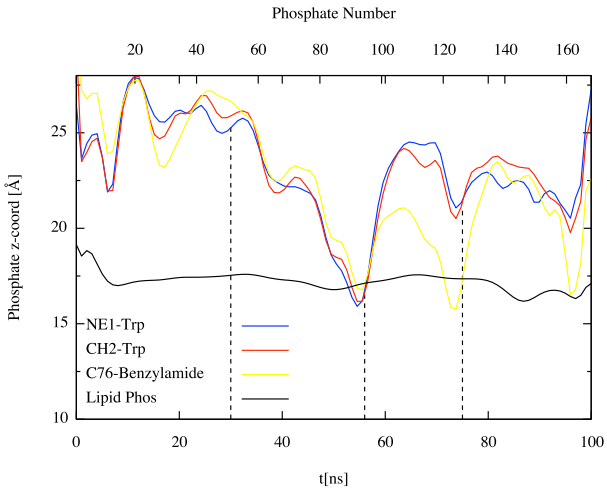

Figure 3.10: *The trend-lines for the z-coordinate of atoms NE1, CH2 (TRP Figure 2.1) and C76 which is the first atom on the C-terminal benzyl ring (A-RTbtR-NHBn), as a function of time (ns). The black line shows the trend of all phosphate atoms z-coordinates in the lipid bilayer leaflet facing the peptides, blotted individually. The dashed lines refers to the snapshots of the trajectory taken at 30, 56 and 75 ns respectively shown in Figure 3.11.*

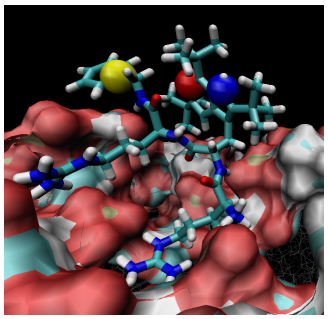

(a) *RTbtR-NHBn peptide at 30 ns.*

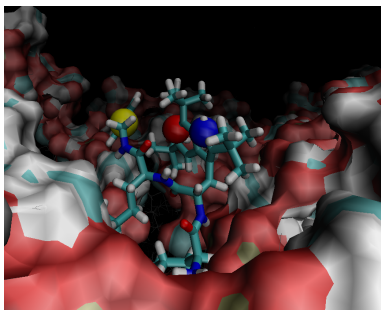

(b) *RTbtR-NHBn peptide at 56 ns.*

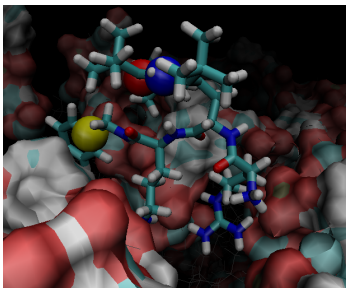

(c) *RTbtR-NHBn peptide at 75 ns.*

Figure 3.11: *Snapshots taken of peptide A, which movement is illustrate by trend-line in Figure 3.10. Taken from a simulation with 8 RTbtR-NHBn peptides. The color of the atoms in the figure match the trend-lines in figure 3.10.*

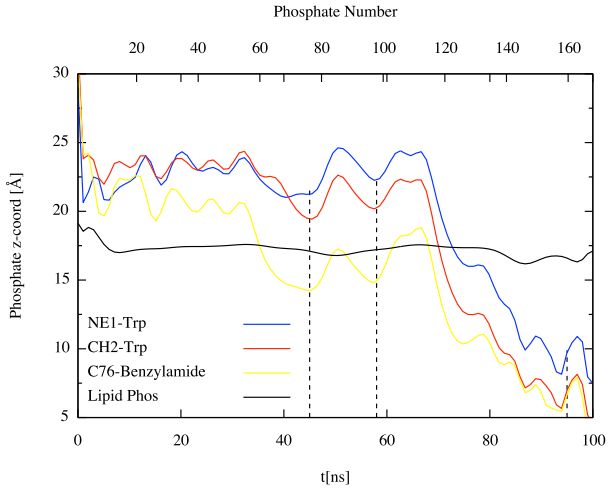

Figure 3.12: *The trend-lines for the z-coordinate of atoms NE1, CH2 (TRP Figure 2.1) and C76 which is the first atom on the C-terminal benzyl ring (E-RTbtR-NHBn), as a function of time (ns). The black line shows the trend of all phosphate atoms z-coordinates in the lipid bilayer leaflet facing the peptides, blotted individually. The dashed lines refers to the snapshots of the trajectory taken at 45, 58 and 95 ns respectively shown in Figure 3.13.*

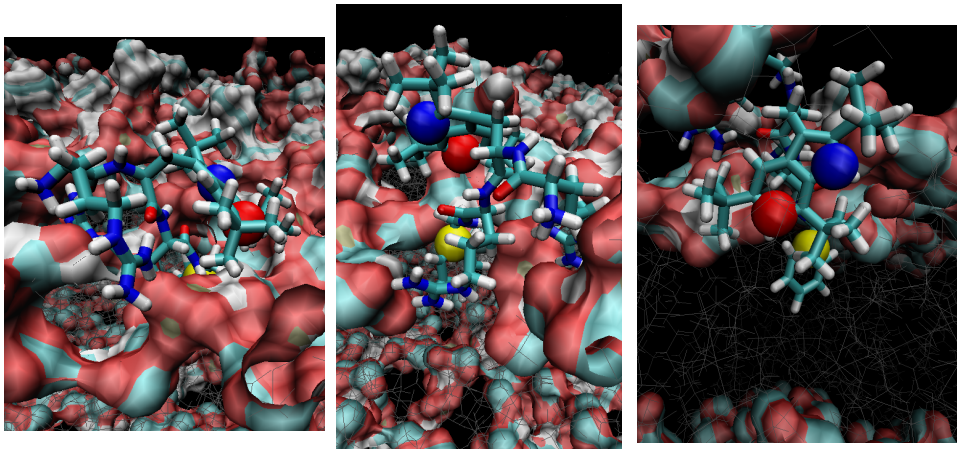

(a) *RTbtR-NHBn peptide at 45 ns.*

(b) *RTbtR-NHBn peptide at 58 ns.*

(c) *RTbtR-NHBn peptide at 95 ns.*

Figure 3.13: *Snapshots taken of peptide E, which movement is illustrate by trend-line in Figure 3.12. Taken from a simulation with 8 RTbtR-NHBn peptides. The color of the atoms in the figure match the trend-lines in figure 3.12.*

lipid has on average increased by less than 1 Å^2. The equilibrated lipid bilayer yielded 62.5±1.3 Å^2 for the DMPC lipids and 63.2±1.2 Å^2 for the DMPG lipids, whereas the total area per lipid was 62.9 Å^2. There is no significant difference between the area per lipids depending on whether they are in the leaflet facing the peptides or not. The only system that stands out due to the area per lipid is the system containing 4 RTbtR-NHBn peptides, which has no increase in the DMPC area and a slight decrease in the DMPG area. In addition the area per lipid in the leaflet facing away from the peptides is smaller than the areas in the leaflet facing the peptides (Table 3.3). The thickness of the bilayer without peptides was 35.35 Å. Similar to the area there is no significant change with peptides present (Table 3.3).

Table 3.3: *Overview of the time average area per lipid in systems containing RWR-NHBn and RTbtR-NHBn peptides and with K^+ as counter-ions. The z+ refers to bilayer leaflet in contact with peptides, whereas z- refers to the leaflet without peptides. The areas obtained during the last half of the simulation time is given in parenthesis.*

Peptide	Leaflet	Area per lipid Å^2			Thickness
		DMPC	DMPG	TOTAL	Å
1RWR	z+	63.47	63.99	63.77	35.00
	z-	63.45	63.93	63.73	
4RWR	z+	63.58(63.56)	63.93(63.85)	63.79(63.73)	35.01(35.17)
	z-	63.42(63.61)	63.95(63.69)	63.74(63.66)	
8RWR	z+	63.57(63.28)	64.12(64.45)	63.89(63.96)	35.03(35.13)
	z-	63.35(63.55)	63.98(64.00)	63.72(63.81)	
1RTbtR	z+	63.60	63.90	63.77	35.06
	z-	63.35	63.97	63.71	
4RTbtR	z+	62.37(62.27)	62.38(62.59)	62.38(62.45)	35.86(35.90)
	z-	61.28(60.91)	60.87(60.95)	61.04(60.93)	
8RTbtR	z+	63.46(62.87)	63.89(63.99)	63.71(63.49)	35.11(35.3)
	z-	63.14(63.10)	63.76(63.65)	63.50(63.42)	

The order parameters S_{CD} calculated for the *sn-1* acyl chains in systems with either 4 or 8 RWR-NHBn and RTbtR-NHBn present are given in Figure in 3.14. As for the area per lipid the S_{CD} were averaged for the three parallel simulations. In correlation with the area per lipid, little change is observed compared to the equilibrated lipid bilayer. With the exception of the systems containing 4 RTbtR-NHBn peptides, where the order parameters are slightly increased compared to those of the bilayer without peptides present. Which is in agreement with the observed smaller area per lipid.

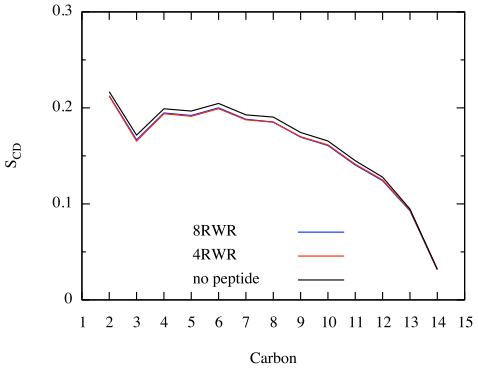

(a) *S_{CD} for bilayer without peptides, with 4 RWR or 8 RWR.*

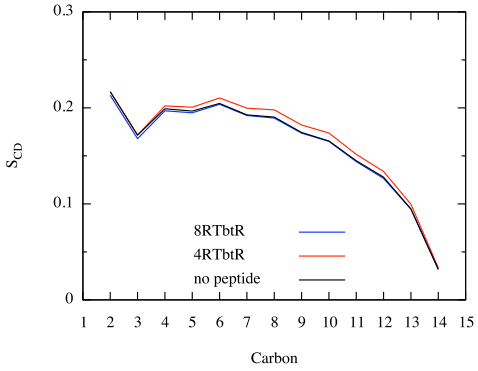

(b) *S_{CD} for bilayer without peptides, with 4 RTbtR or 8 RTbtR*

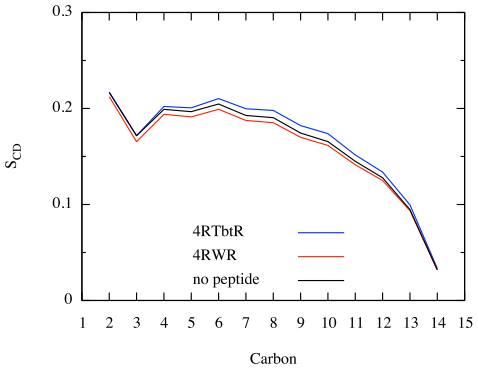

(c)

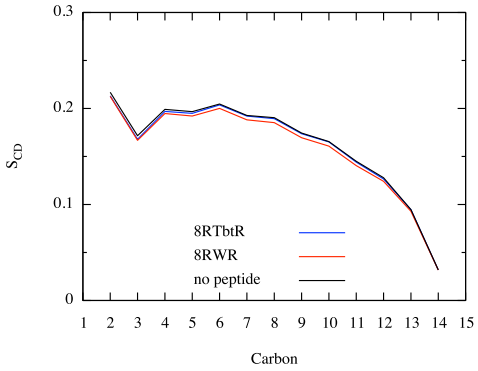

(d)

Figure 3.14: *Lipid tail order parameters S_{CD} from the* sn-1 *chain averaged over three parallel simulations of 100 ns each.*

When examining the trajectories of the of RTbtR-NHBn systems containing 4 peptides it seems like there is much more structural fluctuation within the water lipid interface. The increased fluctuation seem to be largest in the bilayer which do not interact with the peptides. This is illustrated in Figure 3.15, where a pyramid shape can be seen in the lower leaflet due to some polar head groups being closer to the bilayer center. In the top leaflet one peptide is causing a large groove as it "forces" the polar head groups of the lipids towards the bilayer center. The difference between the area per lipid of the two leaflets observed for the systems containing 4 RTbtR-NHBn peptides might be a result of underestimation, as the increased fluctuation of the monolayer might not be accounted for when projecting the area [82].

Fluctuations in the interface region can be illustrated by examining the distribution of phosphate atoms in the lipid head groups [83]. The average distribution of the phosphate atoms as a function of the atoms z-coordinates during the 200 ns simulation was calculated for both system 4 RWR-NHBn and 4 RTbtR-NHBn. The distribution of the two is given in Figure 3.16, where they are compared to the phosphate distribution in bilayers without peptides present. In the case of RWR-NHBn the distribution of phosphate atoms in both leaflets are similar to bilayers without peptides. For systems with RTbtR-NHBn the width of the distribution of phosphates in the leaflet (z+) facing the peptides decreased from 8.7 Å to 7.8 Å, whereas the width of the distribution in the leaflet (z-) not facing the peptides increased from 8.3 Å to 9.1 Å. Thus, the distributions correlates with what is observed in the trajectories. A similar distribution was calculated for systems containing 8 RWR-NHBn and 8 RTbtR-NHBn (not shown), which showed no significant difference compared to bilayers without peptides present. However, by comparing profiles of the average position of each phosphate atom plotted individually, there appear to be a larger displacement between phosphate atoms when peptides are present (Figure 3.17).

When comparing the profiles of phosphates atom position to the trajectories of the simulated systems, it turns out that the low points often belongs to phosphate atoms in contact with peptides. Figure 3.19 shows the profile for system 1, with 4 RTbtR-NHBn peptides Figure (E.1). Peptide D (Figure E.1d) in this system is also illustrated in Figure 3.18. The low points corresponding to phosphate number 68 and 158 in Figure 3.19 belongs to the two lipids which phosphate group can be seen in the bottom of the groove caused by the peptide in Figure 3.19. Another observation is that the major part of the lipids being suppressed by peptide D are DMPG lipids, with one exception. The distribution of lipids around peptide D was calculated over

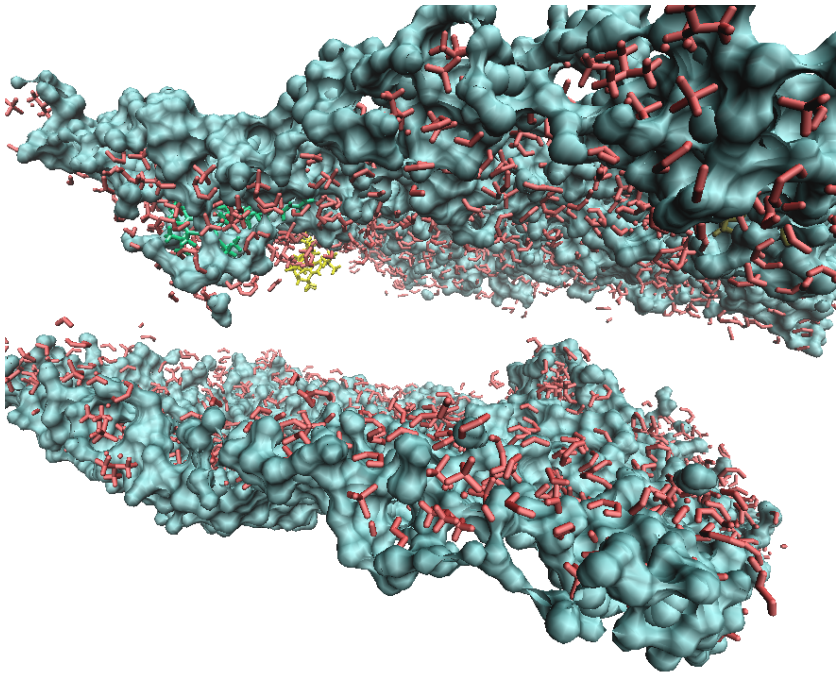

Figure 3.15: *Fluctuation of the lipid bilayer with 4 RTbtR-NHBn present, where 1 of the peptides forces the lipid head groups towards the center of the bilayer. Water within 3 Å of the lipid bilayer surface is illustrated with surf graphics (VMD).*

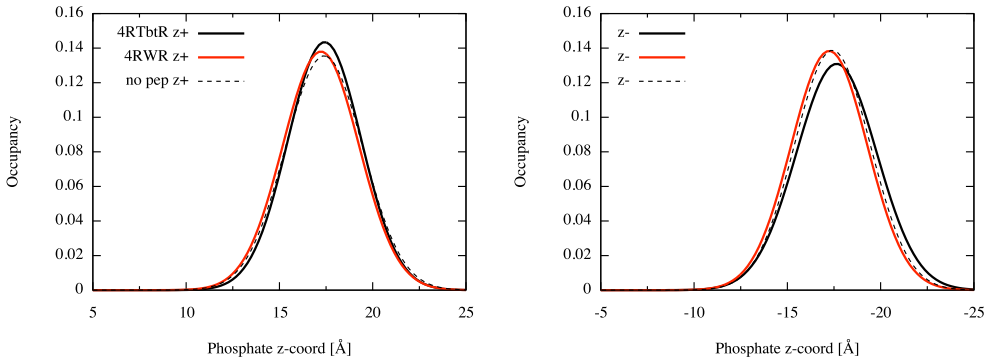

(a) *Leaflet with peptide (z+) and leaflet without peptides (z-) the first 100 ns.*

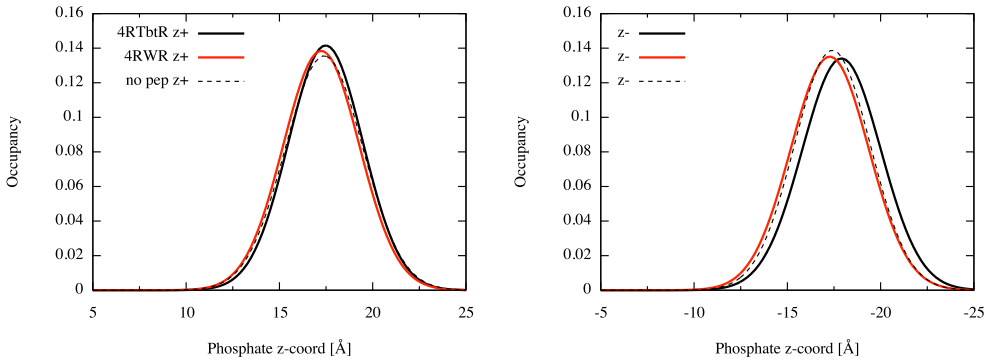

(b) *Leaflet with peptide (z+) and leaflet without peptides (z-) the last 100 ns.*

Figure 3.16: *The average distribution of phosphate atoms in lipid head groups as a function of z-coordinates during the 200 ns simulation of three parallel runs. The plots represent the distribution in a system containing 4 RWR-NHBn peptides (red) and 4 RTbtR-NHBn peptides (black) compared to a system without peptides (dashed lines).*

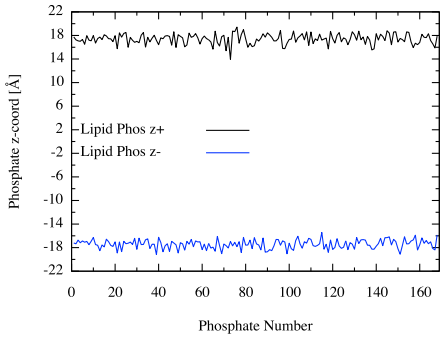

(a) System without peptides. Average position during 100 ns.

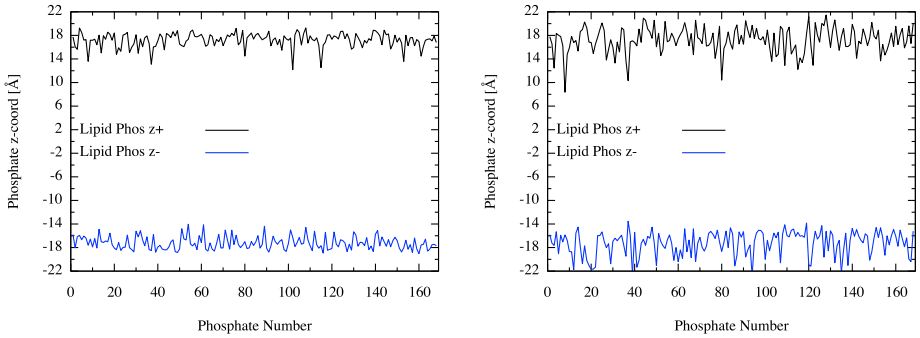

(b) System with 8 RWR-NHBn. Taken from first 100 ns and last 100 ns.

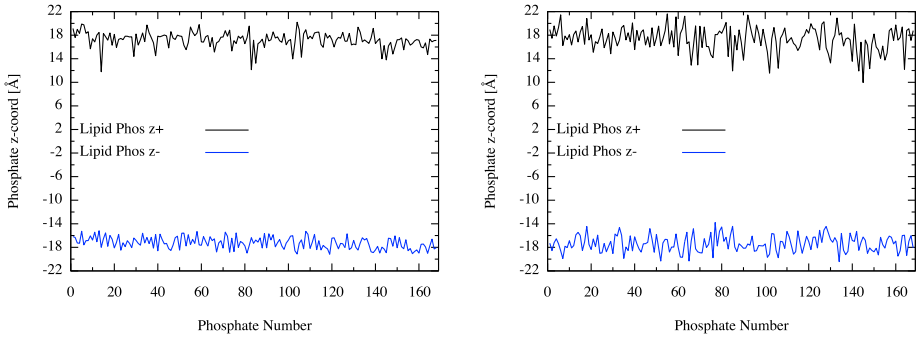

(c) System with 8 RTbtR-NHBn. Taken from first 100 ns and last 100 ns (Figure E.4 and E.5).

Figure 3.17: *Average position along the z-axis of each lipid phosphate atoms, plotted separate for each bilayer leaflet (z+ and z-). The lipid bilayers are oriented parallel to the x- y-plane. The peptides are placed above the z+ leaflet.*

the first 100 ns of the simulation. The result yielded a higher number of DMPG lipids, which is illustrated by the trend-lines in Figure 3.20. Figure 3.18 illustrate how phosphate groups of the lipids are attracted to several regions of the peptide. The obvious is the charged Arg residues and the N-terminal. In addition hydrogen bonding with the nitrogens of the backbone and the indole nitrogen of the Trp residues was observed by analyzing the trajectories. Also, in the case of peptide D in Figure 3.18 the phosphate head groups of the two lipids in the vicinity of the π-system of the Tbt residue persisted in this position throughout the simulation time. The many preferential interactions between DMPGs and AMPs leads to a local increase in the density of peptides at the surface, which has shown to be favorable for the formation of pores [84].

Polyansky *et al.* [85] performed a microsecond long coarse grain molecular dynamics simulation to examine the lateral structure and the main dynamics of phosphatidylethanolamine (PE)/phosphatidylglycerol (PG) mixed bilayer. They found that the antimicrobial peptides can induce growth of phosphatidylglycerol domains. They argued how this can destabilize bacterial membranes due to large fractions of PE lipids which cannot form stable bilayers on their own. The clustering of PG lipids may not be possible to detect during the simulation time of this project. However, it seems like the preferential interactions between DMPG lipids and the RTbtR-NHBn peptide in regions of higher DMPG density induce favorable modes of membrane destabilization. The deeply embedded RTbtR-NHBn peptide observed in systems consisting of 4 peptides might have been a prestage to pore formation.

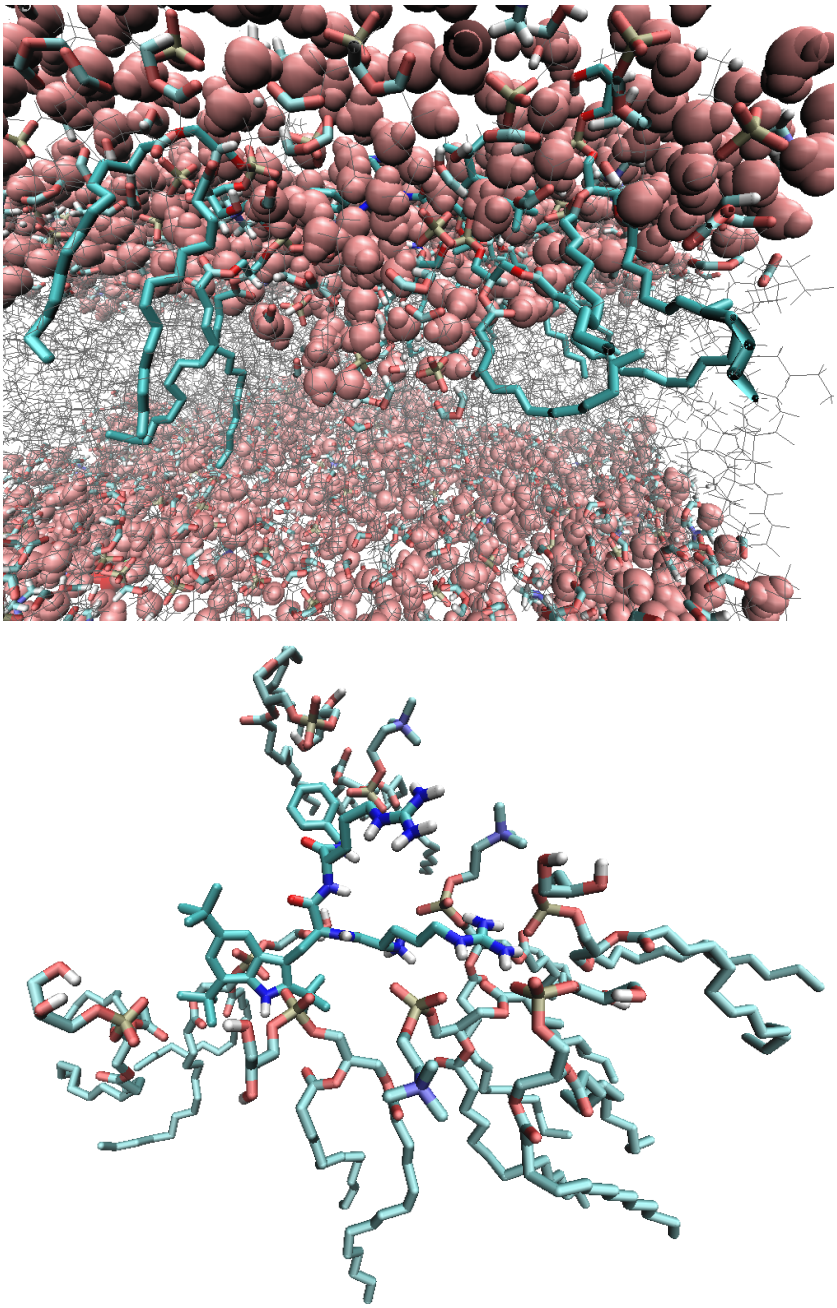

Figure 3.18: *Lipids interacting with the RTbtR-NHBn peptide D, seen from within the bilayer and from above (Figure E.1d).*

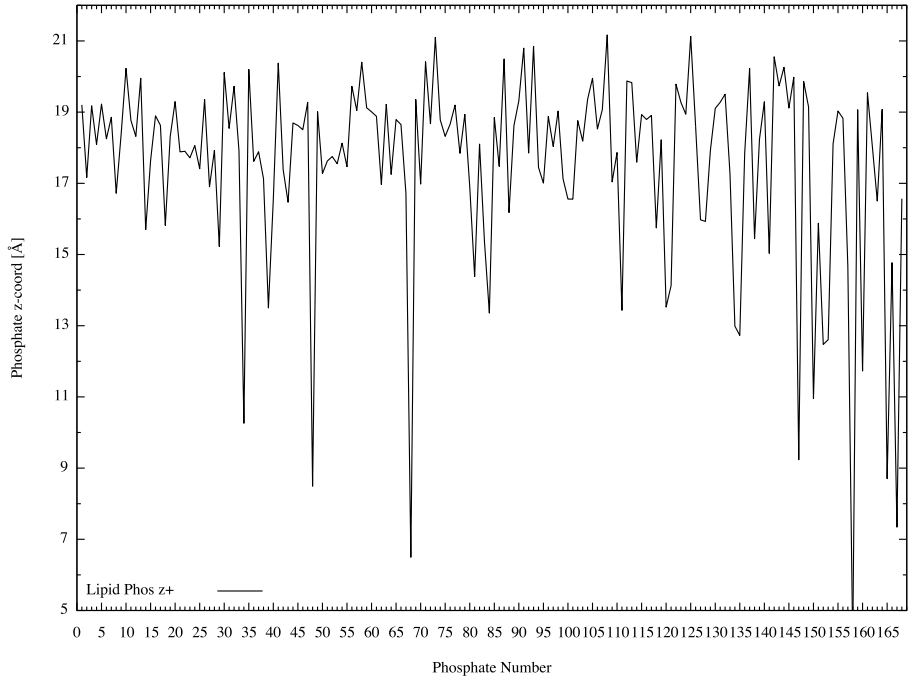

Figure 3.19: *The average z-coordinate of phosphate atoms in the leaflet facing the peptides in systems system 1, with 4 RTbtR-NHBn.*

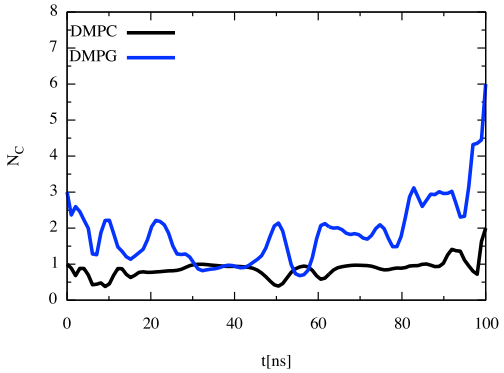

Figure 3.20: *Trend-lines for the distribution of lipids around the RTbtR-NHBn peptides in Figure 3.18.*

Chapter 4

Conclusion

Molecular dynamics (MD) simulations of DMPC/DMPG mixed bilayers with the synthetic antimicrobial peptides RWR-NHBn and RTbtR-NHBn were conducted using the all atom force field CHARMM36 [52]. The analysis of the results were performed using the plugins of the VMD program [54] in combination with basic tcl scripting.

Several lipid bilayer were built composed of either homogeneous DMPC or DMPG lipids in addition to binary mixtures of the two lipids. The system had different combinations of the ions Na^+, K^+ and Cl^-. The area per lipids and order parameters obtained for the DMPC bilayers were in good agreement with the literature values [50, 65] for all combinations of ions. The area per lipid for DMPC ranged from 60.7 $Å^2$ to 61.4 $Å^2$. The area per lipids for the homogeneous DMPG bilayer yielded 65.2 $Å^2$ for systems containing K^+ counter-ions and 64.8 $Å^2$ for the systems with KCl. These values are in good agreement with experimental values [32]. The remaining DMPG bilayers yielded slightly lower values for the average area per lipid. Strong ion interaction yielded an underestimated area per lipid in previous MD studies. The results of this project reveals the improvement in the force field parameters. Due to experimental results indicating a non-ideal mixing behavior of DMPC and DMPG lipids [76], the DMPC/DMPG mixed bilayer system chosen for simulation with peptides had K^+ as counter-ions. This mixed bilayer showed area per lipids and order parameters differing from both homogenous bilayers, with areas per lipid of 62.5 $Å^2$ and 63.2 $Å^2$ for DMPC and DMPG respectively.

A different behavior was observed for the RWR-NHBn and RTbtR-NHBn

peptides. The less bulky Trp residue of RWR-NHBn showed a greater preference for the membrane water interface than the Tbt residue of RTbtR-NHBn. The bulkier hydrophobic residues of RTbtR-NHBn embedded deeper into the membrane after insertion then thous of RWR-NHBn. On the timescale of these simulation the amount of insertions was observed in equal amount for the two peptides. This might be due to the immediate clustering among the hydrophobic components of the RTbtR-NHBn peptides. An increase in displacement of phosphate head groups was observed for the lipid bilayers in presence of both types of peptides. A slight increase in area per lipids was observed in all simulations with peptides, except for the systems with 4 RTbtR-NHBn which showed a slight decrease.

The simulations with peptides did not induce any pore formation at the applied time scale. However, large fluctuations was observed in the leaflet facing away from the peptides in systems with 4 RTbtR-NHBn yielding an increase interfacial width of 0.8 Å. One of the peptides in this system was interacting with several DMPG lipids forcing their head groups towards the membrane interior. This might have been a pre-stage of induced pore formation.

Chapter 5

Future Work

Considering the observed effects of ions on lipid bilayers it would be interesting to examine how different types of ions and physiolgical relevant ion concentrations affects the interactions between antimicrobial peptides and the lipid bilayers.

It would also be interesting to look at how the membrane potential changes with different compositions of lipids and how this further affects the interactions with antimicrobial peptides.

Examining wether the destabilizing effect of the antimicrobial peptides on the lipid bilayer mainly are rlated to regions with higher density of DMPG lipids.

References

[1] K. A. Brogden, "Antimicrobial peptides: pore formers or metabolic inhibitors in bacteria?," *Nature Reviews Microbiology*, vol. 3, no. 3, pp. 238–250, 2005.

[2] T. Heimburg, "Themed issue: Membrane biophysics," 2009.

[3] E. Fahy, S. Subramaniam, R. C. Murphy, M. Nishijima, C. R. Raetz, T. Shimizu, F. Spener, G. van Meer, M. J. Wakelam, and E. A. Dennis, "Update of the lipid maps comprehensive classification system for lipids," *Journal of lipid research*, vol. 50, no. Supplement, pp. S9–S14, 2009.

[4] P. Tripathi, A. Beaussart, G. Andre, T. Rolain, S. Lebeer, J. Vanderleyden, P. Hols, and Y. F. Dufrêne, "Towards a nanoscale view of lactic acid bacteria," *Micron*, vol. 43, no. 12, pp. 1323–1330, 2012.

[5] R. B. Best, X. Zhu, J. Shim, P. E. Lopes, J. Mittal, M. Feig, and A. D. MacKerell Jr, "Optimization of the additive charmm all-atom protein force field targeting improved sampling of the backbone ϕ, ψ and side-chain $\chi 1$ and $\chi 2$ dihedral angles," *Journal of chemical theory and computation*, vol. 8, no. 9, pp. 3257–3273, 2012.

[6] A. A. Nevzorov, T. P. Trouard, and M. F. Brown, "Lipid bilayer dynamics from simultaneous analysis of orientation and frequency dependence of deuterium spin-lattice and quadrupolar order relaxation," *Physical Review E*, vol. 58, no. 2, p. 2259, 1998.

[7] J.-P. Douliez, A. Leonard, and E. J. Dufourc, "Restatement of order parameters in biomembranes: calculation of cc bond order parameters from cd quadrupolar splittings," *Biophysical journal*, vol. 68, no. 5, pp. 1727–1739, 1995.

[8] J. Davies and D. Davies, "Origins and evolution of antibiotic resistance," *Microbiology and Molecular Biology Reviews*, vol. 74, no. 3, pp. 417–433, 2010.

[9] J. L. M. R. K. R. P. W. B. Alberts, A. Johnson, *Molecular Biology of The Cell*. New York: Garland Science, 5st ed., 2008.

[10] W. H. Organization, *The Global Eradication of Smallpox: Final Report of the Global Commission for the Certification of Smallpox Eradication*. Geneva: World Health Organization, 1980.

[11] A. D. Lopez, C. D. Mathers, M. Ezzati, D. T. Jamison, and C. J. Murray, "Global and regional burden of disease and risk factors, 2001: systematic analysis of population health data," *The Lancet*, vol. 367, no. 9524, pp. 1747–1757, 2006.

[12] A. J. Alanis, "Resistance to antibiotics: are we in the post-antibiotic era?," *Archives of medical research*, vol. 36, no. 6, pp. 697–705, 2005.

[13] H. C. Neu, "The crisis in antibiotic resistance," *Science*, vol. 257, no. 5073, pp. 1064–1073, 1992.

[14] H. Zeya and J. K. Spitznagel, "Antibacterial and enzymic basic proteins from leukocyte lysosomes: separation and identification," *Science*, vol. 142, no. 3595, pp. 1085–1087, 1963.

[15] R. J. Dubos, "Studies on a bactericidal agent extracted from a soil bacillus: I. preparation of the agent. its activity in vitro," *The Journal of experimental medicine*, vol. 70, no. 1, p. 1, 1939.

[16] K. OHTANI, T. OKADA, H. YOSHIZUMI, and H. KAGAMIYAMA, "Complete primary structures of two subunits of purothionin a, a lethal protein for brewer's yeast from wheat flour," *Journal of biochemistry*, vol. 82, no. 3, pp. 753–767, 1977.

[17] M. Groves, R. Peterson, and C. Kiddy, "Polymorphism in the red protein isolated from milk of individual cows," 1965.

[18] T. Nakamura, H. Furunaka, T. Miyata, F. Tokunaga, T. Muta, S. Iwanaga, M. Niwa, T. Takao, and Y. Shimonishi, "Tachyplesin, a class of antimicrobial peptide from the hemocytes of the horseshoe crab (tachypleus tridentatus). isolation and chemical structure.," *Journal of Biological Chemistry*, vol. 263, no. 32, pp. 16709–16713, 1988.

[19] J. G. Hirsch, "Phagocytin: a bactericidal substance from polymorphonuclear leucocytes," *The Journal of experimental medicine*, vol. 103, no. 5, pp. 589–611, 1956.

[20] K. Reddy, R. Yedery, and C. Aranha, "Antimicrobial peptides: premises and promises," *International journal of antimicrobial agents*, vol. 24, no. 6, pp. 536–547, 2004.

[21] M. A. R. B. Castanho, *Membrane Active Peptides: Methods and Results on Structure and Function*. California: International University Line, 1st ed., 2009.

[22] A. A. Bahar and D. Ren, "Antimicrobial peptides," *Pharmaceuticals*, vol. 6, no. 12, pp. 1543–1575, 2013.

[23] X. Zhao, H. Wu, H. Lu, G. Li, and Q. Huang, "Lamp: A database linking antimicrobial peptides," *PLoS One*, vol. 8, no. 6, p. e66557, 2013.

[24] G. Wang, X. Li, and Z. Wang, "Apd2: the updated antimicrobial peptide database and its application in peptide design," *Nucleic acids research*, vol. 37, no. suppl 1, pp. D933–D937, 2009.

[25] C. D. Fjell, J. A. Hiss, R. E. Hancock, and G. Schneider, "Designing antimicrobial peptides: form follows function," *Nature reviews Drug discovery*, vol. 11, no. 1, pp. 37–51, 2011.

[26] J. Svenson, W. Stensen, B.-O. Brandsdal, B. E. Haug, J. Monrad, and J. S. Svendsen, "Antimicrobial peptides with stability toward tryptic degradation†," *Biochemistry*, vol. 47, no. 12, pp. 3777–3788, 2008.

[27] R. E. Hancock and H.-G. Sahl, "Antimicrobial and host-defense peptides as new anti-infective therapeutic strategies," *Nature biotechnology*, vol. 24, no. 12, pp. 1551–1557, 2006.

[28] J. Isaksson, B. O. Brandsdal, M. Engqvist, G. E. Flaten, J. S. M. Svendsen, and W. Stensen, "A synthetic antimicrobial peptidomimetic (ltx 109): stereochemical impact on membrane disruption," *Journal of medicinal chemistry*, vol. 54, no. 16, pp. 5786–5795, 2011.

[29] E. Matyus, C. Kandt, and D. P. Tieleman, "Computer simulation of antimicrobial peptides," *Current medicinal chemistry*, vol. 14, no. 26, pp. 2789–2798, 2007.

[30] B. E. Haug, W. Stensen, M. Kalaaji, O. Rekdal, and J. S. Svendsen, "Synthetic antimicrobial peptidomimetics with therapeutic potential," *Journal of medicinal chemistry*, vol. 51, no. 14, pp. 4306–4314, 2008.

[31] R. Karstad, G. Isaksen, B.-O. Brandsdal, J. S. Svendsen, and J. Svenson, "Unnatural amino acid side chains as s1, s1, and s2 probes yield cationic antimicrobial peptides with stability toward chymotryptic degradation," *Journal of medicinal chemistry*, vol. 53, no. 15, pp. 5558–5566, 2010.

[32] J. Pan, F. A. Heberle, S. Tristram-Nagle, M. Szymanski, M. Koepfinger, J. Katsaras, and N. Kučerka, "Molecular structures of fluid phase phosphatidylglycerol bilayers as determined by small angle neutron and x-ray scattering," *Biochimica et Biophysica Acta (BBA)-Biomembranes*, vol. 1818, no. 9, pp. 2135–2148, 2012.

[33] G. W. Feigenson and J. T. Buboltz, "Ternary phase diagram of dipalmitoyl-pc/dilauroyl-pc/cholesterol: nanoscopic domain formation driven by cholesterol," *Biophysical journal*, vol. 80, no. 6, pp. 2775–2788, 2001.

[34] G. Van Meer, D. R. Voelker, and G. W. Feigenson, "Membrane lipids: where they are and how they behave," *Nature reviews molecular cell biology*, vol. 9, no. 2, pp. 112–124, 2008.

[35] R. F. Epand, J. E. Pollard, J. O. Wright, P. B. Savage, and R. M. Epand, "Depolarization, bacterial membrane composition, and the antimicrobial action of ceragenins," *Antimicrobial agents and chemotherapy*, vol. 54, no. 9, pp. 3708–3713, 2010.

[36] H. Goldfine, "Bacterial membranes and lipid packing theory.," *Journal of lipid research*, vol. 25, no. 13, pp. 1501–1507, 1984.

[37] M. A. Haque and N. J. Russell, "Strains of bacillus cereus vary in the phenotypic adaptation of their membrane lipid composition in response to low water activity, reduced temperature and growth in rice starch," *Microbiology*, vol. 150, no. 5, pp. 1397–1404, 2004.

[38] W. W. Navarre and O. Schneewind, "Surface proteins of gram-positive bacteria and mechanisms of their targeting to the cell wall envelope," *Microbiology and Molecular Biology Reviews*, vol. 63, no. 1, pp. 174–229, 1999.

[39] S. Clejan, T. Krulwich, K. Mondrus, and D. Seto-Young, "Membrane lipid composition of obligately and facultatively alkalophilic strains of bacillus spp.," *Journal of bacteriology*, vol. 168, no. 1, pp. 334–340, 1986.

[40] S. Morein, A.-S. Andersson, L. Rilfors, and G. Lindblom, "Wild-type escherichia coli cells regulate the membrane lipid composition in a window between gel and non-lamellar structures," *Journal of Biological Chemistry*, vol. 271, no. 12, pp. 6801–6809, 1996.

[41] S. D. Shoemaker and T. K. Vanderlick, "Intramembrane electrostatic interactions destabilize lipid vesicles," *Biophysical journal*, vol. 83, no. 4, pp. 2007–2014, 2002.

[42] G. Cevc, "Membrane electrostatics," *Biochimica et Biophysica Acta (BBA)-Reviews on Biomembranes*, vol. 1031, no. 3, pp. 311–382, 1990.

[43] R. J. Clarke, "The dipole potential of phospholipid membranes and methods for its detection," *Advances in colloid and interface science*, vol. 89, pp. 263–281, 2001.

[44] S. E. Feller, *Computational modeling of Membrane Bilayers*. London: ACADEMIC PRESS, 1st ed., 2008.

[45] R. Vácha, P. Jurkiewicz, M. Petrov, M. L. Berkowitz, R. A. Bockmann, J. Barucha-Kraszewska, M. Hof, and P. Jungwirth, "Mechanism of interaction of monovalent ions with phosphatidylcholine lipid membranes," *The Journal of Physical Chemistry B*, vol. 114, no. 29, pp. 9504–9509, 2010.

[46] Y. Zhang and P. S. Cremer, "Interactions between macromolecules and ions: the hofmeister series," *Current opinion in chemical biology*, vol. 10, no. 6, pp. 658–663, 2006.

[47] A. R. Leach, *Molecular modelling; principles and applications*. Essex: Person Education, 2st ed., 2001.

[48] B. Alder and T. Wainwright, "Phase transition for a hard sphere system," *The Journal of Chemical Physics*, vol. 27, no. 5, pp. 1208–1209, 1957.

[49] J.-P. Ryckaert, G. Ciccotti, and H. J. Berendsen, "Numerical integration of the cartesian equations of motion of a system with constraints: molecular dynamics of¡ i¿ n¡/i¿-alkanes," *Journal of Computational Physics*, vol. 23, no. 3, pp. 327–341, 1977.

[50] J. F. Nagle and S. Tristram-Nagle, "Structure of lipid bilayers," *Biochimica et Biophysica Acta (BBA)-Reviews on Biomembranes*, vol. 1469, no. 3, pp. 159–195, 2000.

[51] J. Seelig and W. Niederberger, "Two pictures of a lipid bilayer. comparison between deuterium label and spin-label experiments," *Biochemistry*, vol. 13, no. 8, pp. 1585–1588, 1974.

[52] J. B. Klauda, R. M. Venable, J. A. Freites, J. W. O'Connor, D. J. Tobias, C. Mondragon-Ramirez, I. Vorobyov, A. D. MacKerell Jr, and R. W. Pastor, "Update of the charmm all-atom additive force field for lipids: validation on six lipid types," *The journal of physical chemistry B*, vol. 114, no. 23, pp. 7830–7843, 2010.

[53] J. B. K. W. I. Sunhwan Jo, Joseph B. Lim, "Charmm-gui membrane builder for mixed bilayers and its application to yeast membranes," *Biophysical Journal*, vol. 97, no. 1, p. 50–58, 2009.

[54] W. Humphrey, A. Dalke, and K. Schulten, "VMD – Visual Molecular Dynamics," *Journal of Molecular Graphics*, vol. 14, pp. 33–38, 1996.

[55] S. Y. Noskov and B. Roux, "Control of ion selectivity in leut: Two na¡ sup¿+¡/sup¿ binding sites with two different mechanisms," *Journal of molecular biology*, vol. 377, no. 3, pp. 804–818, 2008.

[56] B. Egwolf, Y. Luo, D. E. Walters, and B. Roux, "Ion selectivity of α-hemolysin with β-cyclodextrin adapter. ii. multi-ion effects studied with grand canonical monte carlo/brownian dynamics simulations," *The Journal of Physical Chemistry B*, vol. 114, no. 8, pp. 2901–2909, 2010.

[57] R. M. Venable, Y. Luo, K. Gawrisch, B. Roux, and R. W. Pastor, "Simulations of anionic lipid membranes: Development of interaction-specific ion parameters and validation using nmr data," *The Journal of Physical Chemistry B*, vol. 117, no. 35, pp. 10183–10192, 2013.

[58] J. C. Phillips, R. Braun, W. Wang, J. Gumbart, E. Tajkhorshid, E. Villa, C. Chipot, R. D. Skeel, L. Kale, and K. Schulten, "Scalable molecular dynamics with namd," *Journal of computational chemistry*, vol. 26, no. 16, pp. 1781–1802, 2005.

[59] S. E. Feller, Y. Zhang, R. W. Pastor, and B. R. Brooks, "Constant pressure molecular dynamics simulation: the langevin piston method," *The Journal of Chemical Physics*, vol. 103, no. 11, pp. 4613–4621, 1995.

[60] U. Essmann, L. Perera, M. L. Berkowitz, T. Darden, H. Lee, and L. G. Pedersen, "A smooth particle mesh ewald method," *The Journal of chemical physics*, vol. 103, no. 19, pp. 8577–8593, 1995.

[61] K. Vanommeslaeghe, E. Hatcher, C. Acharya, S. Kundu, S. Zhong, J. Shim, E. Darian, O. Guvench, P. Lopes, I. Vorobyov, *et al.*, "Charmm general force field: A force field for drug-like molecules compatible with the charmm all-atom additive biological force fields," *Journal of computational chemistry*, vol. 31, no. 4, pp. 671–690, 2010.

[62] R. Guixà-González, I. Rodriguez-Espigares, J. M. Ramírez-Anguita, P. Carrió-Gaspar, H. Martinez-Seara, T. Giorgino, and J. Selent, "Membplugin: studying membrane complexity in vmd," *Bioinformatics*, vol. 30, no. 10, pp. 1478–1480, 2014.

[63] W. Shinoda and S. Okazaki, "A voronoi analysis of lipid area fluctuation in a bilayer," *The Journal of chemical physics*, vol. 109, no. 4, pp. 1517–1521, 1998.

[64] L. S. Vermeer, B. L. De Groot, V. Réat, A. Milon, and J. Czaplicki, "Acyl chain order parameter profiles in phospholipid bilayers: computation from molecular dynamics simulations and comparison with 2h nmr experiments," *European Biophysics Journal*, vol. 36, no. 8, pp. 919–931, 2007.

[65] H. I. Petrache, S. W. Dodd, and M. F. Brown, "Area per lipid and acyl length distributions in fluid phosphatidylcholines determined by¡ sup¿ 2¡/sup¿ h nmr spectroscopy," *Biophysical journal*, vol. 79, no. 6, pp. 3172–3192, 2000.

[66] F. Sixl and A. Watts, "Interactions between phospholipid head groups at membrane interfaces: a deuterium and phosphorus nmr and spin-label esr study," *Biochemistry*, vol. 21, no. 25, pp. 6446–6452, 1982.

[67] T. Bayerl, T. Köchy, and S. Brückner, "On the modulation of a high-enthalpy pretransition in binary mixtures of dmpc and dmpg by polar headgroup interaction," *Biophysical journal*, vol. 57, no. 3, pp. 675–680, 1990.

[68] H. Binder and O. Zschörnig, "The effect of metal cations on the phase behavior and hydration characteristics of phospholipid membranes," *Chemistry and physics of lipids*, vol. 115, no. 1, pp. 39–61, 2002.

[69] J. J. Garcia-Celma, L. Hatahet, W. Kunz, and K. Fendler, "Specific anion and cation binding to lipid membranes investigated on a solid supported membrane," *Langmuir*, vol. 23, no. 20, pp. 10074–10080, 2007.

[70] U. R. Pedersen, C. Leidy, P. Westh, and G. H. Peters, "The effect of calcium on the properties of charged phospholipid bilayers," *Biochimica et Biophysica Acta (BBA)-Biomembranes*, vol. 1758, no. 5, pp. 573–582, 2006.

[71] S. A. Pandit, D. Bostick, and M. L. Berkowitz, "Molecular dynamics simulation of a dipalmitoylphosphatidylcholine bilayer with nacl," *Biophysical journal*, vol. 84, no. 6, pp. 3743–3750, 2003.

[72] W. Zhao, T. Róg, A. A. Gurtovenko, I. Vattulainen, and M. Karttunen, "Atomic-scale structure and electrostatics of anionic palmitoyloleoylphosphatidylglycerol lipid bilayers with na¡ sup¿+¡/sup¿ counterions," *Biophysical journal*, vol. 92, no. 4, pp. 1114–1124, 2007.

[73] A. A. Gurtovenko and I. Vattulainen, "Effect of nacl and kcl on phosphatidylcholine and phosphatidylethanolamine lipid membranes: insight from atomic-scale simulations for understanding salt-induced effects in the plasma membrane," *The Journal of Physical Chemistry B*, vol. 112, no. 7, pp. 1953–1962, 2008.

[74] O. Berger, O. Edholm, and F. Jähnig, "Molecular dynamics simulations of a fluid bilayer of dipalmitoylphosphatidylcholine at full hydration, constant pressure, and constant temperature," *Biophysical journal*, vol. 72, no. 5, pp. 2002–2013, 1997.

[75] D. Beglov and B. Roux, "Finite representation of an infinite bulk system: solvent boundary potential for computer simulations," *The Journal of chemical physics*, vol. 100, no. 12, pp. 9050–9063, 1994.

[76] R. N. Lewis, Y.-P. Zhang, and R. N. McElhaney, "Calorimetric and spectroscopic studies of the phase behavior and organization of lipid bilayer model membranes composed of binary mixtures of dimyristoylphosphatidylcholine and dimyristoylphosphatidylglycerol," *Biochimica et Biophysica Acta (BBA)-Biomembranes*, vol. 1668, no. 2, pp. 203–214, 2005.

[77] P. Garidel, C. Johann, L. Mennicke, and A. Blume, "The mixing behavior of pseudobinary phosphatidylcholine-phosphatidylglycerol mixtures as a function of ph and chain length," *European biophysics journal*, vol. 26, no. 6, pp. 447–459, 1997.

[78] E. J. Findlay and P. G. Barton, "Phase behavior of synthetic phosphatidylglycerols and binary mixtures with phosphatidylcholines in the presence and absence of calcium ions," *Biochemistry*, vol. 17, no. 12, pp. 2400–2405, 1978.

[79] W.-M. Yau, W. C. Wimley, K. Gawrisch, and S. H. White, "The preference of tryptophan for membrane interfaces," *Biochemistry*, vol. 37, no. 42, pp. 14713–14718, 1998.

[80] S. Persson, J. Antoinette Killian, and G. Lindblom, "Molecular ordering of interfacially localized tryptophan analogs in ester-and ether-lipid bilayers studied by¡ sup¿ 2¡/sup¿ h-nmr," *Biophysical journal*, vol. 75, no. 3, pp. 1365–1371, 1998.

[81] D. I. Chan, E. J. Prenner, and H. J. Vogel, "Tryptophan-and arginine-rich antimicrobial peptides: structures and mechanisms of action," *Biochimica et Biophysica Acta (BBA)-Biomembranes*, vol. 1758, no. 9, pp. 1184–1202, 2006.

[82] A. R. Braun, E. G. Brandt, O. Edholm, J. F. Nagle, and J. N. Sachs, "Determination of electron density profiles and area from simulations of undulating membranes," *Biophysical journal*, vol. 100, no. 9, pp. 2112–2120, 2011.

[83] H. Leontiadou, A. E. Mark, and S. J. Marrink, "Antimicrobial peptides in action," *Journal of the American Chemical Society*, vol. 128, no. 37, pp. 12156–12161, 2006.

[84] H. W. Huang, "Molecular mechanism of antimicrobial peptides: the origin of cooperativity," *Biochimica et Biophysica Acta (BBA)-Biomembranes*, vol. 1758, no. 9, pp. 1292–1302, 2006.

[85] A. A. Polyansky, R. Ramaswamy, P. E. Volynsky, I. F. Sbalzarini, S. J. Marrink, and R. G. Efremov, "Antimicrobial peptides induce growth of phosphatidylglycerol domains in a model bacterial membrane," *The Journal of Physical Chemistry Letters*, vol. 1, no. 20, pp. 3108–3111, 2010.

Appendix A

Effect of NaCl and KCl on Area Per Lipid Head Group A[$\text{Å}^2/lipid$]

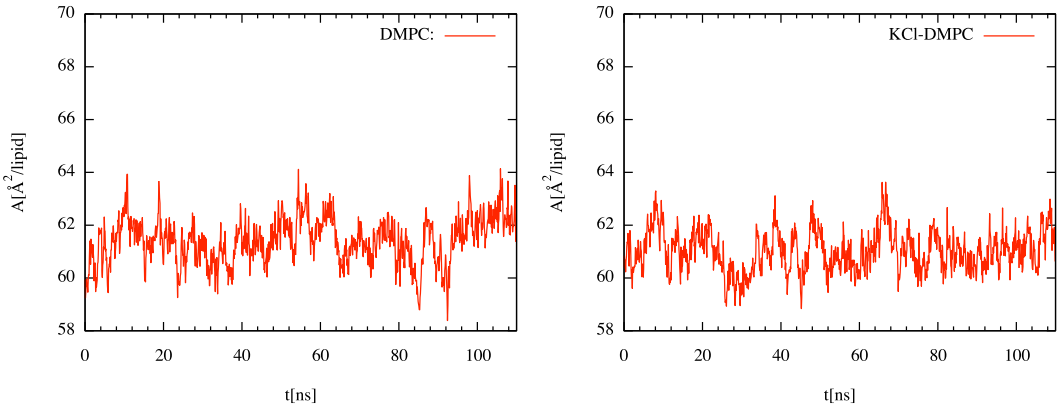

(a) *Without ions.*

(b) *With 154 mM KCl.*

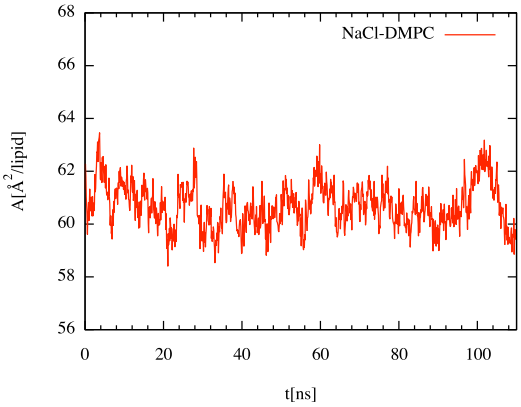

(c) *With 154 mM NaCl.*

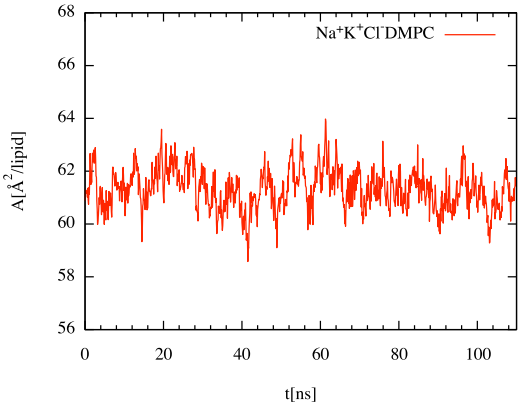

(d) *With in total 154 mM NaCl and KCl.*

Figure A.1: *Area per lipid of various DMPC lipid bilayers.*

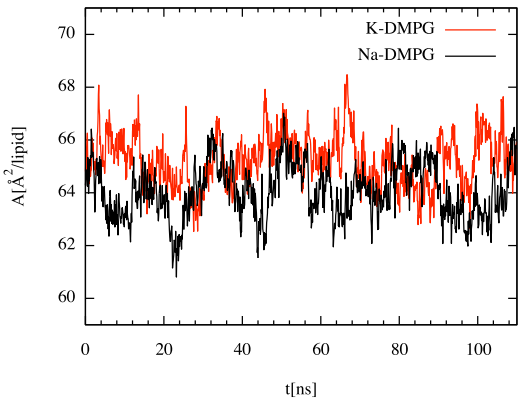

(a) *Two different DMPG lipid bilayer with either Na^+ or K^+ as counter-ions.*

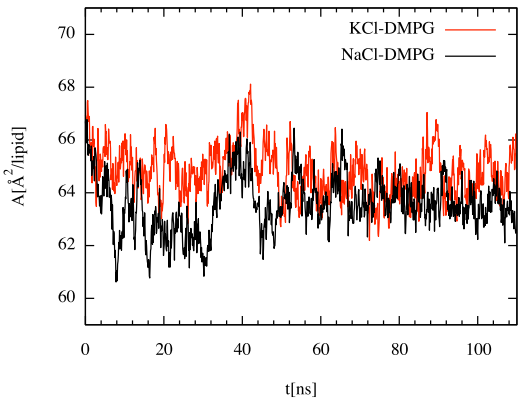

(b) *Two different bilayers with either 154 mM KCl or 154 mM NaCl.*

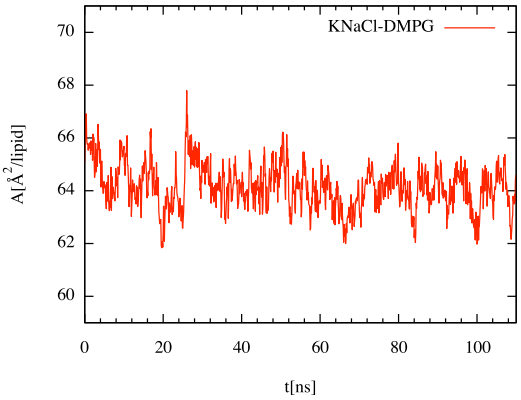

(c) *With 154 mM KCl and NaCl.*

Figure A.2: *Area per lipid of various DMPG lipid bilayers.*

Appendix B

Time Evolution of Cordination Number N_C of Ions with Carbonyl, Phosphate, glycerol and Water Oxygens

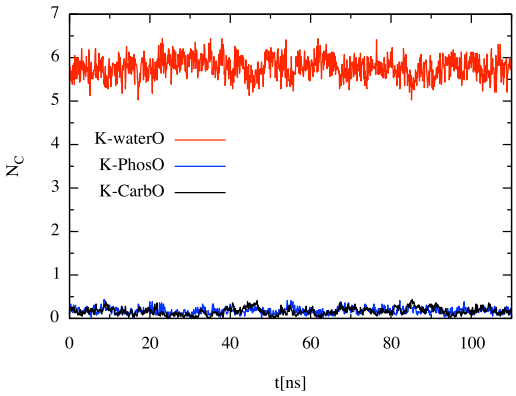

(a) *N_C of K^+ ions in system with 154 mM KCl.*

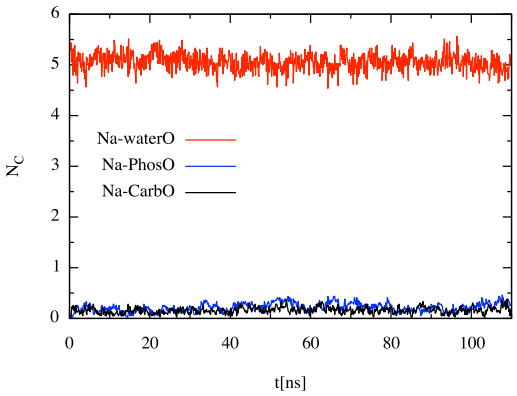

(b) *N_C of Na^+ ions in system with 154 mM NaCl.*

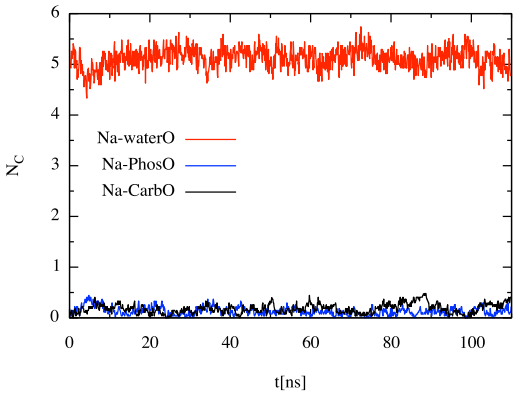

(c) *N_C for Na^+ ions (154 mM NaCl and KCl).*

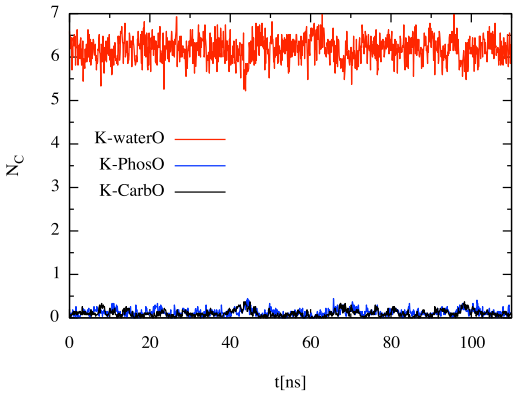

(d) *N_C for K^+ ions (154 mM NaCl and KCl).*

Figure B.1: *Time evolution of coordination number N_C for either K^+ or Na^+ ions with water-, carbonyl- or phosphat oxygens in the DMPC systems.*

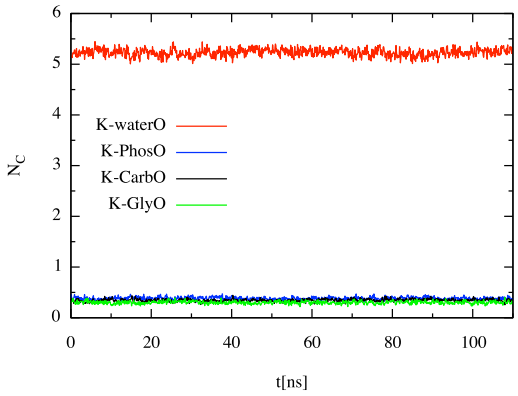

(a) *N_C of K^+ ions (only counter-ions).*

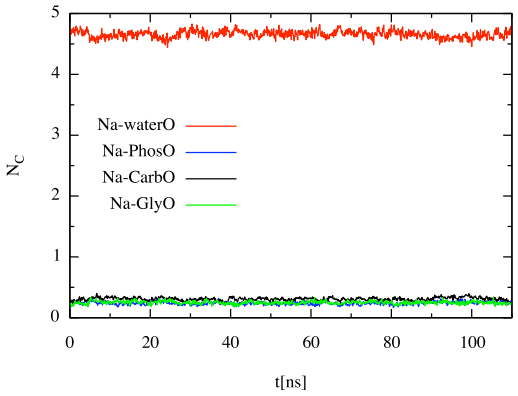

(b) *N_C of Na^+ ions (only counter-ions).*

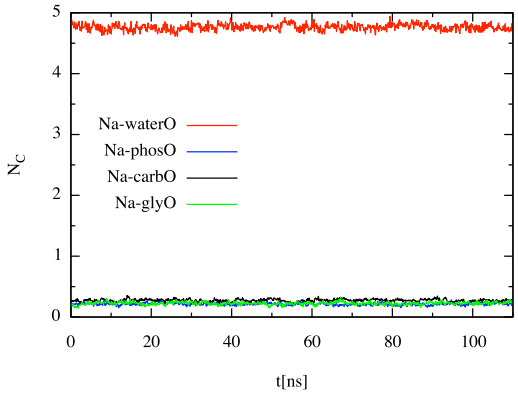

(c) *N_C of Na^+ ions (154 mM NaCl).*

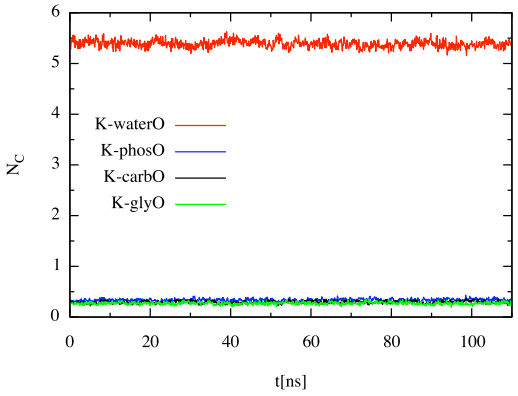

(d) *N_C of K^+ ions (154 mM KCl).*

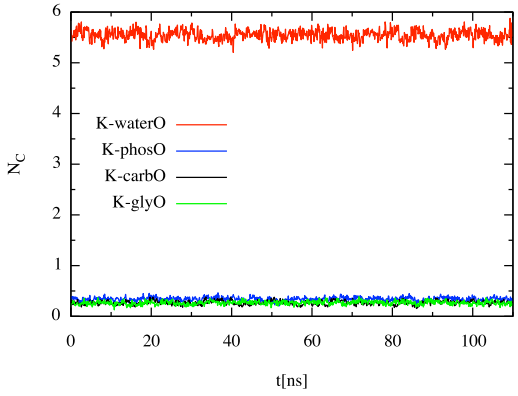

(e) *N_C of K^+ ions (154 mM KCl and NaCl).*

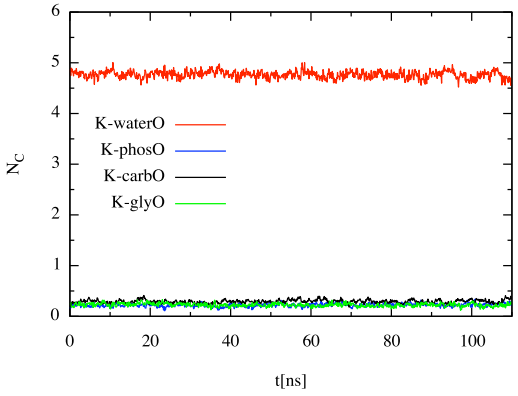

(f) *N_C of Na^+ ions (154 mM KCl and NaCl).*

Figure B.2: *Time evolution of coordination number N_C for either K^+ or Na^+ ions with water-, carbonyl-, phosphat- or glycol oxygens in the DMPG systems.*

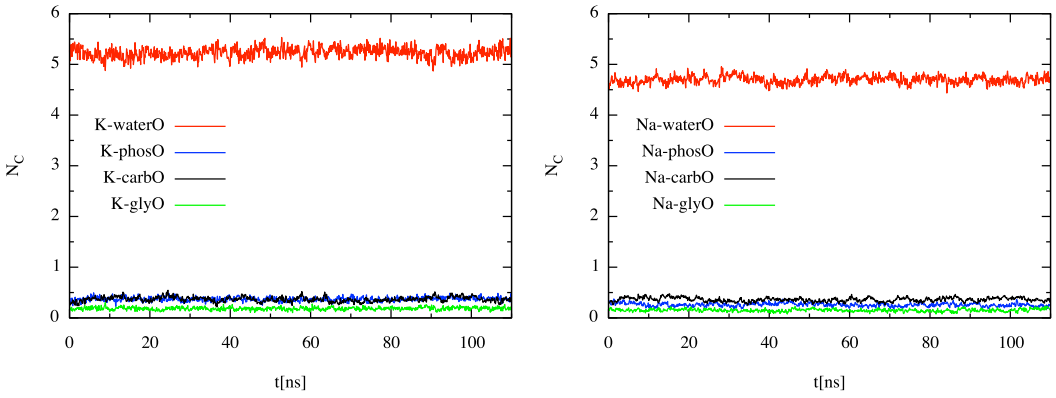

(a) *N_C of K^+ ions, with only counter-ions.*

(b) *N_C of Na^+ ions, with only counter-ions*

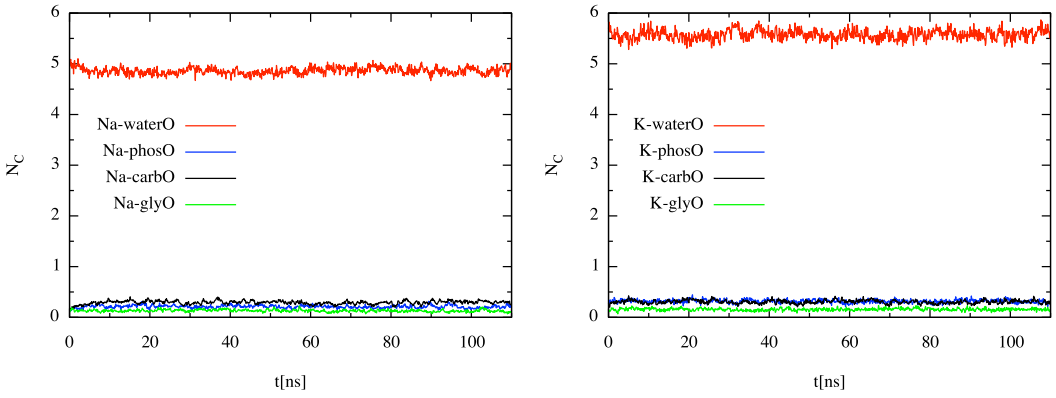

(c) *N_C of Na^+ ions with 154 mM NaCl*

(d) *N_C of K^+ ions with 154 mM KCl*

Figure B.3: *Time evolution of coordination number N_C for either K^+ or Na^+ ions with water-, carbonyl-, phosphat- or glycol oxygens in the mixed DMPC/DMPG systems.*

Appendix C

Order Parameters $\mathbf{S}_{CD}$

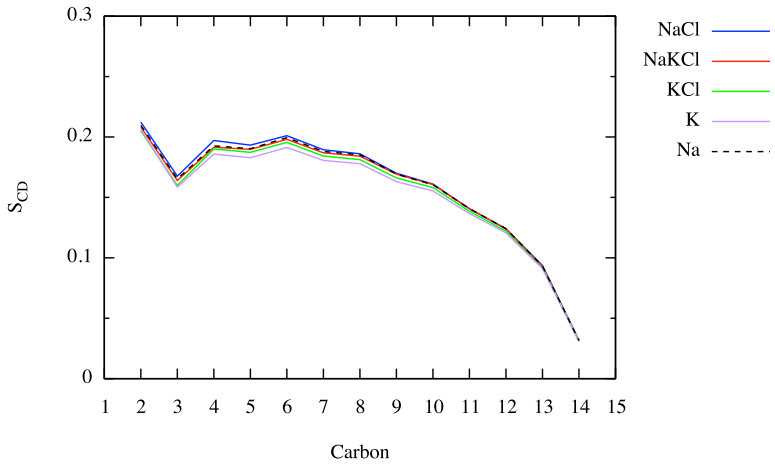

(a) *S_{CD} of the sn-1-chain.*

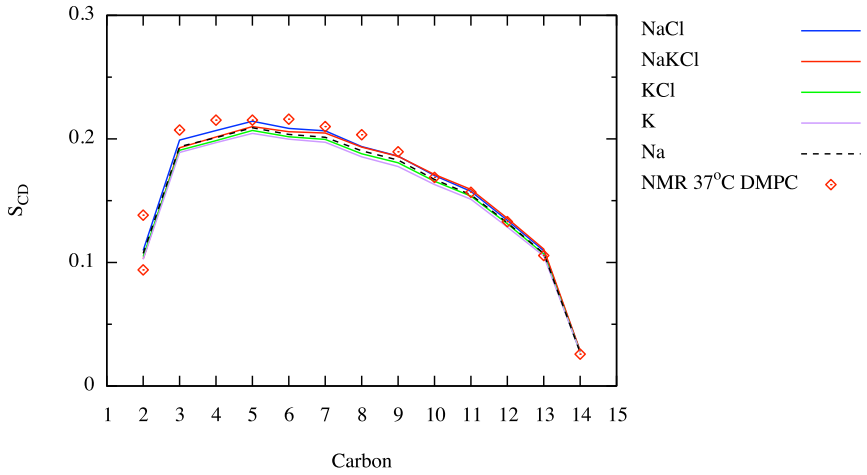

(b) *S_{CD} of the sn-2-chain.*

Figure C.1: *sn-1- (a) and sn-2- (b) acyl chain order parameters (S_{CD}) for all the DMPG systems containing 154 mM NaCl, 154 mM KCl, 154 mM NaCl and KCl, or counter-ions respectively.*

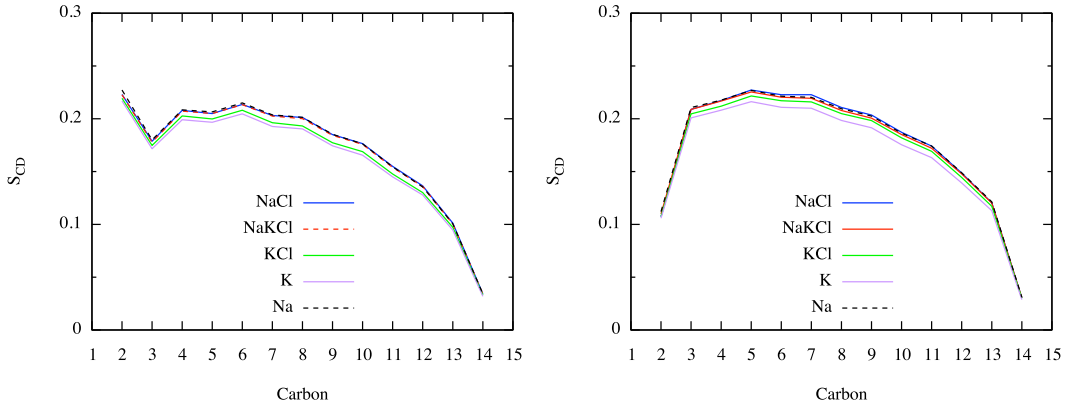

(a) *S_{CD} for sn-1-chain of DMPG lipids.* (b) *S_{CD} for sn-2-chain of DMPG lipids.*

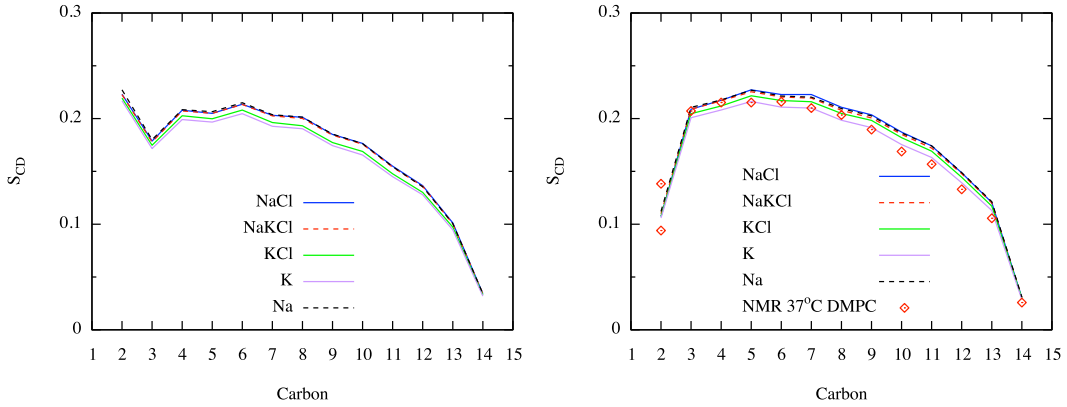

(c) *S_{CD} for sn-1-chain of DMPC lipids.* (d) *S_{CD} for sn-2-chain of DMPC lipids.*

Figure C.2: *sn-1- (a) and sn-2- (b) acyl chain order parameters (S_{CD}) for all the DMPC/DMPG systems containing 154 mM NaCl, 154 mM KCl, 154 mM NaCl and KCl or only counter-ions respectively.*

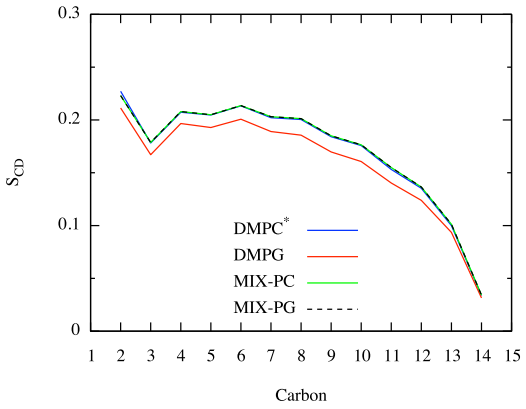

(a) *S_{CD} for sn-1-chain with 154 mM NaCl.*

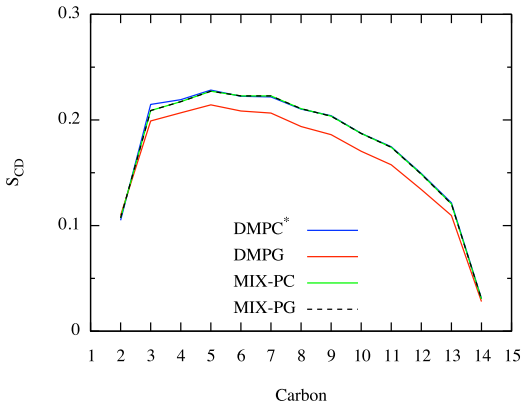

(b) *S_{CD} for sn-2-chain with 154 mM NaCl.*

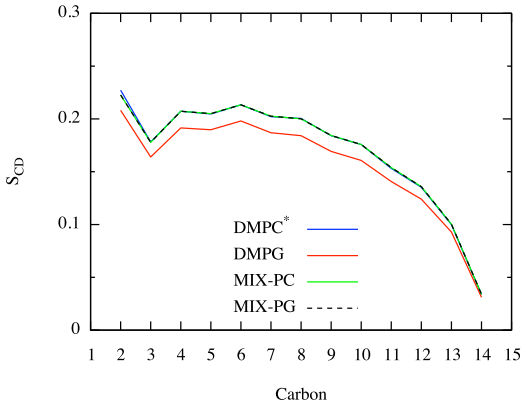

(c) *S_{CD} for sn-1-chain with 154 mM NaKCl.*

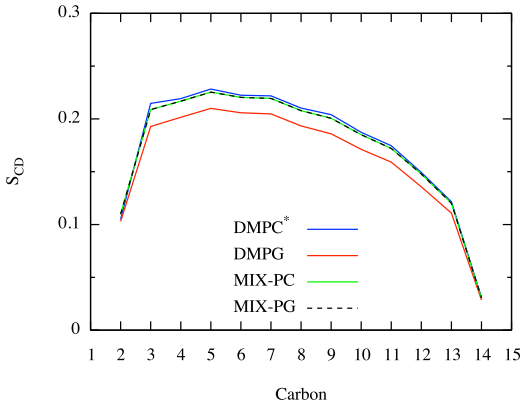

(d) *S_{CD} for sn-2-chain with 154 mM NaKCl.*

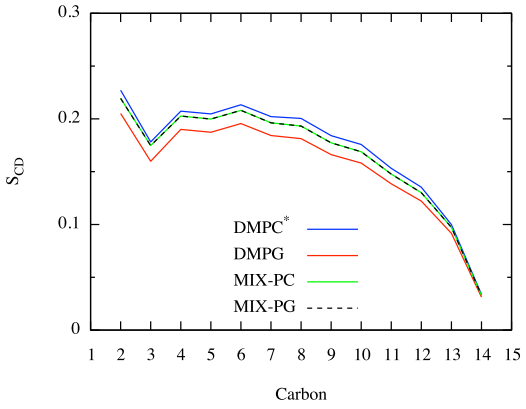

(e) *S_{CD} for sn-1-chain with 154 mM KCl.*

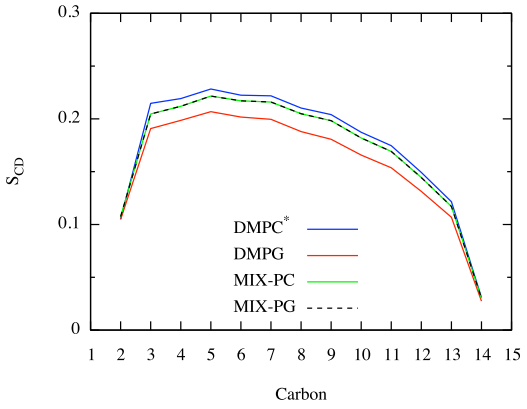

(f) *S_{CD} for sn-2-chain with 154 mM KCl.*

Figure C.3: *The order parameters (S_{CD}) of DMPC * lipids (in system without ions) and DMPG lipids in homogeneous membranes compared with the S_{CD} of a binary mixture of the same lipids, with different ion compositions*

Appendix D

Insertion Trend of the RWR-NHBn Peptide

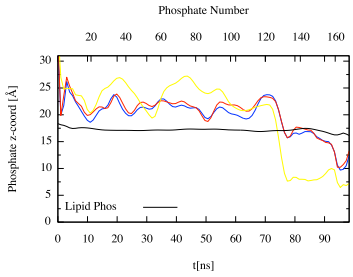

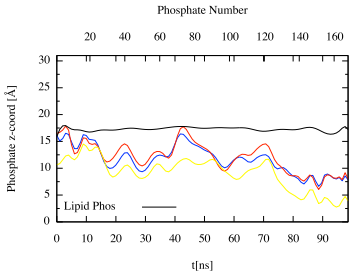

(a) *Pep A; 0 to 200 ns.*

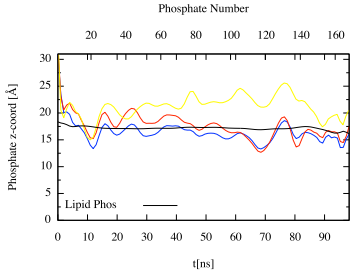

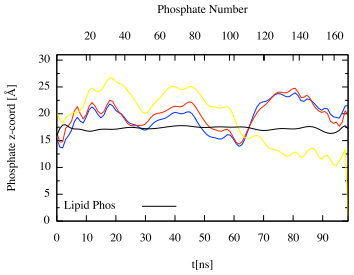

(b) *Pep B; 0 to 200 ns.*

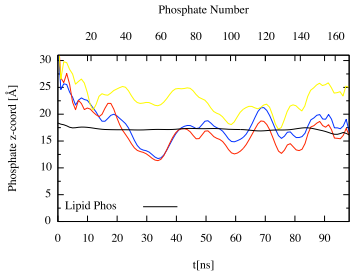

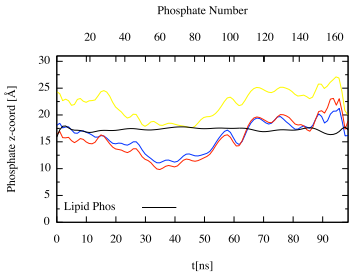

(c) *Pep C; 0 to 200 ns.*

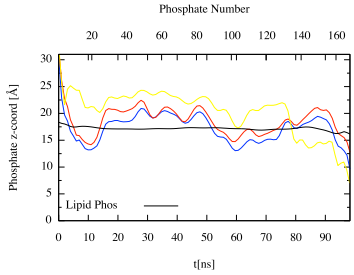

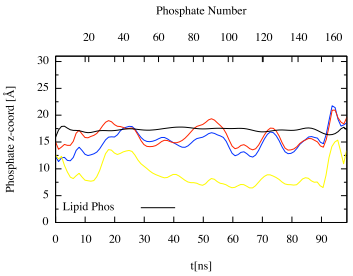

(d) *Pep D; 0 to 200 ns.*

Figure D.1: *System 1, with 4 RWR-NHBn peptides. The trend-lines for the z-coordinate of atoms NE1 (blue) and CH2 (red) on the Tryptophan residue (Figure 2.1). The CG4 atom (yellow) is the first atom on the C-terminal benzyl ring. The z-coord is plottet as a function of time (ns). The black line shows the trend of the phosphate atoms mean z-coordinates in the lipid bilayer leaflet facing the peptides, blotted individually.*

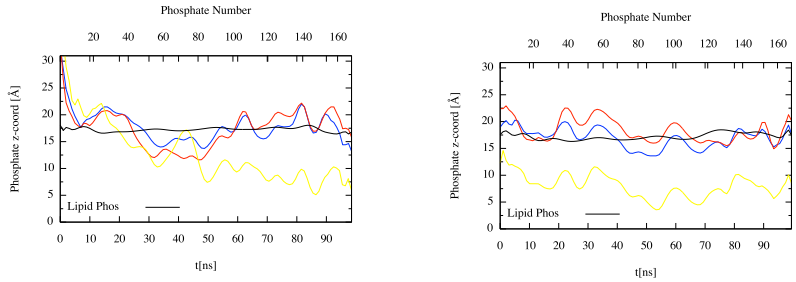

(a) *Pep A; 0 to 200 ns.*

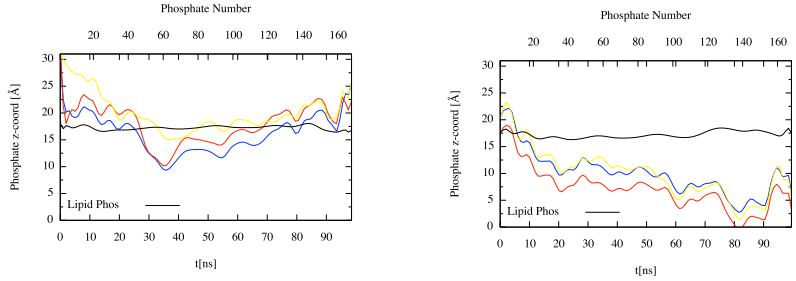

(b) *Pep B; 0 to 200 ns.*

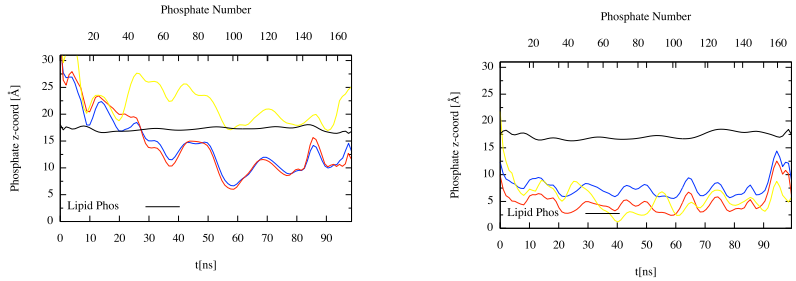

(c) *Pep C; 0 to 200 ns.*

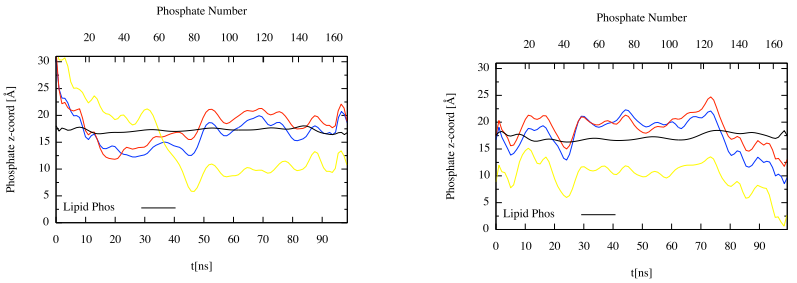

(d) *Pep D; 0 to 200 ns.*

Figure D.2: *System 2, with 4 RWR-NHBn peptides. The trend-lines for the z-coordinate of atoms NE1 (blue) and CH2 (red) on the Tryptophan residue (Figure 2.1). The CG4 atom (yellow) is the first atom on the C-terminal benzyl ring. The z-coord is plottet as a function of time (ns). The black line shows the trend of the phosphate atoms mean z-coordinates in the lipid bilayer leaflet facing the peptides, blotted individually.*

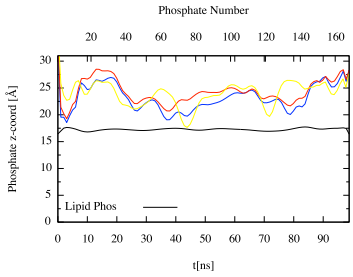

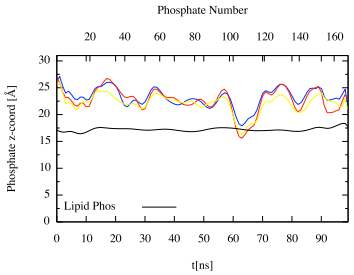

(a) *Pep A; 0 to 200 ns.*

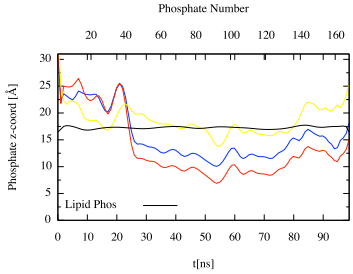

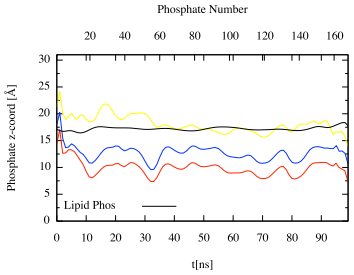

(b) *Pep B; 0 to 200 ns.*

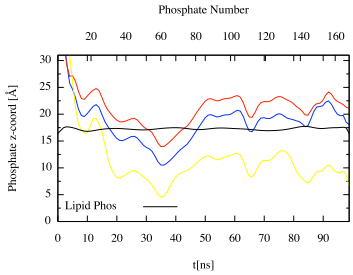

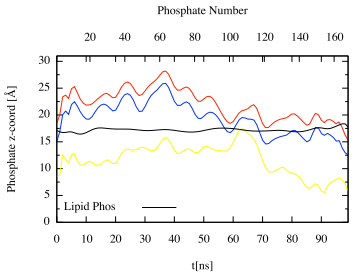

(c) *Pep C; 0 to 200 ns.*

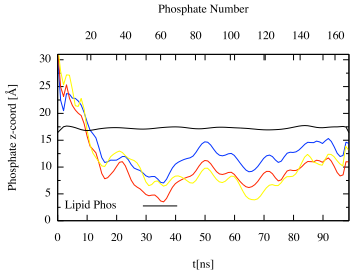

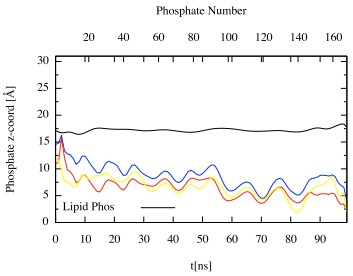

(d) *Pep D; 0 to 200 ns.*

Figure D.3: *System 3, with 4 RWR-NHBn peptides. The trend-lines for the z-coordinate of atoms NE1 (blue) and CH2 (red) on the Tryptophan residue (Figure 2.1). The CG4 atom (yellow) is the first atom on the C-terminal benzyl ring. The z-coord is plottet as a function of time (ns). The black line shows the trend of the phosphate atoms mean z-coordinates in the lipid bilayer leaflet facing the peptides, blotted individually.*

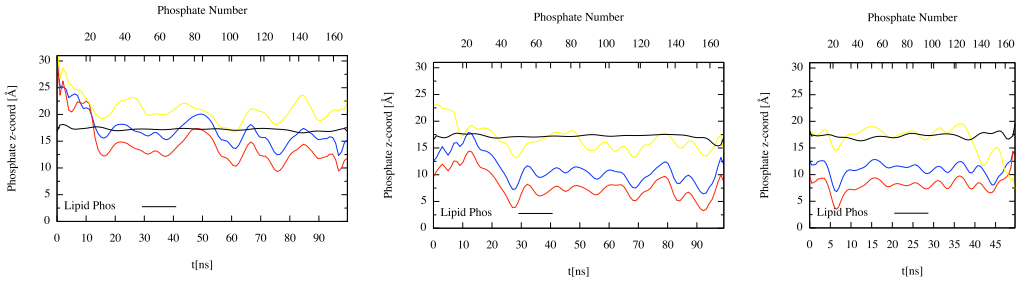

(a) *Pep A; 0 to 250 ns.*

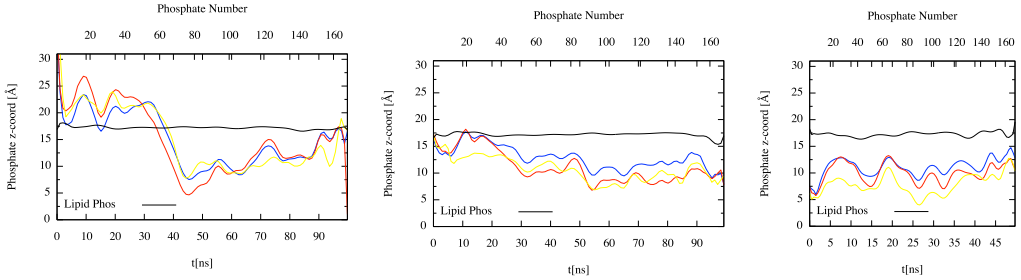

(b) *Pep B; 0 to 250 ns.*

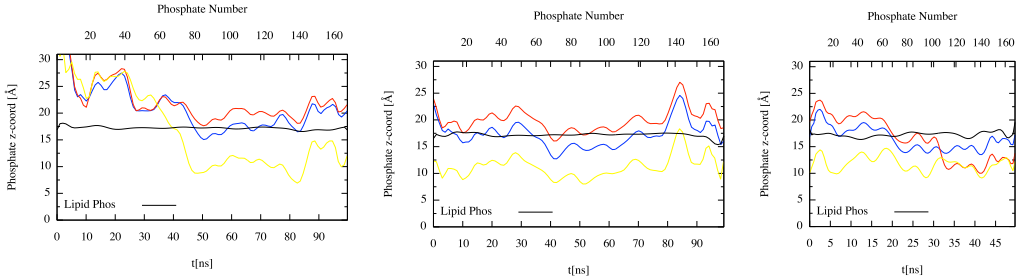

(c) *Pep C; 0 to 250 ns.*

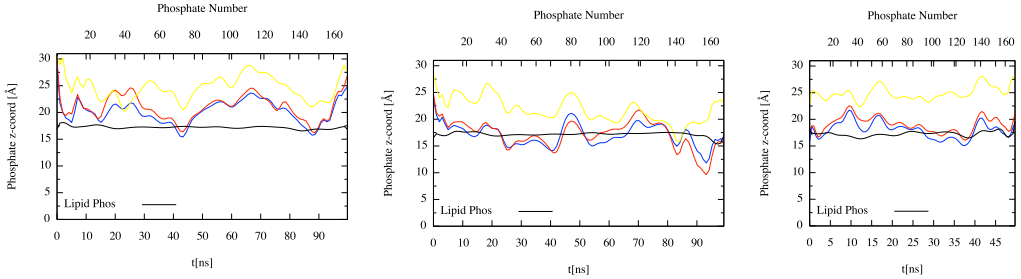

(d) *Pep D; 0 to 250 ns.*

Figure D.4: *System 1, with 8 RWR-NHBn peptides. The trend-lines for the z-coordinate of atoms NE1 (blue) and CH2 (red) on the Tryptophan residue (Figure 2.1). The CG4 atom (yellow) is the first atom on the C-terminal benzyl ring. The z-coord is plottet as a function of time (ns). The black line shows the trend of the phosphate atoms mean z-coordinates in the lipid bilayer leaflet facing the peptides, blotted individually.*

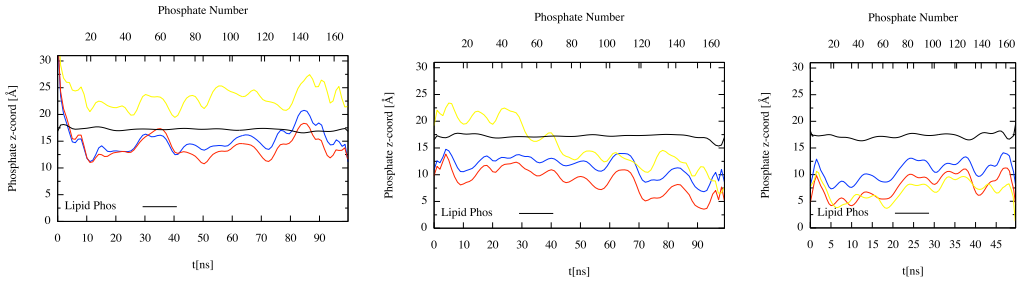

(a) *Pep E; 0 to 250 ns.*

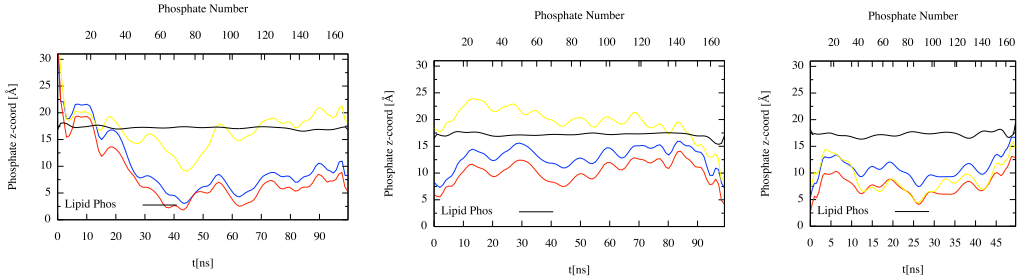

(b) *Pep F; 0 to 250 ns.*

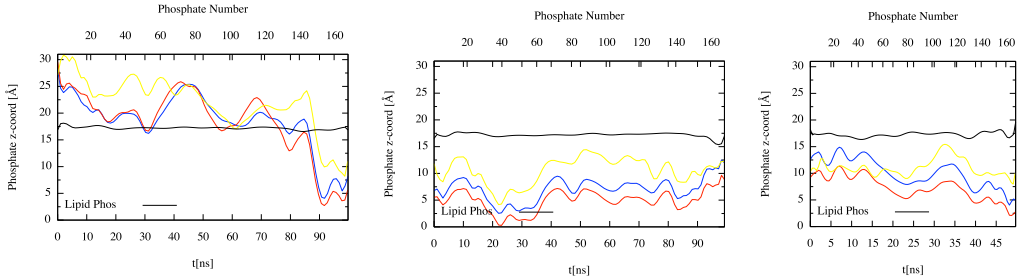

(c) *Pep G; 0 to 250 ns.*

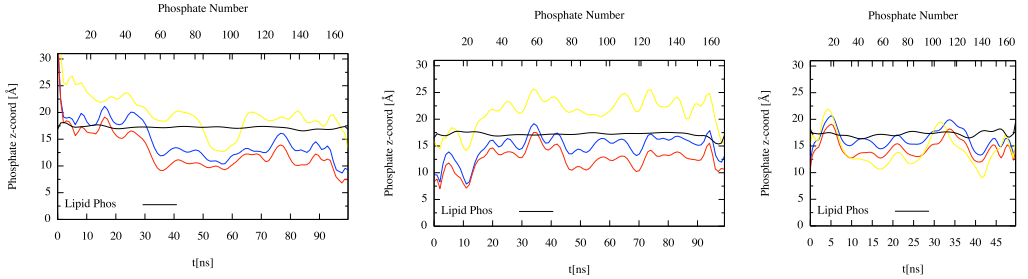

(d) *Pep H; 0 to 250 ns.*

Figure D.5: *System 1, with 8 RWR-NHBn peptides. The trend-lines for the z-coordinate of atoms NE1 (blue) and CH2 (red) on the Tryptophan residue (Figure 2.1). The CG4 atom (yellow) is the first atom on the C-terminal benzyl ring. The z-coord is plottet as a function of time (ns). The black line shows the trend of the phosphate atoms mean z-coordinates in the lipid bilayer leaflet facing the peptides, blotted individually.*

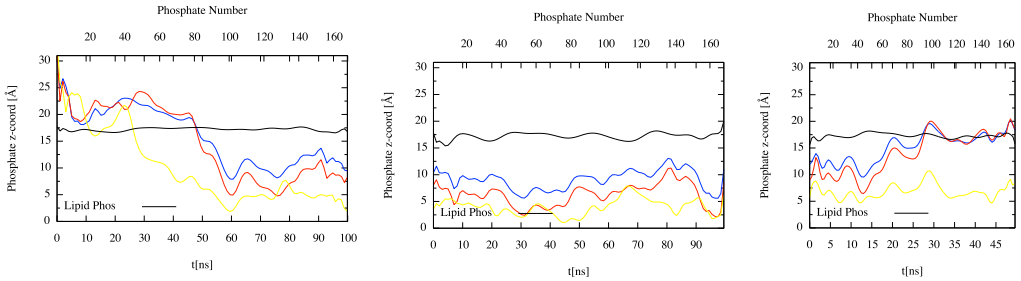

(a) *Pep A; 0 to 250 ns.*

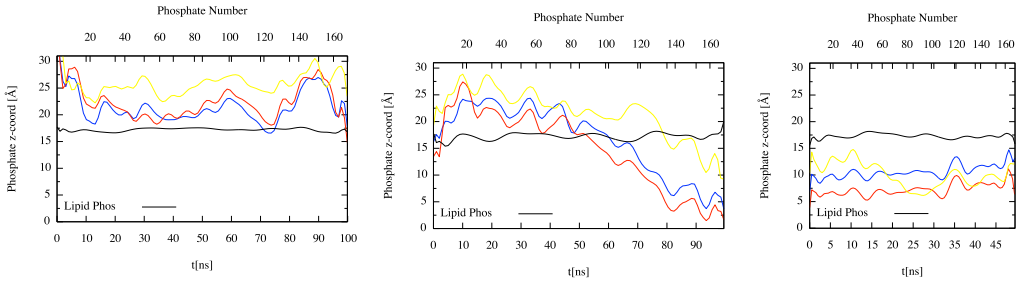

(b) *Pep B; 0 to 250 ns.*

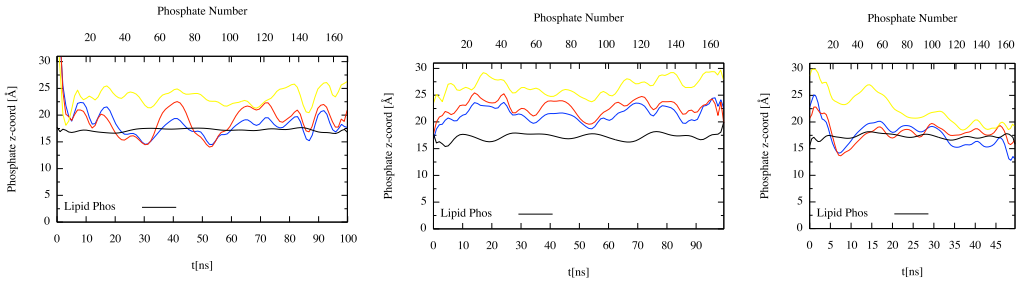

(c) *Pep C; 0 to 250 ns.*

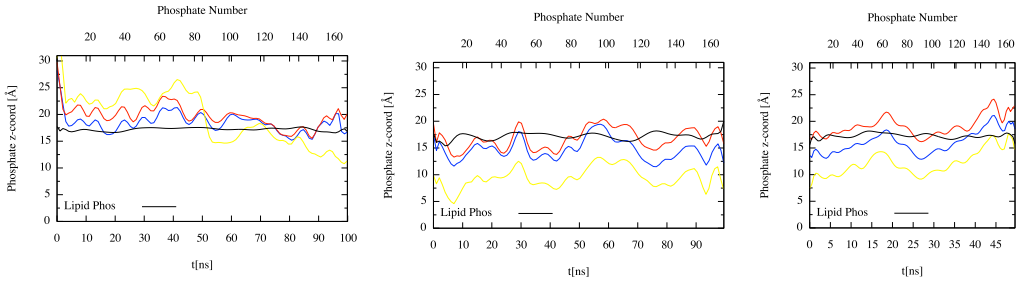

(d) *Pep D; 0 to 250 ns.*

Figure D.6: *System 2, with 8 RWR-NHBn peptides. The trend-lines for the z-coordinate of atoms NE1 (blue) and CH2 (red) on the Tryptophan residue (Figure 2.1). The CG4 atom (yellow) is the first atom on the C-terminal benzyl ring. The z-coord is plottet as a function of time (ns). The black line shows the trend of the phosphate atoms mean z-coordinates in the lipid bilayer leaflet facing the peptides, blotted individually.*

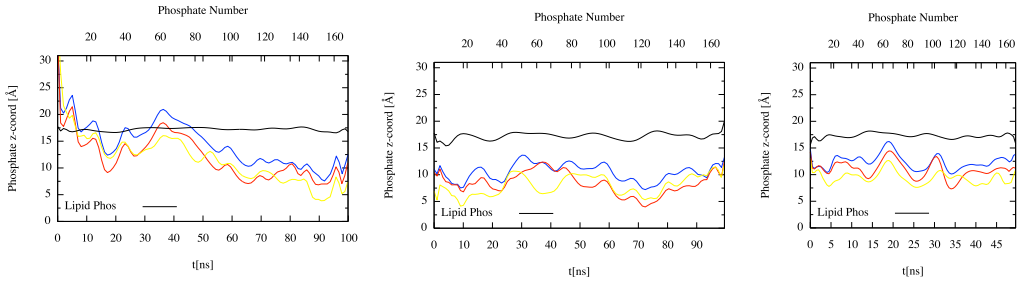

(a) *Pep E; 0 to 250 ns.*

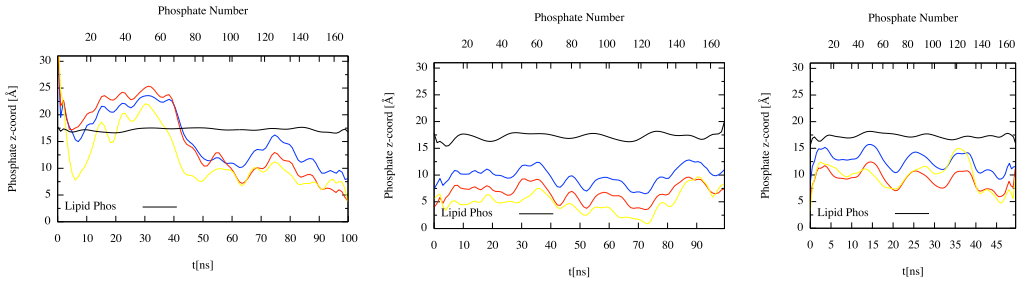

(b) *Pep F; 0 to 250 ns.*

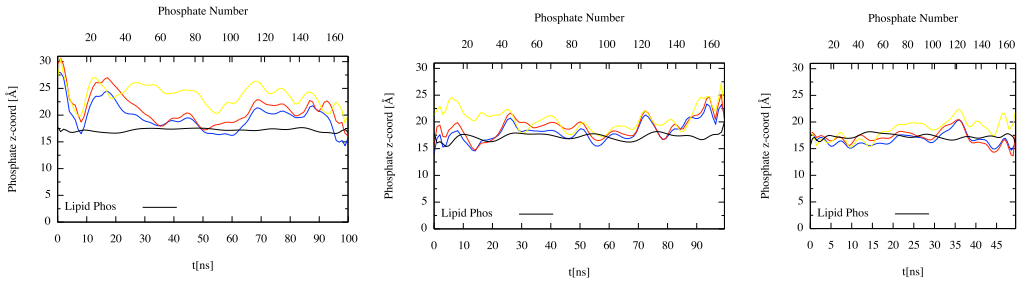

(c) *Pep G; 0 to 250 ns.*

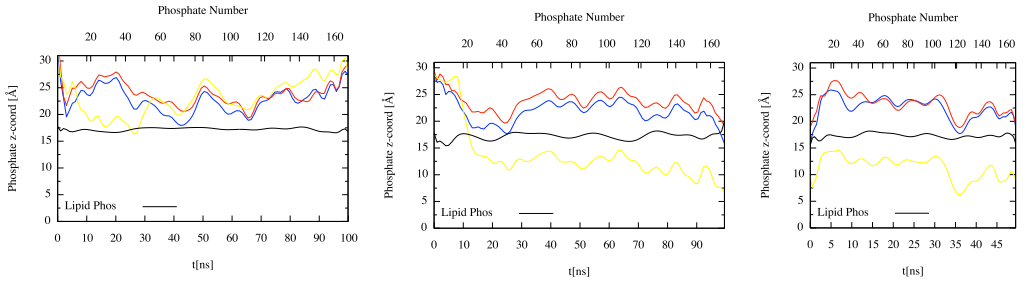

(d) *Pep H; 0 to 250 ns.*

Figure D.7: *System 2, with 8 RWR-NHBn peptides. The trend-lines for the z-coordinate of atoms NE1 (blue) and CH2 (red) on the Tryptophan residue (Figure 2.1). The CG4 atom (yellow) is the first atom on the C-terminal benzyl ring. The z-coord is plottet as a function of time (ns). The black line shows the trend of the phosphate atoms mean z-coordinates in the lipid bilayer leaflet facing the peptides, blotted individually.*

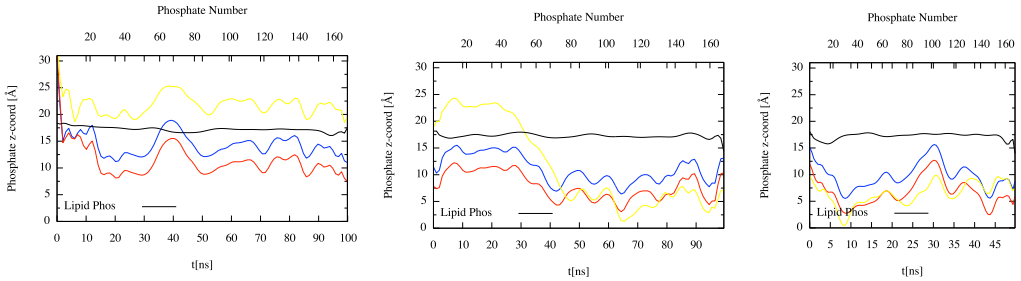

(a) *Pep A; 0 to 250 ns.*

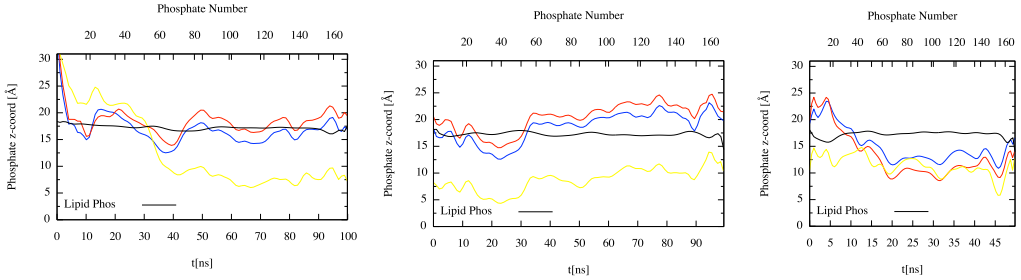

(b) *Pep B; 0 to 250 ns.*

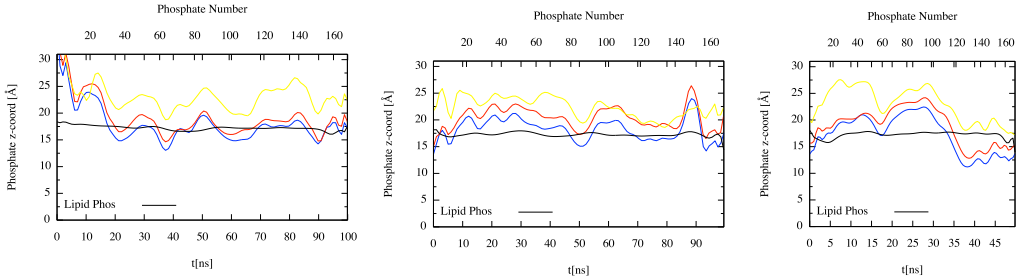

(c) *Pep C; 0 to 250 ns.*

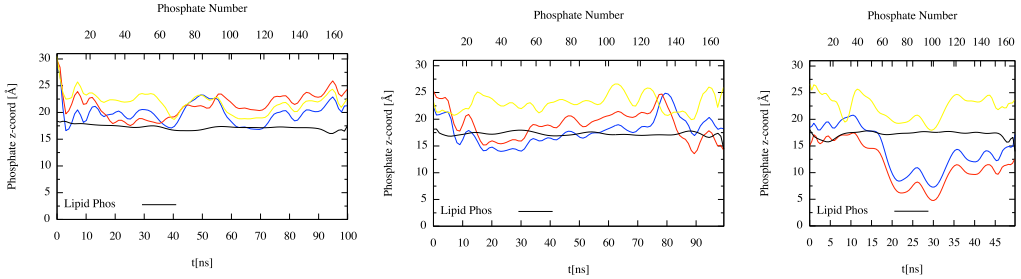

(d) *Pep D; 0 to 250 ns.*

Figure D.8: *System 3, with 8 RWR-NHBn peptides. The trend-lines for the z-coordinate of atoms NE1 (blue) and CH2 (red) on the Tryptophan residue (Figure 2.1). The CG4 atom (yellow) is the first atom on the C-terminal benzyl ring. The z-coord is plottet as a function of time (ns). The black line shows the trend of the phosphate atoms mean z-coordinates in the lipid bilayer leaflet facing the peptides, blotted individually.*

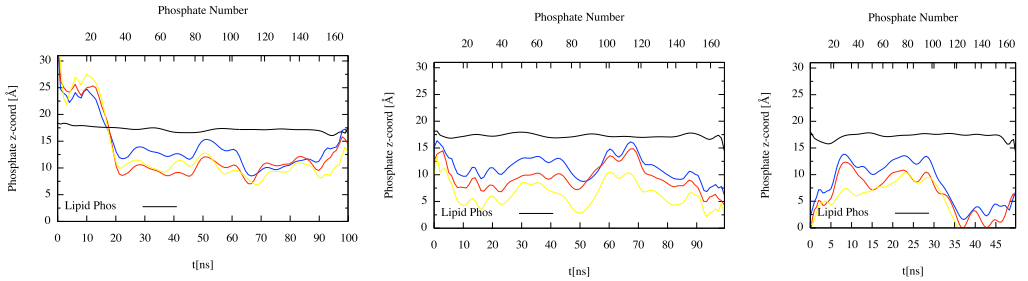

(a) *Pep E; 0 to 250 ns.*

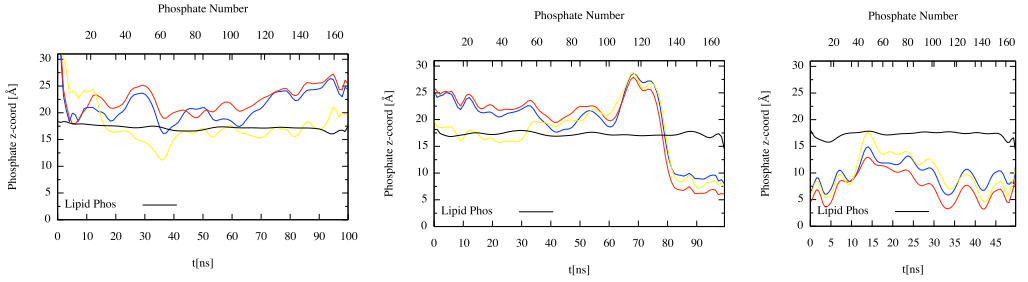

(b) *Pep F; 0 to 250 ns.*

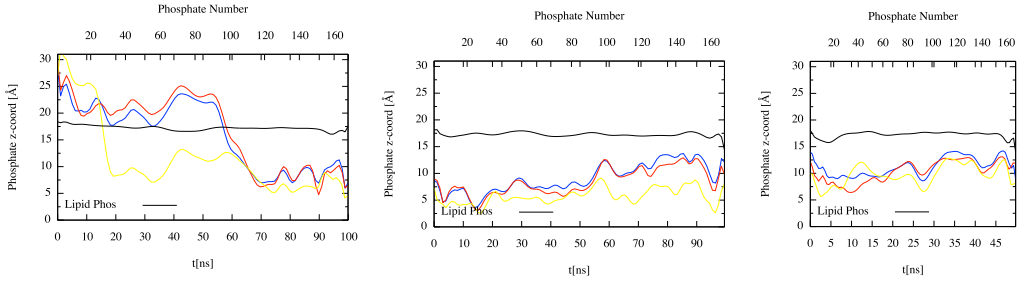

(c) *Pep G; 0 to 250 ns.*

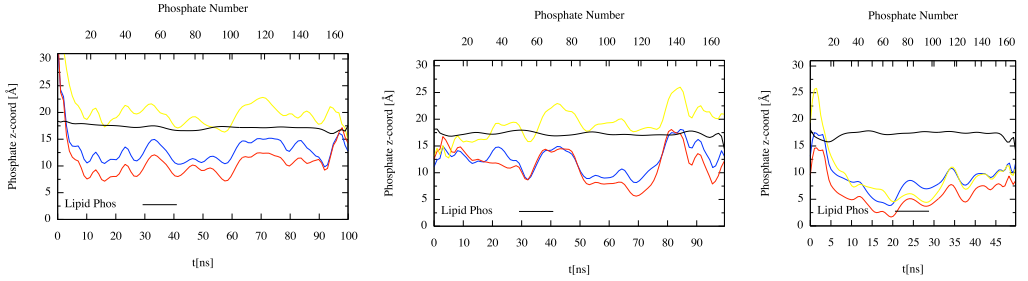

(d) *Pep H; 0 to 250 ns.*

Figure D.9: *System 3, with 8 RWR-NHBn peptides. The trend-lines for the z-coordinate of atoms NE1 (blue) and CH2 (red) on the Tryptophan residue (Figure 2.1). The CG4 atom (yellow) is the first atom on the C-terminal benzyl ring. The z-coord is plottet as a function of time (ns). The black line shows the trend of the phosphate atoms mean z-coordinates in the lipid bilayer leaflet facing the peptides, blotted individually.*

Appendix E

Insertion Trend of the RTbtR-NHBn Peptide

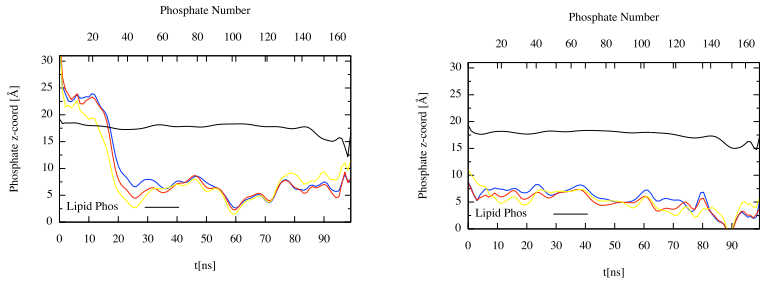

(a) *Pep A; 0 to 200 ns.*

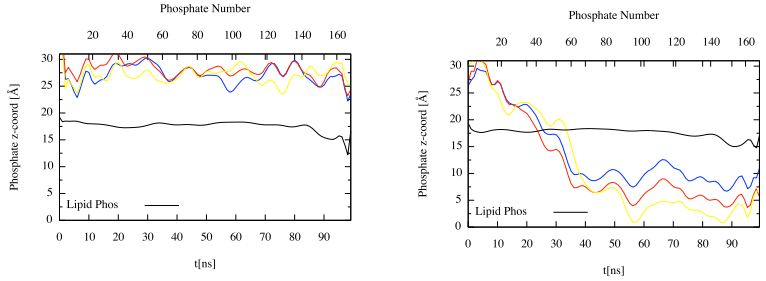

(b) *Pep B; 0 to 200 ns.*

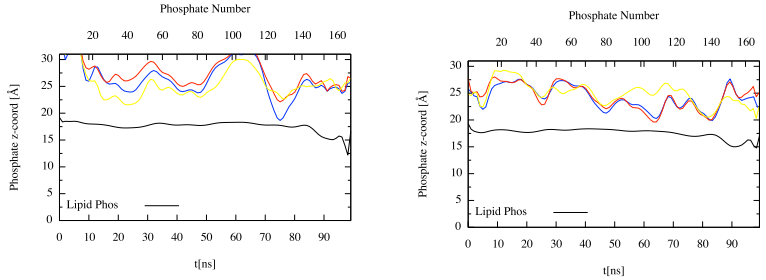

(c) *Pep C; 0 to 200 ns.*

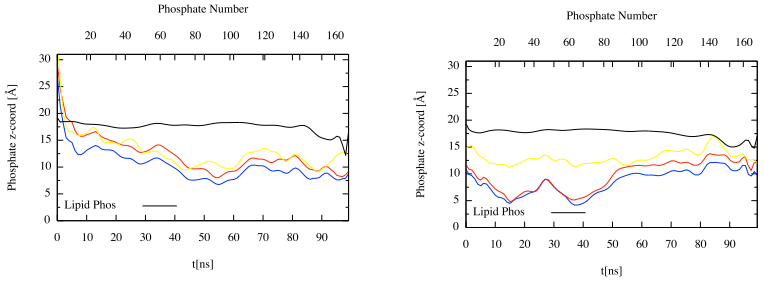

(d) *Pep D; 0 to 200 ns.*

Figure E.1: *System 1, with 4 RTbtR-NHBn peptides. The trend-lines for the z-coordinate of atoms NE1 (blue) and CH2 (red) on the Tryptophan residue (Figure 2.1). The C76 atom (yellow) is the first atom on the C-terminal benzyl ring. The z-coord is plottet as a function of time (ns). The black line shows the trend of the phosphate atoms mean z-coordinates in the lipid bilayer leaflet facing the peptides, blotted individually.*

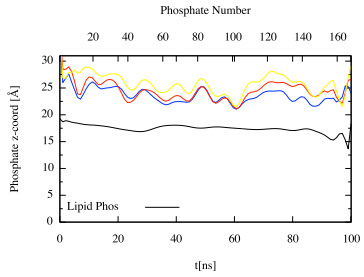

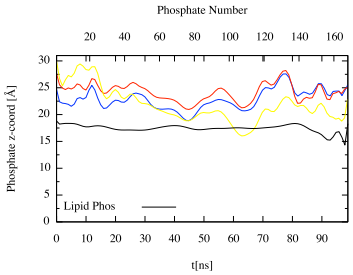

(a) *Pep A; 0 to 200 ns.*

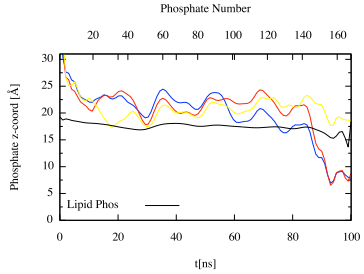

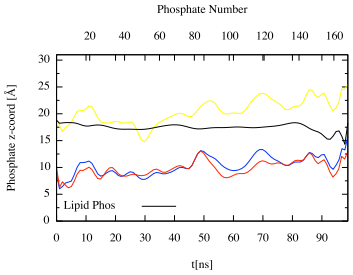

(b) *Pep B; 0 to 200 ns.*

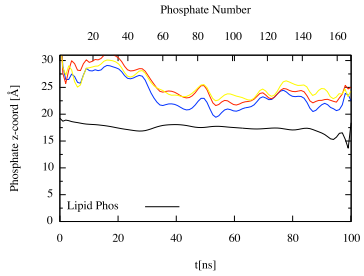

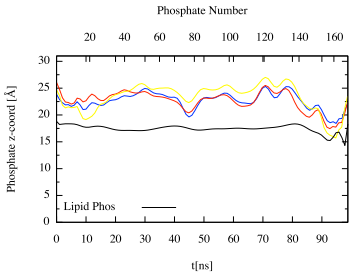

(c) *Pep C; 0 to 200 ns.*

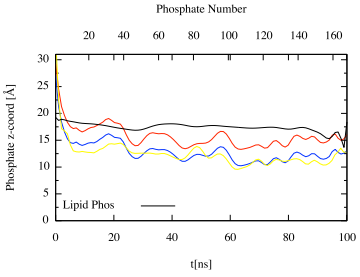

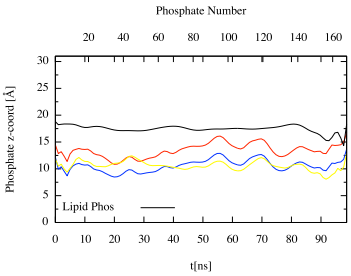

(d) *Pep D; 0 to 200 ns.*

Figure E.2: *System 2, with 4 RTbtR-NHBn peptides. The trend-lines for the z-coordinate of atoms NE1 (blue) and CH2 (red) on the Tryptophan residue (Figure 2.1). The C76 atom (yellow) is the first atom on the C-terminal benzyl ring. The z-coord is plottet as a function of time (ns). The black line shows the trend of the phosphate atoms mean z-coordinates in the lipid bilayer leaflet facing the peptides, blotted individually.*

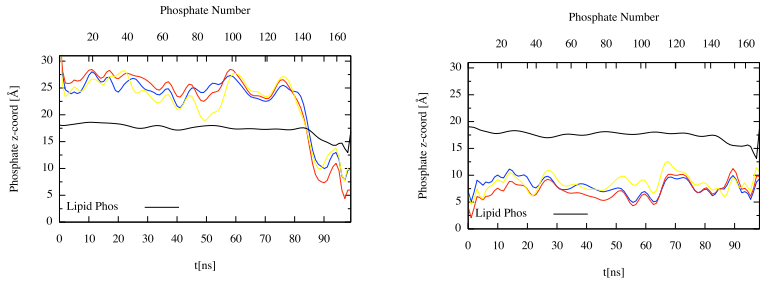

(a) *Pep A; 0 to 200 ns.*

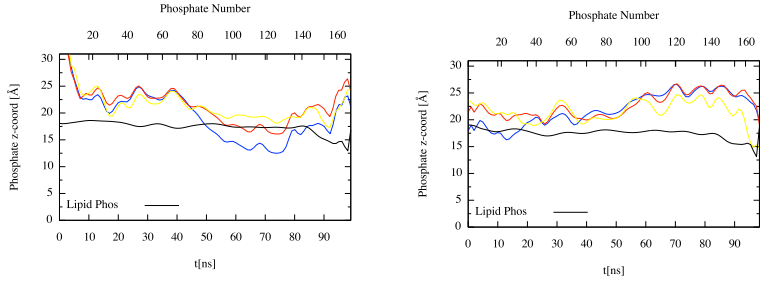

(b) *Pep B; 0 to 200 ns.*

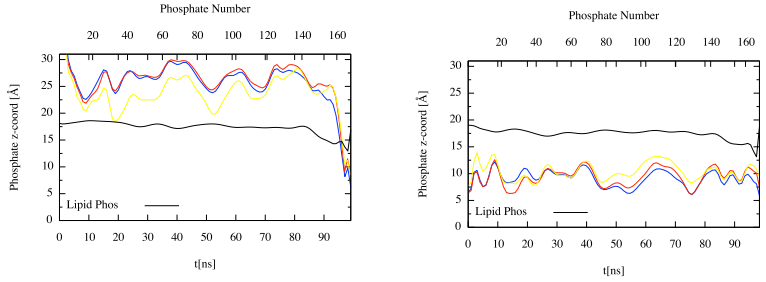

(c) *Pep C; 0 to 200 ns.*

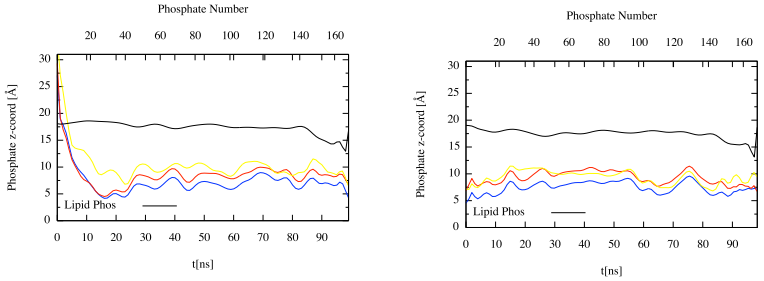

(d) *Pep D; 0 to 200 ns.*

Figure E.3: *System 3, with 4 RTbtR-NHBn peptides. The trend-lines for the z-coordinate of atoms NE1 (blue) and CH2 (red) on the Tryptophan residue (Figure 2.1). The C76 atom (yellow) is the first atom on the C-terminal benzyl ring. The z-coord is plottet as a function of time (ns). The black line shows the trend of the phosphate atoms mean z-coordinates in the lipid bilayer leaflet facing the peptides, blotted individually.*

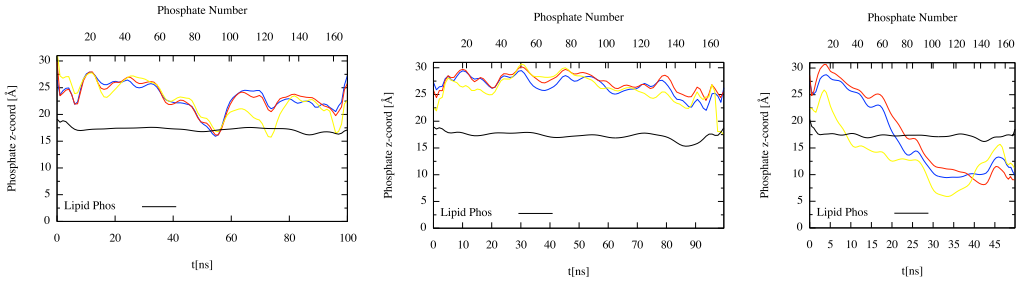

(a) *Pep A; 0 to 250 ns.*

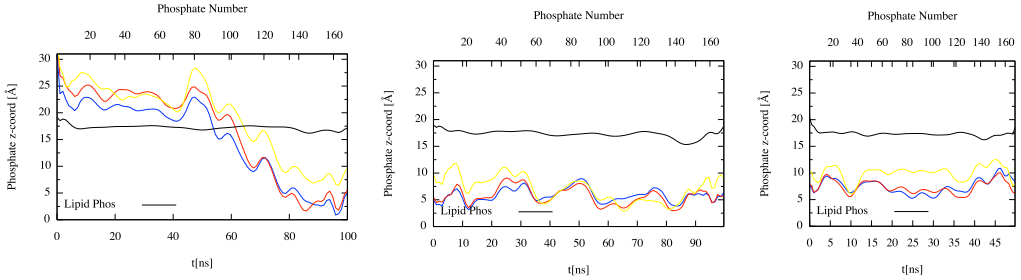

(b) *Pep B; 0 to 250 ns.*

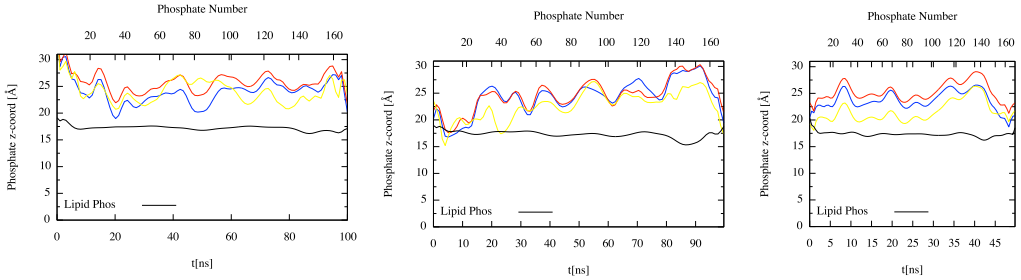

(c) *Pep C; 0 to 250 ns.*

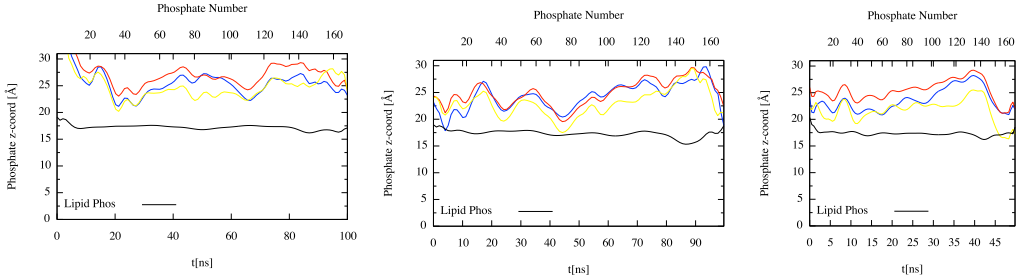

(d) *Pep D; 0 to 250 ns.*

Figure E.4: *System 1, with 8 RTbtR-NHBn peptides. The trend-lines for the z-coordinate of atoms NE1 (blue) and CH2 (red) on the Tryptophan residue (Figure 2.1). The C76 atom (yellow) is the first atom on the C-terminal benzyl ring. The z-coord is plottet as a function of time (ns). The black line shows the trend of the phosphate atoms mean z-coordinates in the lipid bilayer leaflet facing the peptides, blotted individually.*

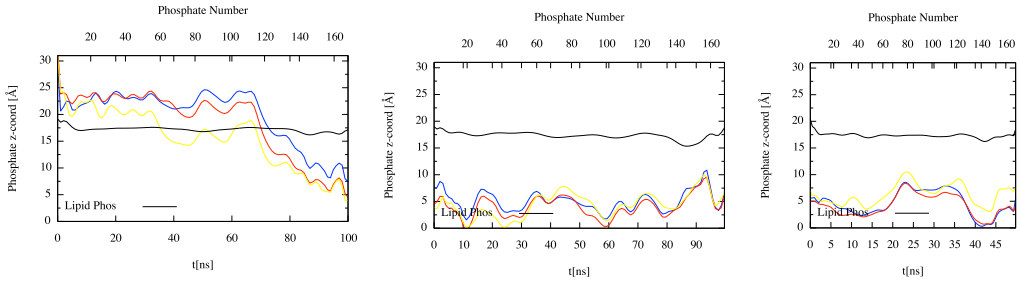

(a) *Pep E; 0 to 250 ns.*

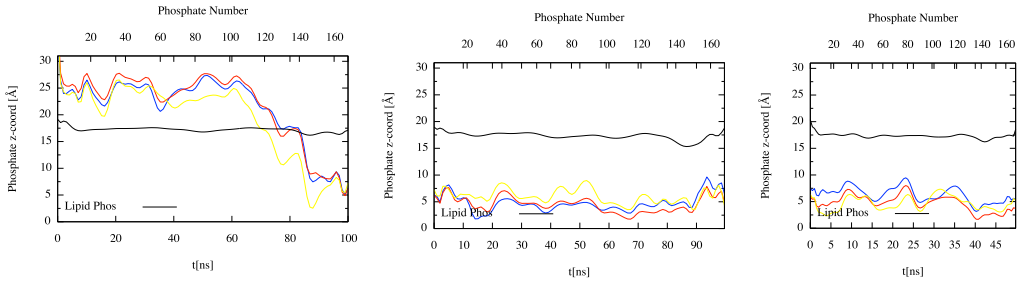

(b) *Pep F; 0 to 250 ns.*

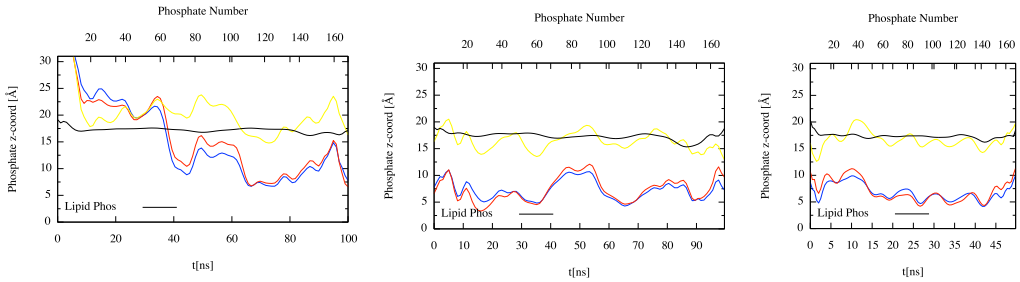

(c) *Pep G; 0 to 250 ns.*

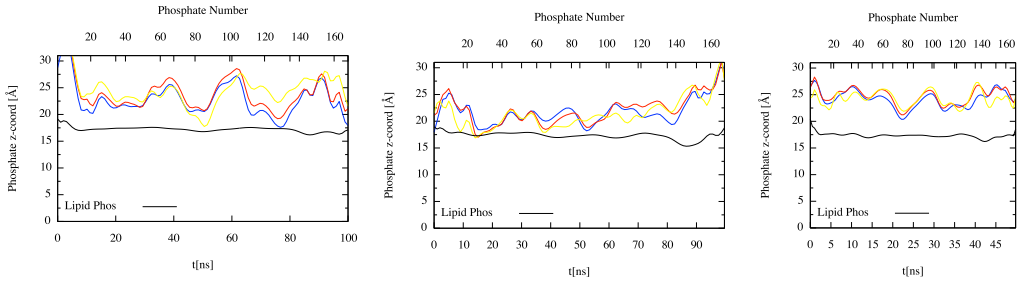

(d) *Pep H; 0 to 250 ns.*

Figure E.5: *System 1, with 8 RTbtR-NHBn peptides. The trend-lines for the z-coordinate of atoms NE1 (blue) and CH2 (red) on the Tryptophan residue (Figure 2.1). The C76 atom (yellow) is the first atom on the C-terminal benzyl ring. The z-coord is plottet as a function of time (ns). The black line shows the trend of the phosphate atoms mean z-coordinates in the lipid bilayer leaflet facing the peptides, blotted individually.*

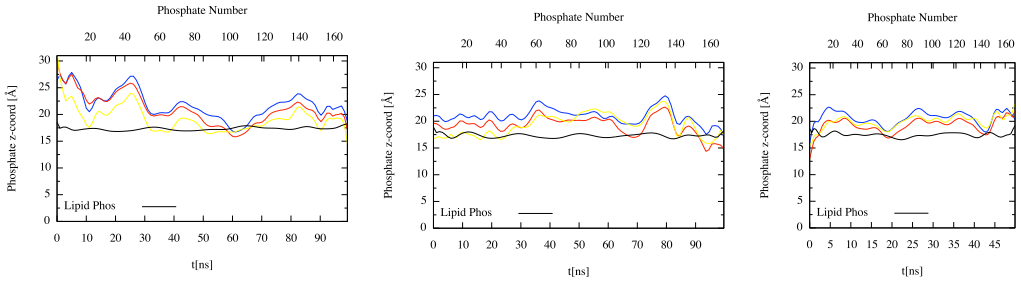

(a) *Pep A; 0 to 250 ns.*

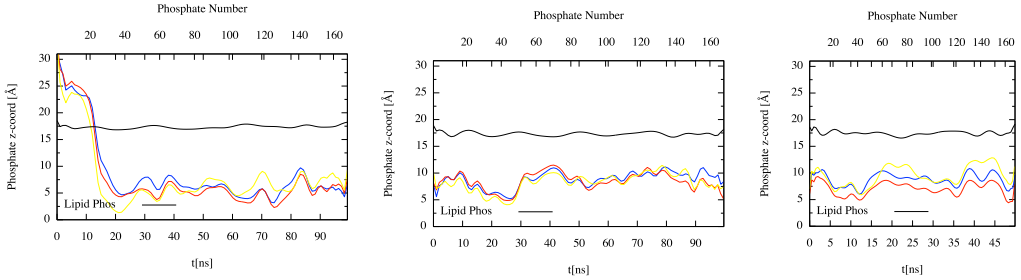

(b) *Pep B; 0 to 250 ns.*

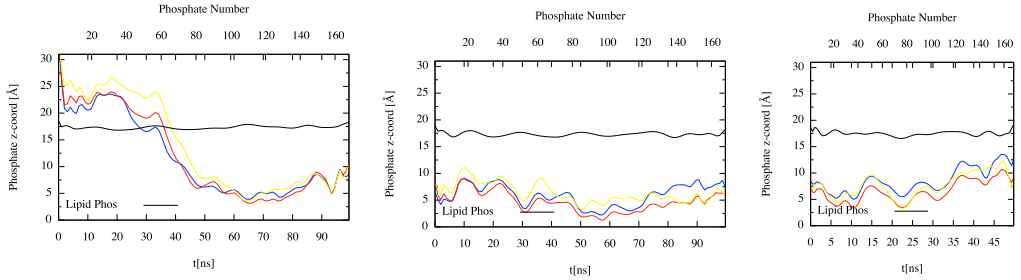

(c) *Pep C; 0 to 250 ns.*

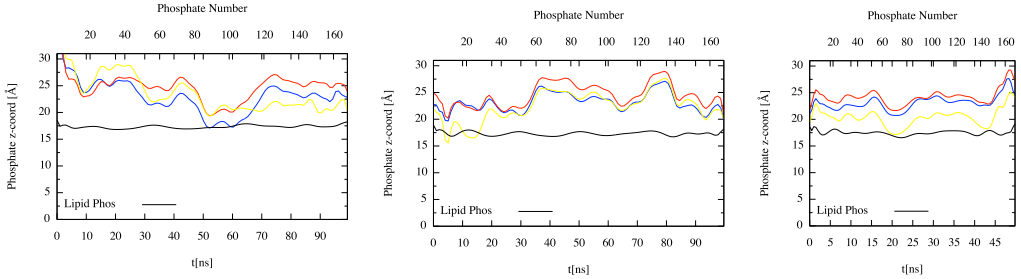

(d) *Pep D; 0 to 250 ns.*

Figure E.6: *System 2, with 8 RTbtR-NHBn peptides. The trend-lines for the z-coordinate of atoms NE1 (blue) and CH2 (red) on the Tryptophan residue (Figure 2.1). The C76 atom (yellow) is the first atom on the C-terminal benzyl ring. The z-coord is plottet as a function of time (ns). The black line shows the trend of the phosphate atoms mean z-coordinates in the lipid bilayer leaflet facing the peptides, blotted individually.*

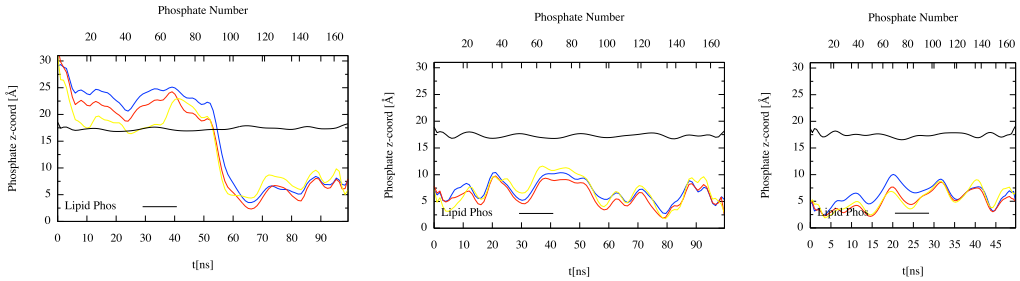

(a) *Pep E; 0 to 250 ns.*

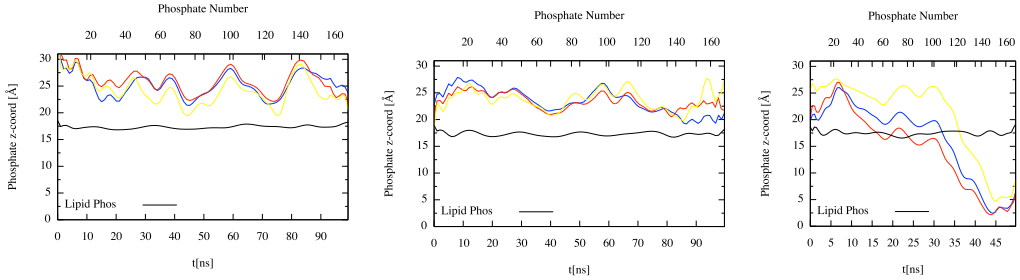

(b) *Pep F; 0 to 250 ns.*

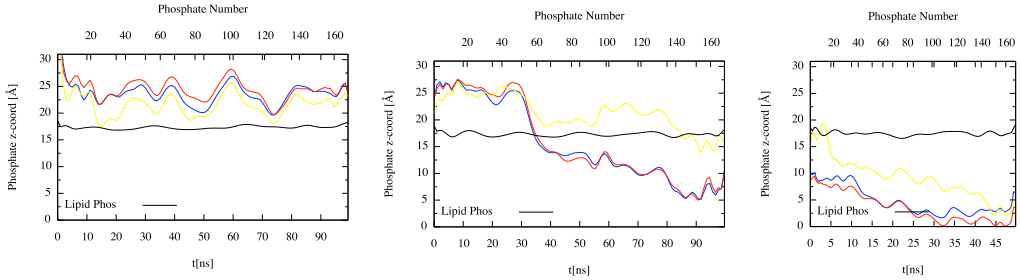

(c) *Pep G; 0 to 250 ns.*

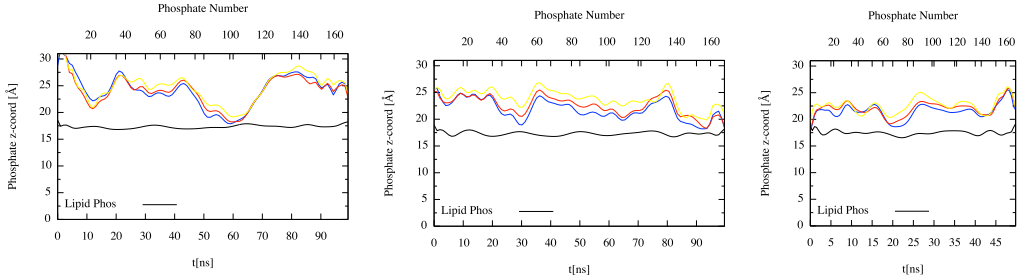

(d) *Pep H; 0 to 250 ns.*

Figure E.7: *System 2, with 8 RTbtR-NHBn peptides. The trend-lines for the z-coordinate of atoms NE1 (blue) and CH2 (red) on the Tryptophan residue (Figure 2.1). The C76 atom (yellow) is the first atom on the C-terminal benzyl ring. The z-coord is plottet as a function of time (ns). The black line shows the trend of the phosphate atoms mean z-coordinates in the lipid bilayer leaflet facing the peptides, blotted individually.*

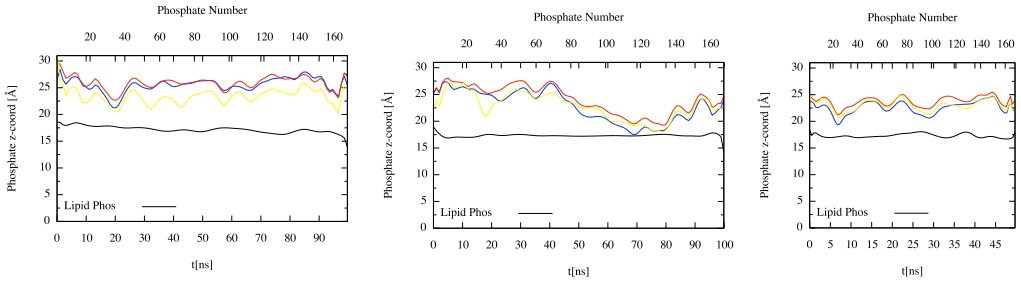

(a) *Pep A; 0 to 250 ns.*

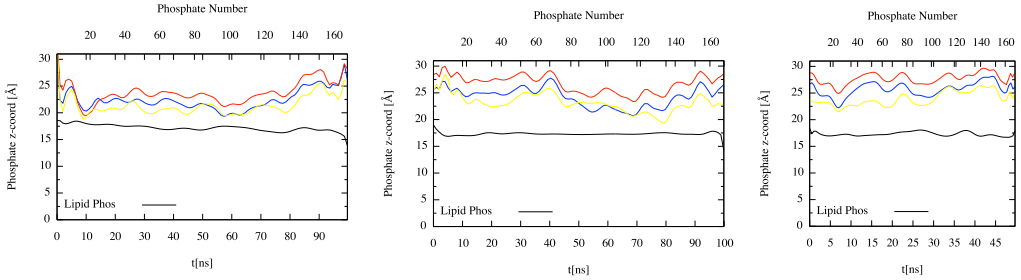

(b) *Pep B; 0 to 250 ns.*

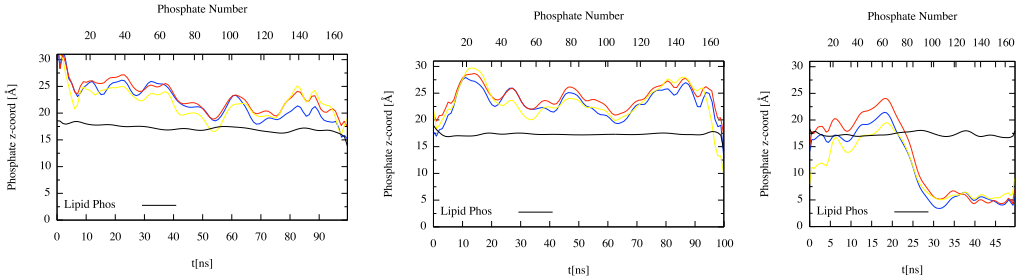

(c) *Pep C; 0 to 250 ns.*

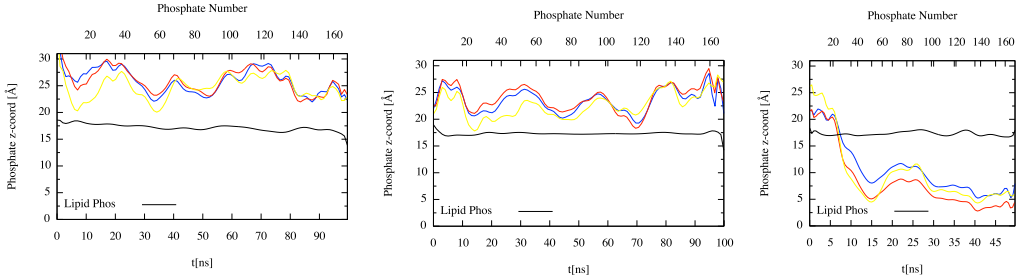

(d) *Pep D; 0 to 250 ns.*

Figure E.8: *System 3, with 8 RTbtR-NHBn peptides. The trend-lines for the z-coordinate of atoms NE1 (blue) and CH2 (red) on the Tryptophan residue (Figure 2.1). The C76 atom (yellow) is the first atom on the C-terminal benzyl ring. The z-coord is plottet as a function of time (ns). The black line shows the trend of the phosphate atoms mean z-coordinates in the lipid bilayer leaflet facing the peptides, blotted individually.*

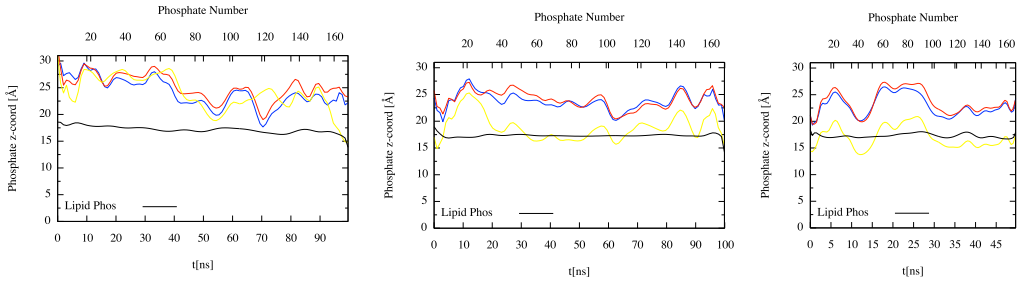

(a) *Pep E; 0 to 250 ns.*

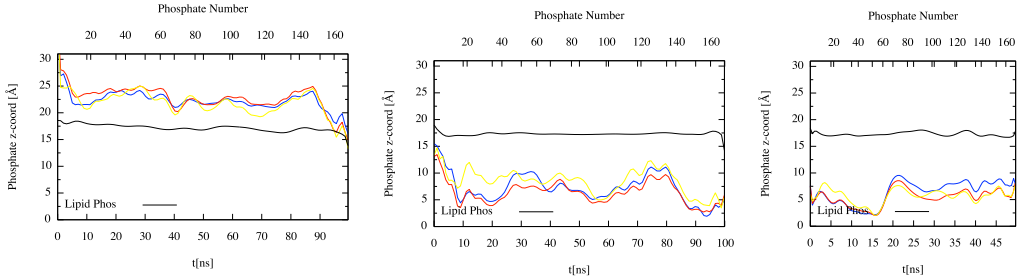

(b) *Pep F; 0 to 250 ns.*

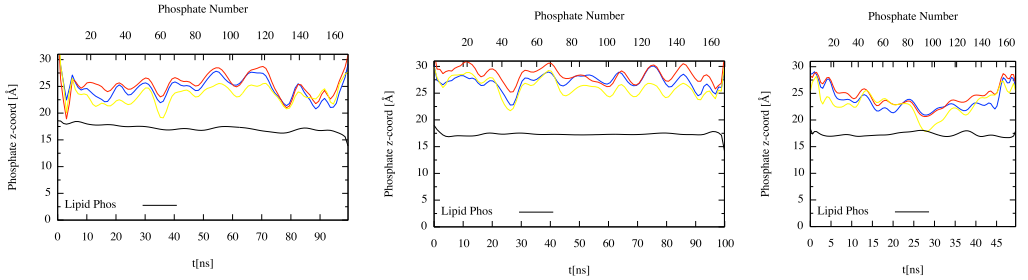

(c) *Pep G; 0 to 250 ns.*

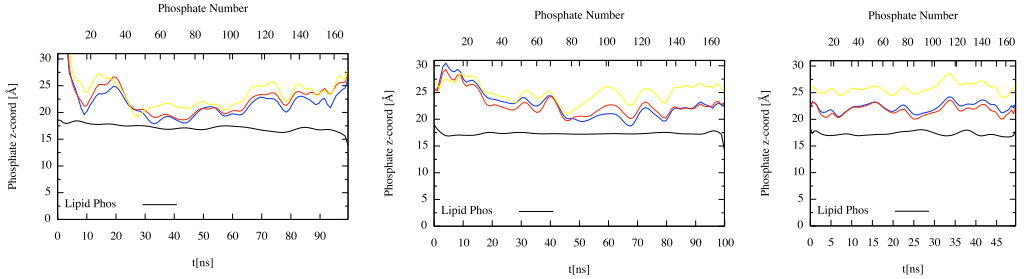

(d) *Pep H; 0 to 250 ns.*

Figure E.9: *System 3, with 8 RTbtR-NHBn peptides. The trend-lines for the z-coordinate of atoms NE1 (blue) and CH2 (red) on the Tryptophan residue (Figure 2.1). The C76 atom (yellow) is the first atom on the C-terminal benzyl ring. The z-coord is plottet as a function of time (ns). The black line shows the trend of the phosphate atoms mean z-coordinates in the lipid bilayer leaflet facing the peptides, blotted individually.*